

# Investigating the Influence of Drought on Sentinel-1 C-band SAR data over Agricultural Crops

A Study in the Netherlands

M. Shorachi





# Investigating the Influence of Drought on Sentinel-1 C-band SAR data over Agricultural Crops

## A Study in the Netherlands

by

**M. Shorachi**

to obtain the degree of Master of Science  
at the Delft University of Technology,

Student number:	4397029	
Thesis committee:	Prof. dr. ir. S.C. Steele-Dunne	Chair
	Dr. V. Kumar	Daily Supervisor
	Dr. ir. A.M.J. Coenders-Gerrits	Assessor
	Dr. ir. F.J. van Leijen	External assessor

# Summary

The stress on global food security is expected to increase due to the continuous growth of the world population, and the more frequently occurring severe agricultural droughts due to climate change. With agricultural crops being one of the most crucial sources of food globally, crop and drought monitoring will become increasingly important in the future for food producers, decision-makers and farmers. Due to the unprecedented amount of available satellite images and their global coverage, satellite remote sensing has become a popular tool for agricultural monitoring purposes. Optical remote sensing provides valuable information on agricultural targets and is currently the main form of satellite remote sensing that is used for agricultural monitoring. However, optical sensors do not always provide temporally reliable data due to cloud cover. Synthetic Aperture Radars (SAR) are able to penetrate clouds and thus reliably provide data at all times. Despite the extensive literature that can be found on the use of high spatio-temporal resolution SAR data, a study investigating the influence of drought on Sentinel-1 data over agricultural crops has yet to be conducted. This research aims to bridge this knowledge gap by utilizing data acquired from Sentinel-1, which provides high resolution dual polarized (VV + VH) data with a return period of six days.

The Sentinel-1 data in this research is acquired and processed in the Google Earth Engine platform and afterwards, data analysis is performed using Python. This results in parcel level SAR (VV, VH and VH/VV) data. Furthermore, surface soil moisture and precipitation data is used to interpret the complex satellite data, distinguish causes for temporal change and identify drought periods. Lastly, gross yield data is used to help validate the observations and conclusions. This research is focused on maize, sugar beet, potato, onion and barley parcels in study areas in the Netherlands during the 2017, 2018 and 2019 agricultural summer season. Studying drought impact in 2018 and 2019 offers a unique opportunity, because of the two consecutive drought summers across central Europe that were most severe in the last 250 years. The Netherlands was also impacted heavily by the consecutive droughts, especially in 2018.

This research demonstrates that phenological changes are reflected in Sentinel-1 data with increasing backscatter intensities during leaf development and stem elongation phases. Subsequently, saturation occurs which halts the rapid increase of backscatter. During harvest, the VH/VV ratio decreases rapidly. Time series of barley behave differently due to its unique vertical structure.

Influences of drought are studied by analyzing parcels in the northern part of the Vechtstromen water board. The results show that VV and VH backscatter values are 2.5, 2 and 1 dB lower during the 2018 drought compared to 2017 for maize, sugar beet and potato parcels, respectively. This is mainly caused by the decreasing vegetation water content. Furthermore, the seasonal VH/VV ratio cycle for maize, onion and barley is shorter in a drought year and shortest in 2018. This is caused by faster crop development and thus an earlier harvest due to dry circumstances. The VH/VV ratio cycle in 2018 was 30, 10 and 20 days shorter compared to 2017 for maize, onion and barley, respectively. However, VH/VV ratio trends for sugar beet and potato did not show a significant difference in 2018 compared to 2017. Lastly, the dry soil - caused by the lingering effects of the 2018 drought - results in significantly lower VH/VV ratio values during the vegetative stages in 2019. However, this did not lead to a lower yield. The aforementioned aggregated observations are also reflected in a majority of individual parcels. The percentage of individual parcels that show responses similar to aggregated responses ranges from 68% to 100%. Moreover, the results show that the overpass time has a large influence on drought response. Descending orbits - which pass around 05:45 - significantly increase the magnitude of the VV and VH backscatter drop during the drought periods, especially for sugar beet and potato crops.

The regional variability was assessed by comparing parcel backscatter from the northern part of the Vechtstromen water board, the Scheldestromen water board and the Flevopolder. Generally, drought impact is found to be most extreme in Vechtstromen, which was expected due to its sandy soil. However, onions in 2018 were impacted most in Scheldestromen according to yield data. This clearly translated into lower VH backscatter and VH/VV ratio values during and after the drought period. Also, regional differences in maize time series caused by irrigation are observed. The results show that areas in which irrigation was allowed with ground and open water had a longer VH/VV ratio cycle in 2018, compared to areas in which irrigation was allowed only with groundwater.

Overall, the usage of Sentinel-1 data for drought monitoring purposes shows tremendous potential. This gives a promising outlook on the use of dense C-band SAR data for the detection of crop drought stress and drought stress monitoring.

# Preface

I wrote this thesis on the influence of drought on Sentinel-1 data over agricultural crops in the Netherlands as completion of the water management track of the civil engineering master at the Delft University of Technology. I would like to express my sincere gratitude to the chair of the committee and my supervisor, Susan Steele-Dunne, for keeping me on the right track while guiding me through this thesis writing process. Furthermore, I would like to thank my daily supervisor Vineet Kumar for always being available whenever I was in need of advice or a brainstorm session. I would also like to thank the rest of the thesis committee, Miriam Coenders and Freek van Leijen, for giving valuable input and feedback during the meetings. Then, I would like to thank Tom Grobbe from the Vechtstromen water board for providing information regarding their irrigation policies. Lastly, I want to thank my family and friends who have supported me throughout the thesis writing process. I especially want to thank my partner for her never-ending patience, invaluable advice, and endless support.

Six years at the TU Delft has equipped me well for the next phases in my life. Plutarch once said that "the mind does not require filling like a bottle, but rather, like wood, it only requires kindling". Even though this thesis marks the end of my time as a student, I will continue learning.

*Maurice Shorachi*  
*Delft, January 2021*

# Contents

Summary	i
Preface	ii
List of Figures	v
List of Tables	viii
Nomenclature	ix
1 Introduction	1
1.1 Research context . . . . .	1
1.2 Problem statement . . . . .	2
1.3 Research objective . . . . .	3
1.4 Report outline. . . . .	3
2 Background	4
2.1 The basics of spaceborne SAR imaging . . . . .	4
2.2 Interaction between SAR and crops . . . . .	5
2.3 Crop response to drought stress. . . . .	7
3 Study Area, Data and Methodology	9
3.1 The Netherlands . . . . .	9
3.1.1 General study areas . . . . .	10
3.1.2 Irrigation study areas . . . . .	11
3.2 Data. . . . .	12
3.2.1 Sentinel-1 SAR data . . . . .	12
3.2.2 Vector, parcel and crop data . . . . .	13
3.2.3 Crop yield data. . . . .	14
3.2.4 Surface soil moisture data . . . . .	15
3.2.5 Precipitation data . . . . .	15
3.3 Methodology . . . . .	16
3.3.1 Extraction of Sentinel-1 data using SandboxNL . . . . .	16
3.3.2 Data Analysis . . . . .	17
4 Results and Discussion	18
4.1 Seasonal crop cycle characterization using C-band Sentinel-1 SAR data . . . . .	18
4.1.1 Impact of phenological changes on C-band SAR data . . . . .	18
4.1.2 Influence of agricultural drought on the interannual variability of C-band SAR data . . . . .	24
4.1.3 Influence of Sentinel-1 viewing geometry and overpass time . . . . .	32
4.1.4 The extent to which drought observations aggregated across all parcels are reflected in individual parcels . . . . .	32
4.2 Regional variability of agricultural drought C-band Sentinel-1 SAR data . . . . .	35
4.2.1 Drought-induced differences between the study areas. . . . .	35
4.2.2 Influence of irrigation on the regional variability of C-band SAR data . . . . .	41
5 Conclusions and Recommendations	44
5.1 Conclusions. . . . .	44
5.2 Recommendations . . . . .	45
Bibliography	47
A BBCH stage tables	55
A.1 Maize . . . . .	55
A.2 Sugar beet. . . . .	57
A.3 Potato. . . . .	58
A.4 Onion . . . . .	60
A.5 Barley . . . . .	61

---

B	Field photo archive	63
C	Python: Post-Processing Code	65
D	Scheldestromen and the Flevopolder results	67
	D.1 Scheldestromen. . . . .	68
	D.2 Flevopolder. . . . .	73

# List of Figures

2.1	Basic SAR scattering mechanisms from incoherent targets. . . . .	5
2.2	The influence of incidence angle on the backscatter coefficient. . . . .	6
2.3	Phenological responses of drought stressed potato crops in different stages. . . . .	8
3.1	30-year average monthly rainfall measured at the Bilt. . . . .	9
3.2	30-year average monthly temperature measured at the Bilt. . . . .	9
3.3	Map of the Netherlands including highlighted general study areas and the irrigation study areas. . . . .	10
3.4	Water system division in the Vechtstromen waterboard area. The red area represents High-Vechtstromen and blue represents Low-Vechtstromen. . . . .	11
3.5	Swaths of the descending Sentinel-1 orbits covering the Netherlands. . . . .	12
3.6	Swaths of the ascending Sentinel-1 orbits covering the Netherlands. . . . .	12
3.7	Sentinel-1 SAR, soil moisture and precipitation data acquisition dates in 2017, 2018 and 2019. . . . .	12
3.8	Normalized gross yield per province expressed in 1000 kg/ha for a) maize, b) sugar beet, c) potato, d) onion and e) barley crops. . . . .	14
3.9	Locations of the soil moisture and precipitation data sources in the general study areas. . . . .	15
3.10	Sentinel-1 SAR data flow diagram. . . . .	16
4.1	The 2017 time series of Sentinel-1 SAR data (VV, VH and VH/VV) from maize parcels in the Flevopolder. The black lines represent the mean value and the gray bands depict the standard deviation across all fields. Precipitation data is displayed in the bottom plot. The green-outlined bars correspond to the general planting and harvest periods. . . . .	19
4.2	Maize field photo taken on the 17th of May (DOY 137) in the Flevopolder. . . . .	19
4.3	Maize field photo taken on the 27th of July (DOY 178) in the Flevopolder. . . . .	19
4.4	The 2017 time series of Sentinel-1 SAR data (VV, VH and VH/VV) from sugar beet parcels in the Flevopolder. The black lines represent the mean value and the gray bands depict the standard deviation across all fields. Precipitation data is displayed in the bottom plot. The green-outlined bars correspond to the general planting and harvest periods. . . . .	20
4.5	Sugar beet field photo taken on the 17th of May (DOY 137) in the Flevopolder. . . . .	21
4.6	Sugar beet field photo taken on the 9th of June (DOY 160) in the Flevopolder. . . . .	21
4.7	The 2017 time series of Sentinel-1 SAR data (VV, VH and VH/VV) from potato parcels in the Flevopolder. The black lines represent the mean value and the gray bands depict the standard deviation across all fields. Precipitation data is displayed in the bottom plot. The green-outlined bars correspond to the general planting and harvest periods. . . . .	21
4.8	Potato field photo taken on the 17th of May (DOY 137) in the Flevopolder. . . . .	22
4.9	Potato field photo taken on the 19th of June (DOY 170) in the Flevopolder. . . . .	22
4.10	The 2017 time series of Sentinel-1 SAR data (VV, VH and VH/VV) from onion parcels in the Flevopolder. The black lines represent the mean value and the gray bands depict the standard deviation across all fields. Precipitation data is displayed in the bottom plot. The green-outlined bars correspond to the general planting and harvest periods. . . . .	22
4.11	centering Onion field photo taken on the 23rd of May (DOY 143) in the Flevopolder. . . . .	23
4.12	Onion field photo taken on the 10th of July (DOY 191) in the Flevopolder. . . . .	23
4.13	The 2017 time series of Sentinel-1 SAR data (VV, VH and VH/VV) from barley parcels in the Flevopolder. The black lines represent the mean value and the gray bands depict the standard deviation across all fields. Precipitation data is displayed in the bottom plot. The green-outlined bars correspond to the general planting and harvest periods. . . . .	24
4.14	The 2017, 2018 and 2019 time series of Sentinel-1 SAR data (VV, VH and VH/VV) from maize parcels in Vechtstromen-Noord. The colored lines represent the mean value and the shaded bands depict the standard deviation across all fields. Surface soil moisture and cumulative precipitation data is displayed in the bottom two plot. The green-outlined bars correspond to the general planting and harvest periods. . . . .	25

4.15	The 2017, 2018 and 2019 time series of Sentinel-1 SAR data (VV, VH and VH/VV) from sugar beet parcels in Vechtstromen-Noord. The colored lines represent the mean value and the shaded bands depict the standard deviation across all fields. Surface soil moisture and cumulative precipitation data is displayed in the bottom two plot. The green-outlined bars correspond to the general planting and harvest periods. . . . .	27
4.16	The 2017, 2018 and 2019 time series of Sentinel-1 SAR data (VV, VH and VH/VV) from potato parcels in Vechtstromen-Noord. The colored lines represent the mean value and the shaded bands depict the standard deviation across all fields. Surface soil moisture and cumulative precipitation data is displayed in the bottom two plot. The green-outlined bars correspond to the general planting and harvest periods. . . . .	28
4.17	Potato field photo taken on the 14th of July in the Flevopolder. . . . .	29
4.18	Potato field photo taken on the 28th of July in the Flevopolder. . . . .	29
4.19	The 2017, 2018 and 2019 time series of Sentinel-1 SAR data (VV, VH and VH/VV) from onion parcels in Vechtstromen-Noord. The colored lines represent the mean value and the shaded bands depict the standard deviation across all fields. Surface soil moisture and cumulative precipitation data is displayed in the bottom two plot. The green-outlined bars correspond to the general planting and harvest periods. . . . .	30
4.20	The 2017, 2018 and 2019 time series of Sentinel-1 SAR data (VV, VH and VH/VV) from barley parcels in Vechtstromen-Noord. The colored lines represent the mean value and the shaded bands depict the standard deviation across all fields. Surface soil moisture and cumulative precipitation data is displayed in the bottom two plot. The green-outlined bars correspond to the general planting and harvest periods. . . . .	31
4.21	Sentinel-1 VH/VV ratio from a maize parcel in 2017 and 2018. . . . .	33
4.22	The 2017, 2018 and 2019 time series of Sentinel-1 SAR data (VV, VH and VH/VV) from maize parcels in all study areas. The colored lines represent the mean value and the shaded bands depict the standard deviation across all fields. Surface soil moisture and cumulative precipitation data is displayed in the bottom two plot. The green-outlined bars correspond to the general planting and harvest periods. . . . .	36
4.23	The 2017, 2018 and 2019 time series of Sentinel-1 SAR data (VV, VH and VH/VV) from sugar beet parcels in all study areas. The colored lines represent the mean value and the shaded bands depict the standard deviation across all fields. Surface soil moisture and cumulative precipitation data is displayed in the bottom two plot. The green-outlined bars correspond to the general planting and harvest periods. . . . .	37
4.24	The 2017, 2018 and 2019 time series of Sentinel-1 SAR data (VV, VH and VH/VV) from potato parcels in all study areas. The colored lines represent the mean value and the shaded bands depict the standard deviation across all fields. Surface soil moisture and cumulative precipitation data is displayed in the bottom two plot. The green-outlined bars correspond to the general planting and harvest periods. . . . .	38
4.25	The 2017, 2018 and 2019 time series of Sentinel-1 SAR data (VV, VH and VH/VV) from onion parcels in all study areas. The colored lines represent the mean value and the shaded bands depict the standard deviation across all fields. Surface soil moisture and cumulative precipitation data is displayed in the bottom two plot. The green-outlined bars correspond to the general planting and harvest periods. . . . .	39
4.26	The 2017, 2018 and 2019 time series of Sentinel-1 SAR data (VV, VH and VH/VV) from barley parcels in all study areas. The colored lines represent the mean value and the shaded bands depict the standard deviation across all fields. Surface soil moisture and cumulative precipitation data is displayed in the bottom two plot. The green-outlined bars correspond to the general planting and harvest periods. . . . .	40
4.27	VH/VV ratio values of maize parcels in the Coevorden, Hardenberg, Tubbergen and Hof van Twente municipalities. . . . .	41
4.28	The 2017, 2018 and 2019 time series of Sentinel-1 SAR data (VV, VH and VH/VV) from maize parcels in the Coevorden, Hardenberg, Tubbergen and Hof van Twente municipalities. The colored lines represent the mean value and the shaded bands depict the standard deviation across all fields. Surface soil moisture and cumulative precipitation data is displayed in the bottom two plot. The green-outlined bars correspond to the general planting and harvest periods. . . .	42
4.29	The 2017, 2018 and 2019 time series of Sentinel-1 SAR data (VV, VH and VH/VV) from potato parcels in the Coevorden, Hardenberg, Tubbergen and Hof van Twente municipalities. The colored lines represent the mean value and the shaded bands depict the standard deviation across all fields. Surface soil moisture and cumulative precipitation data is displayed in the bottom two plot. The green-outlined bars correspond to the general planting and harvest periods. . . .	43

---

B.1	Field photo archive of maize parcel PvD-M2 in the Flevopolder in 2017. . . . .	63
B.2	Field photo archive of sugar beet parcel DB2.1/1.1 in the Flevopolder in 2017. . . . .	64
B.3	Field photo archive of potato parcel DB-A1/A2 in the Flevopolder in 2017. . . . .	64
D.1	2017, 2018 and 2019 Sentinel-1 backscatter data for maize parcels, soil moisture and cumulative precipitation in Scheldestromen. . . . .	68
D.2	2017, 2018 and 2019 Sentinel-1 backscatter data for sugar beet parcels, soil moisture and cumulative precipitation in Scheldestromen. . . . .	69
D.3	2017, 2018 and 2019 Sentinel-1 backscatter data for potato parcels, soil moisture and cumulative precipitation in Scheldestromen. . . . .	70
D.4	2017, 2018 and 2019 Sentinel-1 backscatter data for onion parcels, soil moisture and cumulative precipitation in Scheldestromen. . . . .	71
D.5	2017, 2018 and 2019 Sentinel-1 backscatter data for barley parcels, soil moisture and cumulative precipitation in Scheldestromen. . . . .	72
D.6	2017, 2018 and 2019 Sentinel-1 backscatter data for maize parcels, soil moisture and cumulative precipitation in the Flevopolder. . . . .	73
D.7	2017, 2018 and 2019 Sentinel-1 backscatter data for sugar beet parcels, soil moisture and cumulative precipitation in the Flevopolder. . . . .	74
D.8	2017, 2018 and 2019 Sentinel-1 backscatter data for potato parcels, soil moisture and cumulative precipitation in the Flevopolder . . . . .	75
D.9	2017, 2018 and 2019 Sentinel-1 backscatter data for onion parcels, soil moisture and cumulative precipitation in Flevopolder. . . . .	76
D.10	2017, 2018 and 2019 Sentinel-1 backscatter data for barley parcels, soil moisture and cumulative precipitation in the Flevopolder. . . . .	77

# List of Tables

1.1	Normalized gross yield data for key crops in the Netherlands in 2017, 2018 and 2019, expressed in 1000 kg per harvested hectares. . . . .	2
3.1	General information of Sentinel-1 orbits covering the Netherlands. . . . .	13
3.2	List of most popular arable crops in the Netherlands (2019). . . . .	13
3.3	Number of studied crop parcels in the general study areas (2019) . . . . .	13
4.1	The drought-induced interannual variability observations that are analyzed in this section. . . . .	33
4.2	Individual parcel analysis results for maize parcels in Vechtstromen-Noord. . . . .	34
4.3	Individual parcel analysis results for potato parcels in Vechtstromen-Noord. . . . .	34
4.4	Individual parcel analysis results for barley parcels in Vechtstromen-Noord. . . . .	34
A.1	Maize BBCH stages and corresponding SAR backscatter responses. . . . .	55
A.2	Beet BBCH stages and corresponding SAR backscatter responses. . . . .	57
A.3	Potato BBCH stages and corresponding SAR backscatter responses. . . . .	58
A.4	Bulb vegetable BBCH stages and corresponding SAR backscatter responses. . . . .	60
A.5	Cereal BBCH stages and corresponding SAR backscatter responses. . . . .	61

# Nomenclature

ascN	Ascending relative orbit N
BBCH	A scale system that provides a framework for identifying phenological stages of crops
BRP	Basisregistratie gewaspercelen, a vector file containing the registered parcel boundaries in the Netherlands
CBS	Centraal Bureau voor de Statistiek (Dutch Central Bureau of Statistics)
C-band	A wavelength (or frequency) band with a range of 3.75 - 7.5 cm
dB	Decibel
desN	Descending relative orbit N
DOY	Day Of Year
ESA	European Space Agency
GAI	Green Area Index
GEE	Google Earth Engine
GRD	Ground Range Detected
KNMI	Koninklijk Nederlands Meteorologisch Instituut (The Royal Netherlands Meteorological Institute)
LAI	Leaf Area Index
NDVI	Normalized Difference Vegetation Index
SLC	Single Look Complex
Radar	Radio Detection And Ranging
SAR	Synthetic Aperture Radar
VH	Vertically (V) transmitted and horizontally (H) received
VV	Vertically (V) transmitted and received
VWC	Vegetation Water Content
$\sigma^0$	Backscatter coefficient
$\sigma_{VH}^0$	Scattering of an electromagnetic wave that is vertically (V) transmitted and horizontally (H) received
$\sigma_{VV}^0$	Scattering of an electromagnetic wave that is vertically (V) transmitted and received
$\sigma_{VH/VV}^0$	Cross-pol ratio (SAR index)
$\theta$	Incidence angle

# 1

## Introduction

### 1.1. Research context

With the changing climate and the increasing world population, the stress on global food security is also expected to increase [1, 2]. According to the Food and Agriculture Organization (FAO), 60% more food is needed by 2050 to meet global demand assuming current food trends [3]. Agricultural crops are one of the most crucial sources of food globally. Accordingly, monitoring agricultural crops to predict yield, increase water use efficiency and detect the impact of extreme weather events is vital for ensuring long-term food security. A form of extreme weather events that has adverse effects on crops are severe droughts, which lead to drought stressed crops. Drought stress is an abiotic stress that starts with a meteorological drought, characterized by a lack of precipitation. The lack of precipitation events eventually leads to a precipitation deficit as evaporation processes continue nevertheless. Eventually, a soil moisture deficit occurs that in turn, leads to drought stressed crops. Drought stress poses a major threat to food security, as reduction of yield is to be expected from crops that experience drought stress [4, 5]. This is caused by the shorter lifecycle of the crops, adaptation of the stomatal control and reduction of leaf area, in order to cope with the drought stress [6]. Subsequently, a decrease in crop yield results in an increase in crop price due to reduced supply [7, 8]. Due to climate change, the frequency of severe meteorological droughts [9, 10] and agricultural droughts [4] are expected to increase in the future. Studying temporal patterns on crop parcels assist to find characteristics that indicate drought stress. Food production, amongst other industries, benefits from detection of drought stress as this information allows food producers to anticipate a possible decrease in crop yield and thus are able to take into account the subsequent increase of crop price. Acquiring this information provides the opportunity to import resources from abroad. Also, it provides authorities with additional resources and data that can be used to support decision making regarding water-use and allocation. Furthermore, the temporal data that is acquired can be used to improve crop yield models to give a more accurate and reliable yield estimate which is beneficial for the national economy and food producers. The farmers also benefit from additional resources as it can support decision-making for irrigation in order to increase the water-use efficiency in situations where fresh water is scarce.

Due to the unprecedented amount of freely available satellite images and their global coverage, satellite remote sensing has become a popular tool for agricultural monitoring purposes. Optical imagery is a form of satellite remote sensing that is used for, but not limited to, agricultural purposes. Optical remote sensing operates in the visible, near infrared and thermal infrared spectrum which corresponds to a wavelength range of 0.4-15  $\mu\text{m}$ . The use of optical remote sensing is convenient due to the ease of interpreting the data compared to other forms of remote sensing. Optical remote sensing satellite missions that are currently operative are MODIS, LANDSAT and Sentinel-2 amongst others. While optical imagery provides useful data and indices for crop monitoring purposes such as Normalized Difference Vegetation Index (NDVI), Normalized Difference Water Index (NDWI) and Leaf Area Index (LAI) with very high spatial resolution [11], it is often not temporally reliable due to gaps in data caused by cloud cover. Data acquired by spaceborne optical remote sensing is severely hampered by dense cloud coverage as short wavelengths are unable to penetrate clouds. Throughout the year, two thirds of the Earth's surface is always covered by clouds [12]. In the Netherlands, van der Wal et al. [13] found that the chance to acquire clear satellite images during the growing season in the Netherlands is roughly 20%. Microwave remote sensing has the ability to penetrate clouds and thus is more beneficial to use for this purpose, compared to the aforementioned form of remote sensing. Microwave remote sensing operates in the 1 cm - 1 m spectrum which can be divided in several bands. Active microwave remote sensing has the ability to provide dielectric and geometric properties of target crops [14]. This is ben-

eficial for studying the impact of drought on crops because the dielectric and geometric property of the crops is mostly influenced by water in the crop and in the soil [15]. Examples of active microwave remote sensing satellite missions that are currently operative are RADARSAT-2, TerraSAR-X and Sentinel-1. This research utilizes data acquired from the Sentinel-1 mission which is part of the Copernicus programme from the European Space Agency (ESA). The Sentinel-1 mission consists of two satellites, Sentinel-1A and Sentinel-1B, which were launched in 2014 and 2015 respectively [16]. The main operation imaging mode over the Netherlands is the Interferometric Wide-swath mode (IW) which provides single (VV or HH) and dual polarization (VV+VH and HH+HV) data. This data has a 5 x 20m resolution over a swath of 250 kilometres. The Sentinel-1 satellites are equipped with a C-band Synthetic Aperture radar (SAR) that operates at the centre frequency of 5.405 GHz [16] and is thus not affected by clouds. The main reason for using Sentinel-1 over alternative microwave remote sensing satellite missions is mainly due to the combination of high spatio-temporal resolution, world-wide availability, and open data policy. Both satellites are located in the same orbital plane, making it possible to combine the data resulting in a short revisit time. However, in the growing season of 2015 and 2016, only data from Sentinel-1A was available. Hence, the years 2017, 2018 and 2019 are considered in this research to obtain a dataset with the highest temporal resolution. A maximum temporal resolution of 1-2 days in the Netherlands can be achieved when combining ascending and descending orbits of both satellites [17]. This makes the Sentinel-1 mission very convenient for agricultural monitoring purposes.

This research is focused on key agricultural crop parcels in the Netherlands which includes silage maize, sugar beet, consumption potato, onion and summer barley crop parcels. The Dutch agricultural sector is an important asset of the Dutch economy as the Netherlands is the second largest exporter of agricultural goods in the world, while also being a net-exporter. In 2018, agricultural goods originating from Dutch soil are estimated at 65.4 billion euros, which accounts for 8.4% of GDP [18, 19]. Detection of drought stress experienced by crops and reliable crop phenology data is thus of importance to the Dutch economy as a whole.

Studying drought impact in 2018 and 2019 offers a unique opportunity because of the two consecutive drought summers across central Europe. Hari et al. [20] found that the consecutive droughts of 2018-2019 were the most severe in the last 250 years and that similar events will occur more frequently in the future. The Netherlands was also severely impacted by the 2018 and 2019 droughts, which resulted in a significant drop in yield for most crops. The gross yield per harvested hectares for the key crops in the Netherlands is provided by Centraal Bureau voor de Statistiek (CBS) in Table 1.1. This table shows that the normalized gross yield in 2017 is higher than in the aforementioned years and that 2018 was the most impacted year for all crops except for summer barley.

Table 1.1: Normalized gross yield data for key crops in the Netherlands in 2017, 2018 and 2019, expressed in 1000 kg per harvested hectares [21].

<b>Crop</b>	<b>2017</b>	<b>2018</b>	<b>2019</b>
Silage maize	48.9	39.9	43
Sugar beet	93.3	76.4	83.9
Consumption potato	52.8	41.2	47.9
Onion	55.7	35.5	50.3
Summer barley	6.1	6.7	6.6

## 1.2. Problem statement

As discussed in the previous section, drought has adverse effects on crop growth, yield and thus food security and the economy surrounding food production. Furthermore, a lack of information on the state of the crops can also lead to bad use of available fresh water, which is detrimental in time of droughts. Since severe agricultural droughts are expected to occur more frequently in the future, due to the effects of climate change [4, 9, 10], it will become increasingly important to monitor the growth and the condition of crops.

Studies in the past have used data provided by microwave remote sensing missions for the aforementioned purposes. The issue with these missions is that they generally either have low spatial resolution or low temporal resolution. Studies in the past have used ASCAT, SMOS and SMAP for natural ecosystem monitoring [22–29]. While the temporal resolution of these missions are relatively high, the spatial resolution is generally in the order of kilometres. The data from these missions can thus not be used for studies on parcel level. Missions like RADARSAT-2, ALOS-2 and TERRASAR-X have also been used in the past for crop monitoring purposes [30–33]. The issue with data provided by the aforementioned satellite missions is the relatively low temporal resolution. Since crop phenology changes rapidly during the growing period, it is extremely likely that key phenological stages will not be captured by data retrieved from low temporal resolution satellite missions.

In recent years, studies have also successfully utilized Sentinel-1 data for crop monitoring and phenological stage detection for a diverse set of crops [14, 34–37]. However, despite the extensive literature that can be found on SAR and agriculture, a study investigating the influence of drought on Sentinel-1 data over agricultural crops has yet to be conducted. Hence, a knowledge gap exists regarding the influence of drought stressed crops on dense C-band SAR data. Sentinel-1 offers a unique opportunity to bridge this gap due to the high-spatiotemporal data it provides.

### 1.3. Research objective

The objective of this research is to close the aforementioned knowledge gap by analyzing the influence of drought on the Sentinel-1 SAR data over agricultural crops and the potential of using Sentinel-1 data to monitor drought stress experienced by crops. This leads to the following research question:

#### *Research Question*

**What is the influence of drought on C-band Sentinel-1 SAR data over agricultural parcels of key crops in the Netherlands?**

This research question is divided into 6 sub-questions:

1. How are phenological changes of key crops in the Netherlands reflected in C-band Sentinel-1 SAR data?
2. How is drought reflected in the interannual variability of C-band Sentinel-1 SAR data?
3. What is the influence of viewing geometry and overpass time on C-band Sentinel-1 SAR data?
4. Are the drought observations aggregated across all parcels reflected in individual parcels?
5. What is the drought-induced regional variability of C-band Sentinel-1 SAR data?
6. Is the influence of irrigation during drought reflected in C-band Sentinel-1 SAR data?

This research intends to serve as a foundation for further research into agricultural drought monitoring using microwave remote sensing.

### 1.4. Report outline

This thesis includes a background, methodology, results & discussion and a conclusion. In Chapter 2, the basics of SAR remote sensing are described in order to support interpretation of the results obtained in this research. This includes the interaction between microwaves and vegetation, the different SAR parameters and their influence, and the Sentinel-1 SAR observables and their characteristics. In Chapter 3, background information about the Netherlands is given and the study areas are highlighted in the first section. In the second section, ancillary data that is acquired and used in this research is specified. In the third section, Sentinel-1 data acquisition and data analysis is described. The results of this research are presented in Chapter 4. The results are discussed and interpreted through the knowledge gained from other studies and the background chapter. The conclusion of this research is provided in Chapter 5. At last, since this research intends to serve as for further research into monitoring agricultural droughts using microwave remote sensing, recommendations for further research are also provided in Chapter 5.

# 2

## Background

### 2.1. The basics of spaceborne SAR imaging

SAR is a type of radar in which microwaves are transmitted and received to retrieve information and is thus a form of active remote sensing. Due to the ability of SARs to penetrate clouds, the transmitted microwaves interact with the Earth's surface and part of the signal scatters back in the direction of the radar. A measure of reflective strength of the target is the scattering cross section, denoted by  $\sigma [m^2]$ . However, a more common measure of radar backscatter is the backscatter coefficient which is the normalized cross section defined per unit ground area, denoted by  $\sigma^0 [\frac{m^2}{m^2}]$ .  $\sigma^0$  can be expressed by rewriting the radar range equation and dividing by the ground area:

$$\sigma^0[-] = \frac{P_r (4\pi)^2 R^4}{AP_t G A_e} \quad (2.1)$$

where:

$P_r$  = power received by the radar [W]

$R$  = distance to the radar [m]

$A$  = target area [ $m^2$ ]

$P_t$  = power transmitted by the radar [W]

$G$  = gain of the transmitting antenna [-]

$A_e$  = effective aperture [ $m^2$ ]

While the backscatter coefficient is dimensionless in the linear domain, the backscatter coefficient is commonly converted to the logarithmic domain using

$$\sigma^0 [dB] = 10 * \log_{10}(\sigma^0 [-]). \quad (2.2)$$

The information contained in this backscatter depends mostly on three system parameters: incidence angle, operating frequency (or wavelength) and polarization. The incidence angle is defined as the angle between the incident wave and the normal. The incidence angle range of Sentinel-1 is 29.1° - 46.0°. The operating frequency, which is defined as the frequency of the waves that are transmitted by the SAR, of Sentinel-1 is 5.405 GHz which is within the C-band range. As for polarization, four combinations exist, which can be divided in two types: co-polarized (VV and HH) and cross-polarized (VH and HV). Sentinel-1 provides dual VV + VH or HH + HV polarization. In Europe the main conflict-free mode is IW with VV + VH polarization [38]. This means that waves are transmitted in the vertical (V) plane and received in either the vertical (V) or horizontal (H) plane. Co-polarized and cross-polarized images contain different types of information. Besides the aforementioned system parameters, the backscatter is also influenced by target parameters at the Earth's surface such as surface roughness, dielectric constant, geometrical structure and orientation. The influence of the system parameters and the relevant target parameters are discussed in Section 2.2. Sentinel-1 data is available in several levels. Level-0 contains raw SAR data which is difficult to work with. Level-1 Sentinel-1 data, which are products intended for data users, consists of Ground Range Detection (GRD) and as Single Look Complex (SLC) data. To summarize the difference between the aforementioned images, SLC images are less processed than GRD images. Additionally, phase information in GRD images is lost during processing [39].

Due to the complexity of SAR it is desirable to simplify by defining several scattering mechanisms. Three basic scattering mechanisms from incoherent targets are: scattering from a rough surface, double-bounce scattering from a pair of orthogonal surfaces and volume scattering of randomly oriented dipoles [40]. These mechanisms are depicted in Figure 2.1. The total backscatter from a target consists of a summation of surface scattering, double-bounce scattering and volume scattering:

$$\sigma_{\text{tot}}^0 = \sigma_{\text{surface}}^0 + \sigma_{\text{double bounce}}^0 + \sigma_{\text{volume}}^0 \quad (2.3)$$

where  $\sigma^0$  is the backscatter coefficient. The relation between the simplified scattering mechanisms and Sentinel-1 C-band SAR data is explained in Section 2.2. The results discussion chapter will also be referring to the scattering mechanisms in order to interpret the data.

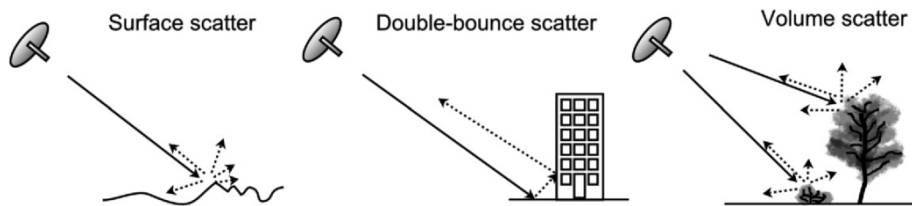


Figure 2.1: Basic SAR scattering mechanisms from incoherent targets [41].

## 2.2. Interaction between SAR and crops

Targeting crop parcels will lead to backscatter from the crop canopy and from the soil underneath. With regards to the simplified scattering mechanisms, surface scatter is caused by the direct backscatter from the top layer of the canopy and direct soil backscatter that is often attenuated by the canopy layer. Double-bounce scattering takes place in the form of soil-canopy interaction where the wave bounces off the soil and subsequently bounces off the canopy back to the SAR sensor. Volume scattering occurs within the crop canopy layer itself in the form of multiple bounces. Generally, total backscatter consists mostly of ground backscatter in the early and late growth stages, while backscatter from the canopy is dominant in-between.

### Target Parameters

The response of the canopy layer is influenced by target parameters like the dielectric constant, size, stem density and orientation of the crops. The aforementioned target properties all depend on the phenological stage and condition of the crop that change throughout the growing period [14]. Hence, the measured response has a direct correlation with biophysical parameters like Leaf Area Index (LAI), above ground biomass and canopy height.

The dielectric constant is the dominant factor that determines the behaviour of SAR backscatter response. The microwave transmitted by the Sentinel-1 radar is scattered by crops due to a change in the dielectric constant when the wave collides with the crop. This dielectric discontinuity is mostly caused by the presence of water in the crops [15]. The dielectric constant of water and air is approximately 80 and 1, respectively [42]. Water has a high dielectric constant, because water molecules are dipoles and will thus rotate when being exposed to an electromagnetic field. The dielectric constant has a positive correlation with the measured SAR backscatter, which means that scattering by a target with high dielectric constant results in high backscatter values. While this correlation has been observed when measuring backscatter from soil, this correlation is however not so straightforward when measuring backscatter from crops. Backscatter from crops is more complex due to the geometrical structure of the crop canopy, which is more sophisticated and changes throughout the growing season [15].

The size of the crop and the density of its stems and leaves also influence the backscatter. A larger and denser crop leads to more attenuation and thus less backscatter from the soil which might eventually lead to saturation. Saturation of SAR response occurs when the target crops keeps accumulating biomass while the SAR backscatter is no longer responsive or sensitive to the increasing biomass. Furthermore, a denser crop provides more surfaces, which enables multiple bounces and therefore increases volume scattering. The effects of the aforementioned on polarized backscatter is explained in the system parameter paragraph.

The intensity of the measured backscatter is also influenced by the orientation of the crops and the rows in which the crops are planted, relative to the transmitted wave propagation. The measured intensity is generally higher when the crop rows are situated perpendicular to the transmitted wave, compared to parallel [43, 44].

### System parameters

Besides the aforementioned target parameters, operating frequency (or wavelength), incidence angle and polarization are important system parameters that influence the information that is captured within the backscatter. Increasing the wavelength (i.e. decreasing the operating frequency) results in an increase of the penetration depth [45]. Microwave remote sensing has 7 frequency bands ranked from high to low wavelength: P-band, L-band, S-band, C-band, X-band, Ku-band and Ka-band. Hence, L-band (15-30 cm wavelength) microwaves penetrate deeper into the crop canopy than C-band (7.5–3.75 cm wavelength) microwaves. This results in better crop interaction with L-band for tall crops like maize. However, for shorter canopies, L-band soil backscatter can interfere with soil backscatter, which results the possibility of canopy backscatter being overshadowed by soil backscatter during the growing season. C-band microwaves are more suitable when measuring shorter crop canopies. C-band microwaves do not fully penetrate tall canopies, hence it is possible that saturation of the radar signal will occur [45, 46]. The point of saturation depends on the crop type and the operating frequency [47].

The penetration depth is also affected by the incidence angle. Larger incidence angles result in smaller penetration depths. This is because the path length through the canopy is longer with a large incidence angle and results in a higher canopy backscatter contribution and a lower ground backscatter contribution to the total backscatter due to canopy attenuation. Smaller incidence angles reduce the path length through the canopy and thus increase the penetration depth. The attenuation of the canopy backscatter is then reduced, leading to a higher ground backscatter contribution and lower canopy backscatter contribution to the total backscatter [34, 48]. Furthermore, the incidence angle also influences the backscatter intensity. Incidence angle has a negative correlation with backscatter intensity. Hence, data derived with a low incidence angle relatively contain higher backscatter intensities. This correlation is influenced by the surface roughness. The influence of the incidence angle on the radar backscatter coefficient can be seen in Figure 2.2.

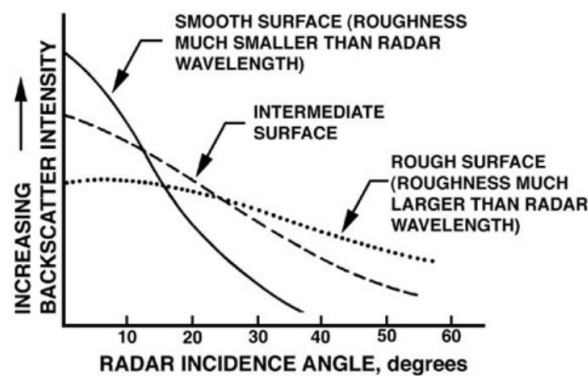


Figure 2.2: The influence of incidence angle on the backscatter coefficient, adapted from [49].

Polarized backscatter yields specific information, which can be used to distinguish and dissect the different type of backscatter from the total backscatter. Sentinel-1 provides co-polarized (VV) and cross-polarized (VH) backscatter. The degree of polarization depends on crop type, growth stage and polarization. VV backscatter mainly contains soil information as surface scattering is the main contributor to VV backscatter. On the other hand, VH backscatter depends on scattering within the crop canopy as it is mainly a function of volume scattering. Multiple scattering results in depolarization of waves, which increases the cross-polarized backscatter intensity. Hence, VH generally increases throughout the vegetative growth stages due to the increasing ability to accommodate multiple scattering within the crop canopy. Therefore, cross-polarized backscatter should in theory be well correlated with biophysical parameters. Jiao et al. [50] found that cross-polarized backscatter was well correlated with LAI for maize and soy bean crops with a correlation coefficient of  $r = 0.95$  and  $r = 0.73$  respectively. According to Wiseman et al. [30], cross-polarized backscatter is highly sensitive to biomass for soy bean crops ( $r = 0.81$ ). Cross-polarized backscatter tends to decrease when the crop matures due to a reduction of vegetation water content [34]. Furthermore, cross-polarized data is not affected by the row angle [51]. VV backscatter can also increase during the vegetative growth stages of the crops because of the soil-canopy interaction. This interaction cannot be distinguished from regular soil backscatter in the VV polarization. Likewise, VH backscatter may also contain soil returns due to the soil-canopy interaction [52].

An index that correlates well with crop phenology other than the VH backscatter is the cross-pol (VH/VV) ratio. The cross-pol ratio is an index that is frequently used for crop monitoring purposes in recent years. It is calculated using

$$\sigma_{VH/VV}^0 = \frac{\sigma_{VH}^0[-]}{\sigma_{VV}^0[-]} \quad (2.4)$$

where  $\sigma_{VH}^0$  and  $\sigma_{VV}^0$  are divided in the linear domain. Since VH backscatter increases more relative to VV backscatter during crop growth, the cross-pol ratio will also increase during the vegetative stages of the crop. The cross-pol ratio also reduces the influence of soil moisture and soil-canopy interaction, which makes it very suitable index for crop monitoring purposes. Furthermore, the cross-pol ratio is relatively stable compared to VH and VV polarization backscatter [36]. Veloso et al. [34] observed that the VH/VV ratio is in agreement with the on-site (Green Area Index) GAI and fresh biomass measurements for barley and maize. The VH/VV ratio can thus be used for biophysical parameter retrieval. The study also mentions that the VH/VV ratio reduces errors caused by acquisition systems and environmental factors. Vreugdenhil et al. [14] found from Random Forest analysis that the VH/VV ratio is the most important variable to estimate Vegetation Water Content (VWC). More recently, Khabbazan et al. [35] states that the VH/VV ratio is especially sensitive to fresh biomass formation during the vegetative stages of the crop. The VH/VV ratio decreases during the senescence stages of the crop as VWC reduces.

### 2.3. Crop response to drought stress

As discussed in the introduction chapter, droughts have an adverse effect on yield which is caused by the shorter lifecycle of the crops, adaptation of the stomatal control and reduction of leaf area, in order to cope with the water deficit [6]. Hence, crops change their structure and characteristics in order to adapt to the water deficit. Since the SAR response depends on the geometrical structure of the object and its features, it is expected that the water deficit caused by the drought will be observable in the SAR response. Only drought impact on the above ground biomass will be sensed with radar. The drought response is crop-specific and depends on the length and the timing of the drought as well as the hydrometeorological parameters such as temperature.

#### Maize

Severe drought stress of maize crops is characterized by rolling leaves. This is only alleviated when the crops receive water. According to Kurt Thelen [53], crops that experience drought stress before the tassel and silk emergence can result in small ear size. The potential kernel row number, which is the number of kernels in a cross-section, is determined by the state of the crop from approximately the 8-leaf to the 12-leaf stage. The potential kernel number per row is determined from approximately the 12-leaf until the 17-leaf stage. Drought stress during the vegetative phase thus could reduce both ear length and number of kernels on the ears. The reduction of the ear size cannot be undone by providing water on a later stage. Furthermore, drought stress during silking and pollination results in the largest decrease in yield. This is caused by a lack of synchronization between silking and shedding of the pollen during pollination. The pollen grains may not remain viable and silking might be delayed. If maize crops have tasseled and shed their pollen while blisters have not appeared yet, the crop will barren [53].

Anami et al. [54] mentions that drought stress during the vegetative phase typically reduces plant and leaf sizes. Drought stress during the tasseling and silking stages decreases ear size and potential yield. Crop drought stress during flowering and pollination results in a delay of the silking, reduction of silk length and inhibits embryo development after pollination. At last, drought stress during the grain filling stage typically results in lower yield as kernel size is reduced. Furthermore, it may also result in dying of leaves, shorter grain filling stage and increased lodging.

Schmidhalter et al. [55] found that the earliest observation of drought stressed maize are a decrease in leaf elongation and an increase in largest root diameter. This was followed by an increase in root length and number of fine roots.

#### Sugar beet

According to Abdollahian-Noghabi and Froud-Williams [56] (as cited in Shaw et al. [57]), root growth is less impacted than shoot growth in dry soil. Hence, the shoot to root ratio decreases during drought stress. Sugar beet typically has the ability to recover leaf area relatively well when receiving water after experiencing drought stress. The sugar beet root storage experiences the greatest reduction of dry matter accumulation during a drought.

To analyze the response of sugar beets to droughts and drought timings, Brown et al. [58] set up a study where a set of sugar beets were exposed to an 8-week early drought (directly after planting) and another set of

sugar beets that were exposed to an 8-week late drought which takes place after 8 weeks. The study concluded that the early drought had severe adverse effects on the fibrous roots. Also, the leaf canopy expansion slowed down which resulted in a decrease of radiation interception and water use. The late drought experiment took place after an extensive fibrous root system was established. When this drought took place, the available water was quickly depleted causing an early senescence. The yield of the sugar beets that experienced the early drought was lower compared to the late drought.

### Potato

Timing is an important factor that influences phenological responses to drought stress. Figure 2.3 summarizes the phenological responses of potato crops that experience drought stress at different stages. Albiski et al. [59] observed that drought stress decreased the length, stem thickness, leaf area, root number length and thickness, and water content of potato crops. Dalla Costa et al. [60] performed a study where they exposed potatoes to three irrigation regimes, 40%, 60% and 80% of maximum evapotranspiration, evenly over the crop cycle. The study concluded that biomass and yield decreased almost proportionally to water consumption. Another experiment that was performed withheld 80 mm irrigation in three stages: tuber initiation, early tuber growth and late tuber growth. They found that drought stress during tuber initiation had the highest impact on yield and biomass.

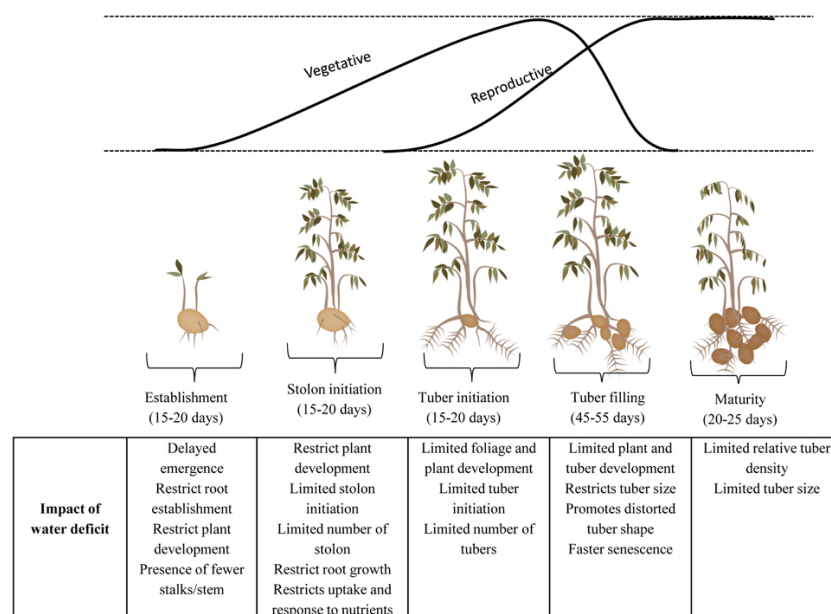


Figure 2.3: Phenological responses of drought stressed potato crops in different stages [61].

### Onion

Lis et al. [62] found that drought stress during the seedling stage speeds up foliar emergence, increases the number of leaves, accelerates bulb formation by 15 days and increases the final weight of the bulb. Drought stress occurring at the start of bulb formation, delays foliar emergence, decreases the number of leaves and final bulb weight. Bhatt et al. [63] also analyzed the drought stress impact by imposing a drought of 15 days, 30 days after transplanting. They found that the leaf area and the bulb growth significantly decreased during the 15 days of drought.

### Barley

H. Samarah [64] studied the effect on drought stress on barley. They imposed three drought treatments on the crops, 100%, 60% and 20% of field capacity from grain filling till grain maturity. He found that the dry weight of the drought stressed crops reached their individual maximum faster than the well-watered crops. This indicates that drought stressed barley crops have a higher growth rate than mildly stressed and well-watered plants. This agrees with the findings of Harfenmeister et al. [65] which concluded that high temperatures, solar radiation and little precipitation leads to a higher growth rate of barley crops.

# 3

## Study Area, Data and Methodology

The effect of drought on crops mainly depend on the following factors:

- frequency and timing of the drought;
- area and its soil type;
- type of crop;
- availability of (stored) water in the system;
- possibility to irrigate.

Hence, acquiring data about the aforementioned factors assists to analyze the influence of drought on the C-band SAR data over crop parcels. Firstly, this chapter introduces the study areas within the Netherlands and their characteristics. Then, the acquisition of ancillary data used in this research is described. Furthermore, a methodology is presented that defines how the Sentinel-1 data is acquired and how this data is used in order to answer the research questions.

### 3.1. The Netherlands

As stated in the introduction, this research focuses on parcels of key crops in the Netherlands. The Netherlands has a temperate maritime climate, which is characterized by its relatively cool summers and moderate winters. The average annual rainfall measured in the Bilt, which is located in the centre of the Netherlands, over the last 30 years equals 840.9 mm [66]. The monthly variation of precipitation and temperature in the Netherlands is presented in Figure 3.1 and 3.2, respectively. It can be noted that the rainfall is distributed relatively uniformly over the months and no clear rain season is observed. The western part of the Netherlands also deals with salt water intrusion, because it is situated beneath sea level. The salt water intrusion increases during periods of drought, which could lead to complications for agriculture amongst other sectors. In terms of soil type, the dutch soil mostly consists of sand, clay and peat [67]. The Netherlands experienced severe droughts during summer crop seasons of 2018 and 2019 that significantly impacted the agricultural sector.

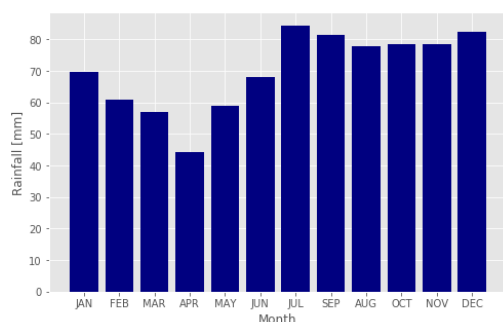


Figure 3.1: 30-year average monthly rainfall measured at the Bilt [66].

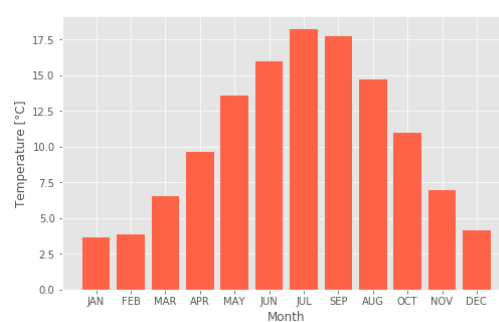


Figure 3.2: 30-year average monthly temperature measured at the Bilt [66].

### 3.1.1. General study areas

This research is mainly focused on three areas which include the Northern part of the Vechtstromen water board area (Vechtstromen-Noord), the Scheldestromen water board area and the Flevopolder. The study areas are indicated in Figure 3.3.

Vechtstromen-Noord is located in the eastern part of the Netherlands. Only the northern part of the Vechtstromen waterboard is considered to reduce the difference in the number of parcels for the studied crops. The northern part of the study area is located in the Drenthe province and the lower part in the Overijssel province. The soil of Vechtstromen-Noord consists mostly of sand and to a lesser extent of peat (moor). Soil characteristics affect soil water retention and thus the drought stress experienced by crops. Generally, sand retains water relatively poorly compared to clay. According to van Hussen et al. [68], which is a report regarding the economical damage caused by the 2018 drought, parcels located in the high sandy soils in the eastern part of the Netherlands experienced more intense drought stress and thus a large decrease in yield. Furthermore, VanderSat [69] used satellite data to find that the municipality of Emmen - which is located within Vechtstromen-Noord - showed the highest drought vulnerability in 2018.

Scheldestromen is located in the province of Zeeland, in the south-west corner of the Netherlands. The dominant soil type in the Scheldestromen is clay. During droughts, salt intrusion can become an issue in Scheldestromen which may lead to an early ban on open water irrigation. According to van Hussen et al. [68], Zeeland experienced a large yield loss during the drought of 2018 as well. This yield loss was partly caused by the ban on open water irrigation and the salinization of the soil and the groundwater. With a decrease in yield of approximately 70%, especially onions parcels were impacted by the drought in this region.

The Flevopolder is a reclaimed island in the Flevoland province located in the centre of the Netherlands. Increasing areas for agricultural activities was one of the main purposes of land reclamation for the Flevopolder. With clay as its soil type, the Flevopolder is known to be relatively drought resistant. The crops were thus not impacted as heavily by the droughts as the other study areas. The motivation to choose the Flevopolder as a study area is to analyze if the degree of drought stress is also observable.

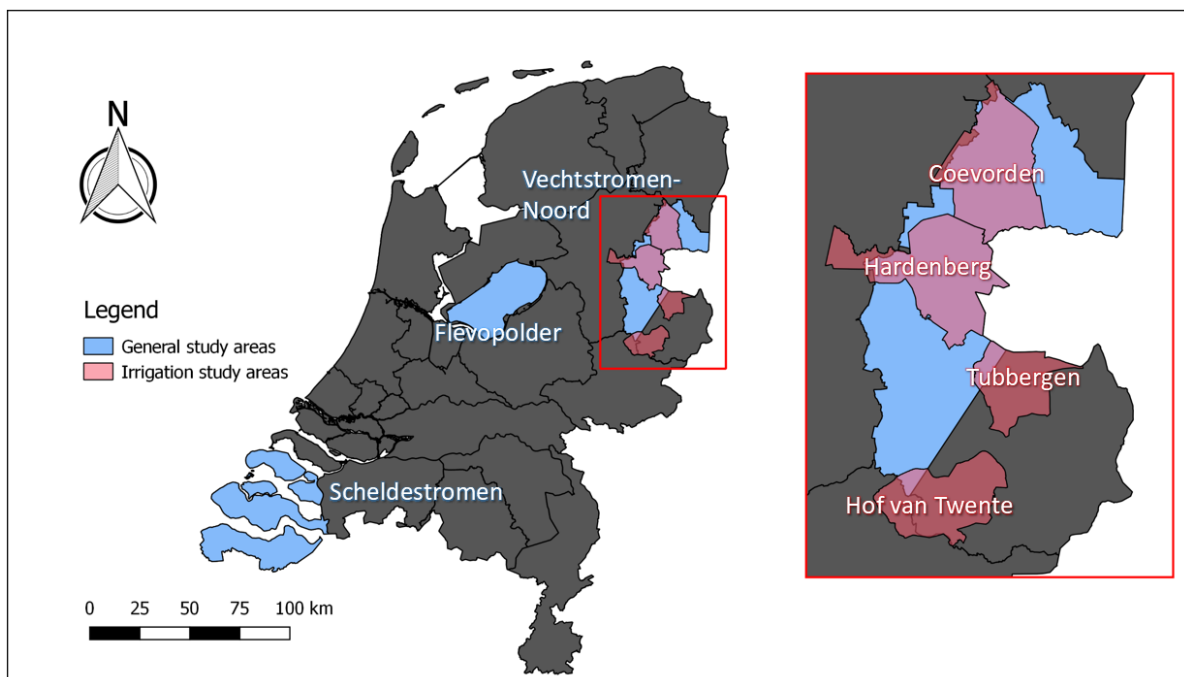


Figure 3.3: Map of the Netherlands including highlighted general study areas and the irrigation study areas.

### 3.1.2. Irrigation study areas

In order to study the influence of irrigation policies, it is of importance to isolate the effects of irrigation on the SAR backscatter as much as possible. Therefore, an analysis in a more detailed level of the Vechtstromen waterboard is required. Comparing areas in close vicinity minimizes the soil and hydrometeorological differences. Hence, a larger share of the observable differences can be appointed to irrigation. The general irrigation policy of Vechtstromen is that open water irrigation is allowed as long as there is sufficient surface water available. Hence, as long as there is still water flowing over the next weir, irrigation is allowed. The Vechtstromen waterboard can be divided into 'high-Vechtstromen' and 'low-Vechtstromen'. This division is depicted in Figure 3.4 in which the blue area represents low-Vechtstromen and the red area represents high-Vechtstromen. The water level in low-Vechtstromen is maintained through water supplied by the Rhine system, while surface water supply cannot be used to maintain the water level in high-Vechtstromen. This means that farmers in high-Vechtstromen are less likely to use open water for irrigation, because there is no water source available to refill the open waters once the open water resources are used up. Hence, mostly groundwater is used for irrigation during droughts in high-Vechtstromen. Farmers situated in low-Vechtstromen can use both open water and groundwater for irrigation during a drought. In addition to the general irrigation policy, open water irrigation was used during the drought periods in 2018 and 2019 in high-Vechtstromen. Overall, if available, irrigation with open water is preferred as high cost efficiencies are achieved due to lower energy use. Furthermore, the temperature of groundwater is generally low and contains more iron and chloride which is not beneficial for crop growth. It is expected that comparing parcels with a low economic value crop in high-Vechtstromen and low-Vechtstromen will show apparent differences. For example, silage maize parcels are mainly irrigated with open water due to its low economic value and will thus likely show drought-induced changes in backscatter in areas where farmers are not allowed to irrigate with open water.

To assess the influence of irrigation on the regional variability, the following municipality areas are studied: Coevorden, Hardenberg, Tubbergen and Hof van Twente. The municipalities are indicated in Figure 3.3. Coevorden and Hardenberg are located in low-Vechtstromen while Tubbergen and Hof van Twente are located in high-Vechtstromen.

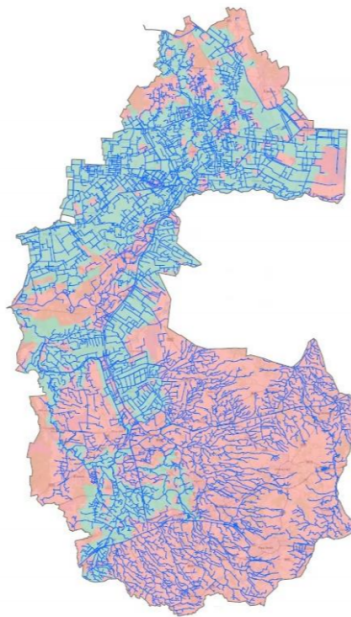


Figure 3.4: Water system division in the Vechtstromen waterboard area. The red area represents High-Vechtstromen and blue represents Low-Vechtstromen [70].

## 3.2. Data

To create a better understanding of drought influence on Sentinel-1 SAR data over agricultural crops, data is required. This includes Sentinel-1 SAR, crop parcel, yield, precipitation and surface soil moisture data. This section specifies how this data is acquired and utilized.

### 3.2.1. Sentinel-1 SAR data

The Sentinel-1 orbits that cover a significant part of the Netherlands are relative orbits 37, 110, 139, 15, 88 and 161. The pass type and local time of passage of these orbits is presented in Table 3.1. The swaths of the descending and ascending orbits are shown in Figure 3.5 and 3.6, respectively. It is observed that Vechtstromen-Noord is covered by orbits 37, 88, 139 and 161. Scheldestromen is covered by orbits 15, 110 and parts of 37 and 88. Data acquired from orbit 37 and 88 are still used for the analysis of parcels in Scheldestromen, since both orbits cover most of the parcels in that area. At last, Flevopolder is covered by orbits 37, 88, 110 and partly 15 and 161. Data from orbits 15 and 161 are not used in the analysis of the parcels in Flevopolder as the majority of the parcels are not within the swaths of the orbits and hence should not be included.

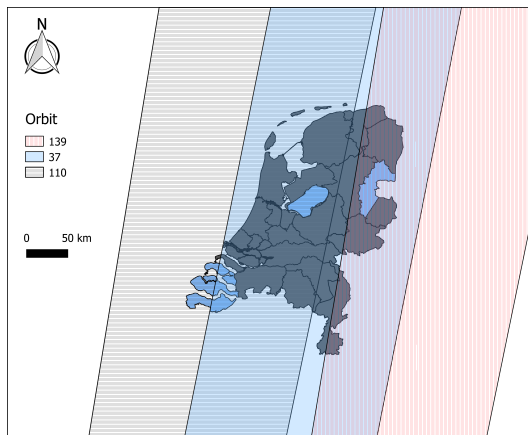


Figure 3.5: Swaths of the descending Sentinel-1 orbits covering the Netherlands.

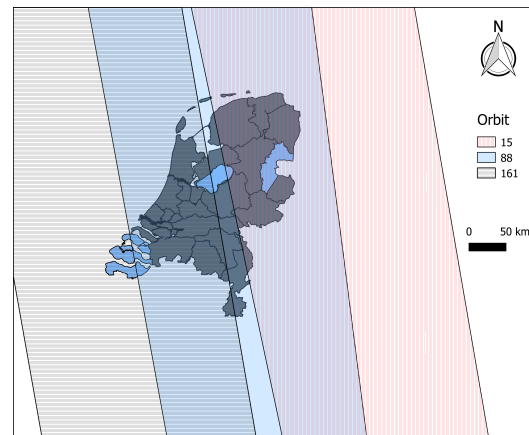


Figure 3.6: Swaths of the ascending Sentinel-1 orbits covering the Netherlands.

The acquisition dates of the orbits, surface soil moisture and precipitation Sentinel-1 data is shown in Figure 3.7. Only data during the agricultural summer season of 2017, 2018 and 2019 is included. The chosen period extends from the 1st of March until the 30th of October in all years. In total, 116, 118, 119, 119, 121 and 121 images are acquired for orbit 15, 88, 161, 139, 37 and 110 respectively. This data is acquired through the Google Earth Engine (GEE) platform. The GEE platform provides satellite imagery which is stored in their public data archives. The method used to acquire specific Sentinel-1 SAR data for this research is further described in Section 3.3.

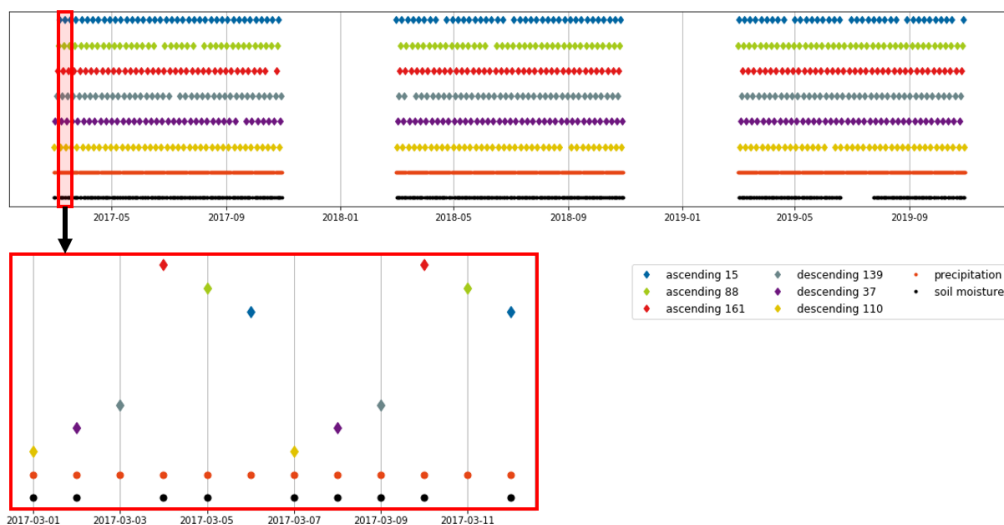


Figure 3.7: Sentinel-1 SAR, soil moisture and precipitation data acquisition dates in 2017, 2018 and 2019.

Table 3.1: General information of Sentinel-1 orbits covering the Netherlands.

Relative orbit	Pass type	Local time	$\theta_{\text{Vechtstromen-Noord}}$	$\theta_{\text{Scheldestromen}}$	$\theta_{\text{Flevopolder}}$
15	asc	17:16	33.8° - 36.3°	-	-
37	des	05:49	36.1° - 34.7°	45.1° - 44.4°	41.6° - 39.5°
88	asc	17:25	42.4° - 44.0°	30.1° - 31.1°	36.3° - 39.5°
110	des	05:58	-	41.0° 35.7°	33.7° - 30.4°
139	des	05:41	44.4° - 42.5°	-	-
161	asc	17:33	-	36.4° - 40.2°	44.5° - 45.9°

### 3.2.2. Vector, parcel and crop data

Since only crop parcels within the study areas are of interest, vector files containing the study area are required. Water board and municipality boundary vector files acquired through the ArcGIS Hub [71] are used and edited to include the study areas. Scheldestromen is already available as an attribute in the water board boundary vector file. The Vechtstromen-Noord attribute is created by manually dividing the Vechtstromen water board into two parts. The Flevopolder attribute is created by merging the municipality areas of Lelystad, Almere, Dronten and Zeewolde.

The impact of drought on crop growth is different for each crop. It is not necessary to classify the crop parcels, as the Ministry of Economic Affairs and Climate in the Netherlands provides the Basisregistratie Gewaspercelen (BRP) datasets that contains registered parcel boundaries and its crop type through the PDOK platform [72]. As mentioned before, the years 2017, 2018 and 2019 are analyzed in this research, thus the BRP of these year are used. For additional information on using SAR for crop classification purposes, you may refer to the following studies [73–76]. The most prevalent crop parcels in the Netherlands according to the 2019 BRP dataset are presented in Table 3.2.

Table 3.2: List of most popular arable crops in the Netherlands (2019) [21, 72].

Crop	No. of parcels	Cultivated area [ha]
Silage maize	71758	187 400
Winter wheat	21435	112 203
Consumption potatoes	17300	78 887
Sugar beet	15793	79 176
Seed potatoes	8764	43 688
Starch potatoes	7830	44 949
Summer barley	6621	22 570
Grain maize	5399	12 668
Onions	4986	27 583

It is of importance that a diverse collection of crops is chosen to ensure the robustness of the methodology and the reliability of the results. Since droughts in the Netherlands mostly occur during the summer period, only summer crops are considered. In this research, the following crops are studied: silage maize, consumption potatoes, sugar beets, summer barley and onions. The number of crop parcels in the study areas is presented in Table 3.3.

Table 3.3: Number of studied crop parcels in the general study areas (2019) [72].

Crop	Vechtstromen-Noord	Scheldestromen	Flevopolder
Silage Maize	4084	1394	300
Sugar Beets	817	2413	660
Consumption Potatoes	541	2722	882
Onions	71	879	767
Summer Barley	773	312	75

To identify and compare the phenological stages of different crops based on pictures or literature, the BBCH-scale system [77] is used. The BBCH-scale system provides a framework that defines a code for each growth stages of different crop species. The code consists of two digits (1-9) where the first digit of the code refers to the principal growth stage and the second digit refers to the secondary growth stage. Due to the lack of appropriate field data, findings from literature are used in order to connect Sentinel-1 time series to BBCH stages for all studied crops. Many of these studies performed case studies in which they use SAR data to monitor several crops and visited the crop parcels at different times in the cropping season to gather field

data and determine the phenological stage of the crop. Findings from Khabbazan et al. [35] are mainly used as they performed their study in the Flevopolder and also used the BBCH framework. Furthermore, they also analyzed maize, sugar beet, potato and wheat (which is similar to barley). The result of this analysis is presented as BBCH stage tables which can be found in Appendix A. Also, ancillary ground information in the form of a digital photo archive of maize, sugar beet and potato parcels used in the study by Khabbazan et al. [35] is utilized. These photos can be found in Appendix B. In addition, field photos from online sources are also used.

### 3.2.3. Crop yield data

The crop yield is acquired through the agricultural crop yield dataset from the StatLine database provided by the CBS [21]. CBS provides the total gross yield and the normalized gross yield for all key crops in the

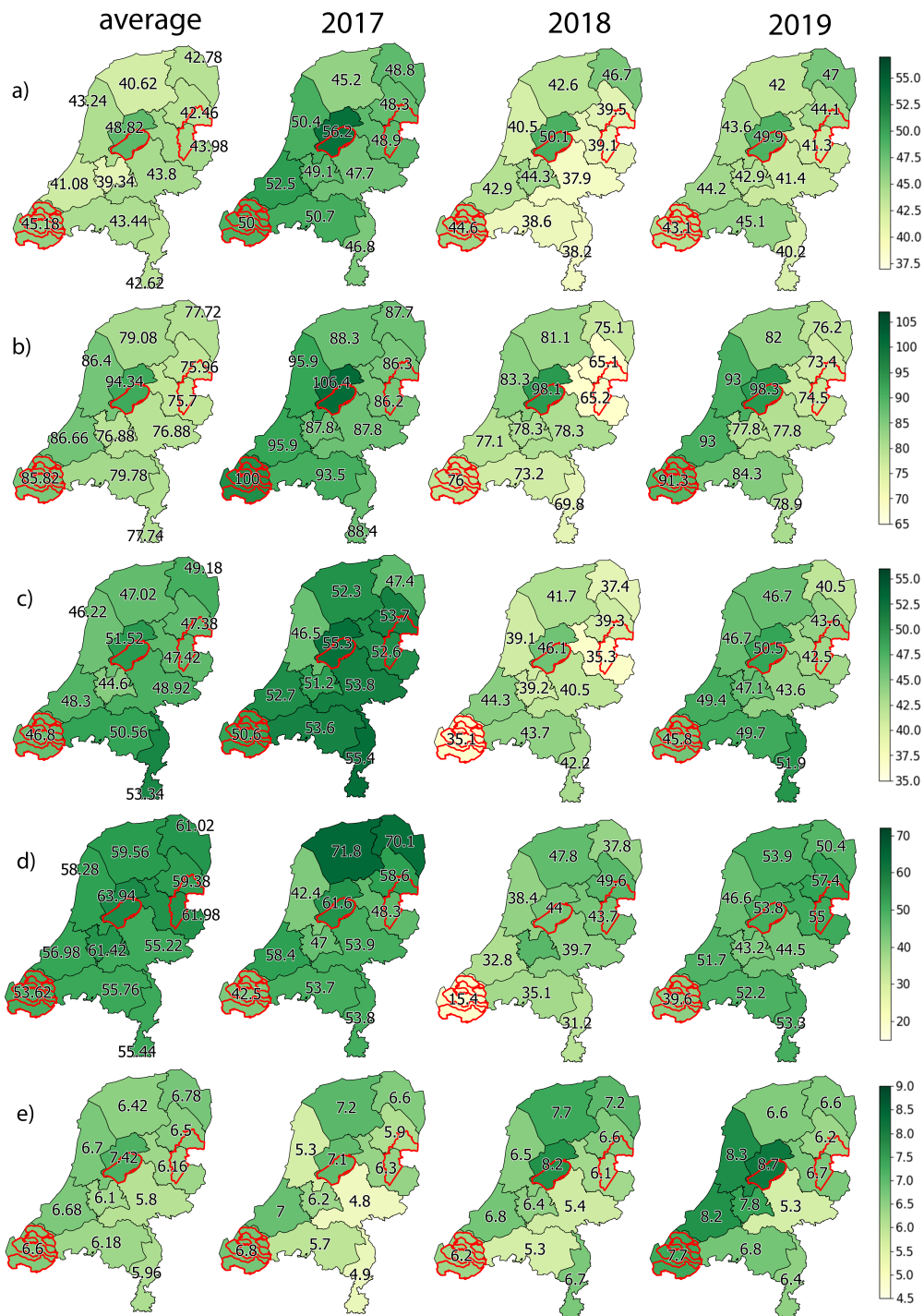


Figure 3.8: Gross normalized yield per province expressed in 1000 kg/ha for a) maize, b) sugar beet, c) potato, d) onion and e) barley crops [21].

Netherlands. Normalized yield is the total gross yield per harvested hectare and is available on national level and province level. Normalized gross yield data is utilized to assist validation of the results and conclusions. Gross yield data is not directly dependent on drought intensity due to the farmers' ability to irrigate. Furthermore, the impact of drought stress on yield depends on crop type and timing of the drought. Despite the fact that yield data is not a direct function of drought, it still can be of use when evaluating the impact of drought on crops in 2018 and 2019. In Figure 3.8, the normalized gross yield of each crop aggregated over province areas for the study period are presented. The average normalized gross yield is calculated by averaging the reference years 2016, 2015, 2014, 2012 and 2011. The year 2013 is excluded because of large negative precipitation anomalies in July [78]. Since the Vechtstromen-Noord study area is located in two provinces, the yield is calculated by taking the average of the Overijssel and Drenthe crop yield values.

### 3.2.4. Surface soil moisture data

Daily surface soil moisture data aggregated over municipality areas is provided by VanderSat [79]. The L-band volumetric soil moisture product provides satellite observed soil moisture at 5 cm depth [80]. The soil moisture data is generated by a retrieval algorithm, the Land Parameter Retrieval Model, combining data retrieved from the SMAP and AMSR-E satellites, achieving a 100x100m resolution [81, 82]. As can be seen in Figure 3.7, a data gap can be observed in the soil moisture data around mid 2019. This data gap is caused by the SMAP satellite not being functional at that time.

The surface soil moisture data is used to 1) identify areas that are heavily impacted by the drought, 2) determine the period of drought and 3) distinguish the causes for temporal changes in backscatter. To distinguish the causes for temporal changes in backscatter, the surface soil moisture data should be independent of the Sentinel-1 SAR data. Since the retrieval algorithm utilizes passive microwave sensing data, and thus not data acquired from the Sentinel-1 satellites, the surface soil moisture data is independent. Increasing measured backscatter does not necessarily translate to crop growth as precipitation may also cause increasing measured backscatter due to the high dielectric constant of water. By using surface soil moisture, crop growth can be distinguished from precipitation when increasing measured backscatter is observed. The surface soil moisture of the Coevorden, Goes and Zeewolde municipality areas are used for the Vechtstromen-Noord, Scheldestromen and Flevopolder study areas, respectively. The municipalities are highlighted in Figure 3.9.

### 3.2.5. Precipitation data

Precipitation data is acquired from local weather stations of the Royal Netherlands Meteorological Institute (KNMI) [66]. Similar to surface soil moisture data, precipitation data is mainly used to determine the period of the drought and to help distinguish the causes for temporal changes in backscatter. The KNMI provides accurate daily precipitation data, measured at 48 weather station scattered throughout the Netherlands. The precipitation data acquired by the weather stations in Hoogeveen, Vlissingen and Lelystad are used for the for the Vechtstromen-Noord, Scheldestromen and Flevopolder study areas, respectively. The location of the weather stations are highlighted in Figure 3.9.

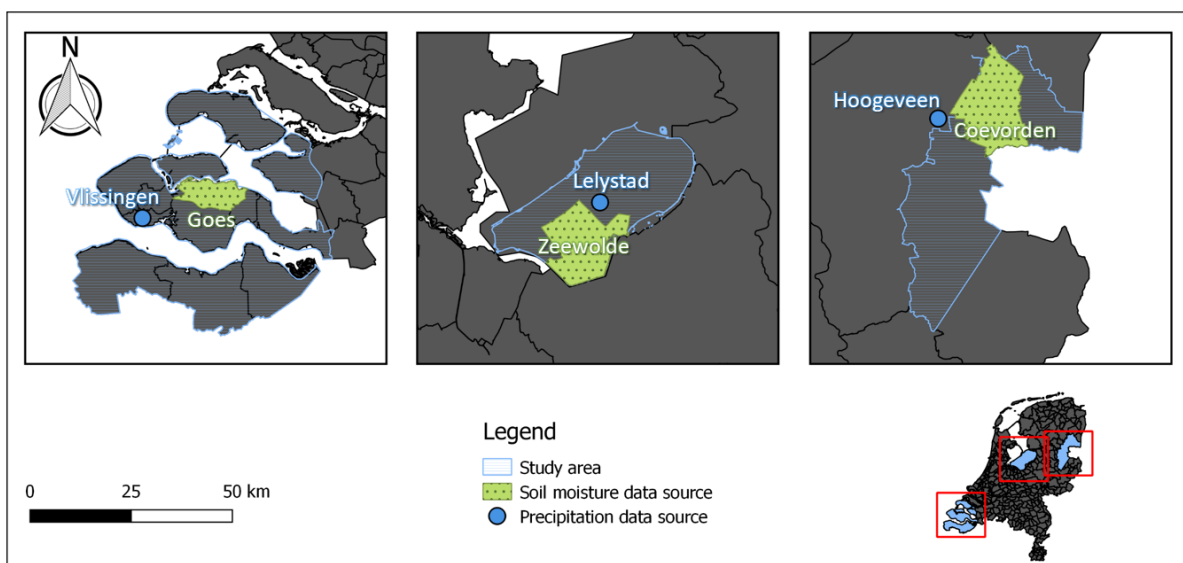


Figure 3.9: Locations of the soil moisture and precipitation data sources in the general study areas.

### 3.3. Methodology

#### 3.3.1. Extraction of Sentinel-1 data using SandboxNL

Sentinel-1 data can be acquired through the Sentinel data hub [83] and processed in Sentinel Application Platform (SNAP). However, this requires a lot of disk space since the Sentinel-1 SAR images are relatively large in size. Furthermore, only data originating from specific crop parcels in specific regions is of interest in this study. Also, three cropping seasons are analyzed meaning that lots of SAR images are needed to perform the temporal analysis. Hence, this acquisition method is not desirable since lots of computer storage is required.

Sentinel-1 data can also be extracted through the GEE platform. As such, it is not required to save the Sentinel-1 SAR images locally as Sentinel-1 SAR GRD images are already available in the GEE image collection. Figure 3.10 presents the flow diagram that is used to acquire and process data to enable analysis for this research. The GRD images in the image collection underwent several preprocessing steps [84]. First, the orbit file is applied by updating the orbit metadata with a restituted orbit file. Then, the invalid data and low intensity noise on the edges of the scene are removed. Subsequently, additive noise in the sub-swaths is removed (thermal noise removal). Afterwards, radiometric calibration takes place in which sensor calibration parameters are used to compute the intensity of the backscatter. At last, terrain correction is applied by converting the data from ground range geometry to  $\sigma^0$ . This results in a Sentinel-1 SAR GRD image [84].

The Sentinel-1 SAR data is then directly fetched from the GEE image collection using the SandboxNL toolbox described in Kumar et al. [85]. SandboxNL performs cloud filtering using metadata combined with user-defined administrative vector data such as the waterboard boundaries, municipality boundaries and the BRP. The input of SandboxNL defines the needs of the user and which data is exported from the GEE based platform. The SandboxNL toolbox takes the following input:

- crop name;
- name of region of interest;
- start date;
- end date;
- pass type (Ascending or Descending);
- relative orbit number.

After defining the input and metadata, a spatial filter is applied to join the selected region of interest and the parcel coordinates of the selected crops. A buffer is applied to remove the outer 10 meters crop parcels, to prevent backscatter from targets other than the selected crops. Afterward, a mask is applied to remove unreliable values at the Sentinel-1 image borders by using a threshold of -35 dB. The Sentinel-1 images are then temporally stacked within the selected period and the pixels (VV, VH and VH/VV) within the selected crop parcels are averaged. The result is a table containing the mean and standard deviation of Sentinel-1 backscatter data (VV, VH and VH/VV) per parcel in a linear scale. The table is exported as a Comma Separated Values (CSV) file from SandboxNL to the google drive output folder. The temporal resolution of the output is

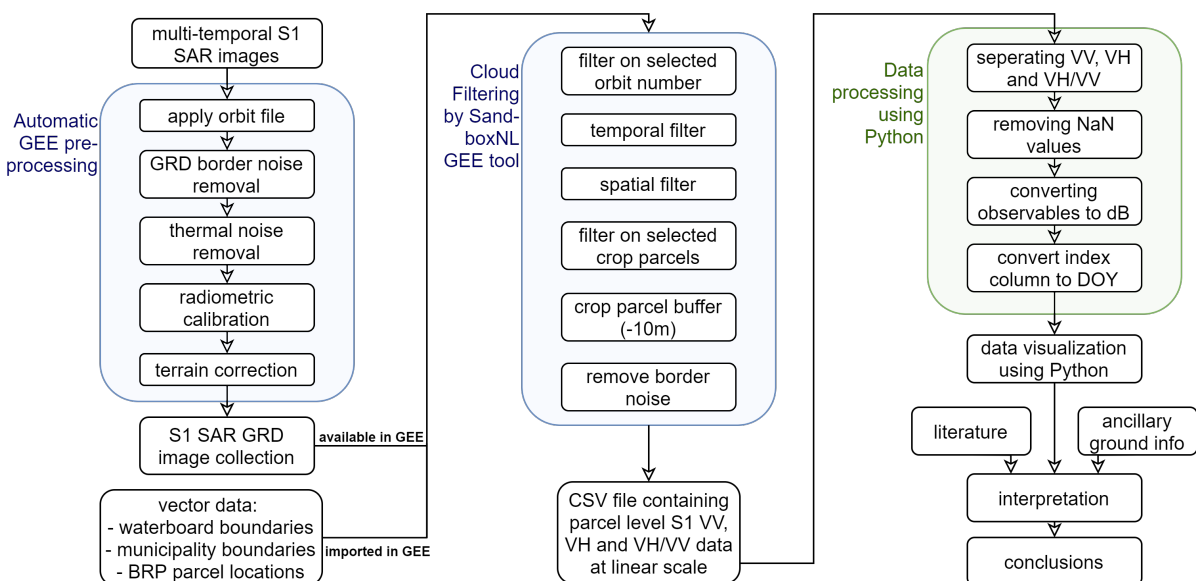


Figure 3.10: Sentinel-1 SAR data flow diagram.

6 days. It is possible to combine data from different orbits to achieve a temporal resolution of 1-2 days. To combine data from different orbits, a correction for the impact of varying incidence angle should be applied to remove the static mean bias between the orbits. However, in this research the orbits are not combined as it is important for this study to know the impact of the incidence angle on the Sentinel-1 time series of crops during drought. Furthermore, descending orbits pass in the morning and the ascending orbits pass in the evening in the Netherlands. Since the targets are agricultural crops, which are active water managers, it is not desirable to combine descending and ascending orbits due to parameters like VWC having a daily cycle.

### 3.3.2. Data Analysis

The extracted Sentinel-1 data values are then processed in Python. The Python code that is used for this script can be found in Appendix C. Since the CSV file contains mean and standard deviation values of VV, VH and VH/VV backscatter data, the first step of post processing is the data separation. New Pandas DataFrames are created for the mean and standard deviation of VV, VH and VH/VV. Then, all rows and columns that consist of solely Not a Number (NaN) values are removed. Next, all backscatter values in the DataFrames are converted from linear scale to logarithmic scale. At last, strings in the index column are converted to Day of Year (DOY). The Sentinel-1 SAR data is now ready to be visualized in combination with the soil and precipitation data.

To assess the influence of phenological changes on the Sentinel-1 time series, parcels in the Flevopolder during the 2017 agricultural summer season are studied in Section 4.1.1. This choice was made based on the availability of ancillary ground information such as field photos in the Flevopolder during this season. The results include Sentinel-1 backscatter time series (VV, VH and VH/VV) averaged over all corresponding crop parcels in the Flevopolder along with precipitation data from the Lelystad KNMI weather station. The general planting and harvest periods for the corresponding crops are also indicated.

The influence of drought on the interannual differences between 2017, 2018 and 2019 is analyzed for crop parcels in Vechtstromen-Noord. As mentioned in Section 3.1.1, the municipality of Emmen - which is located within Vechtstromen-Noord - showed the highest drought vulnerability in 2018 [69]. The results include Sentinel-1 backscatter time series (VV, VH and VH/VV) averaged over all corresponding crop parcels in Vechtstromen-Noord along with surface soil moisture data from the Coevorden municipality area and precipitation data from the Hoogeveen KNMI weather station. The results include data from four orbits that cover Vechtstromen-Noord. The title of the columns indicate the relative orbit number, the corresponding overpass time and incidence angle with respect to the centre of the study area. For the analysis on the influence of drought on the interannual differences, descending orbit 37 data is used for references to specific dates in the graphs. In order to analyze the influence of the incidence angle and the overpass time on the time series, data acquired from all relative orbits covering Vechtstromen-Noord is compared.

Crop parcels in Vechtstromen-Noord are also studied to determine if the drought observations, aggregated across all crop parcels, are reflected back in individual parcels. To rule out differences in soil type, crop type and farmers' decision-making, only common parcels are analyzed. Common parcels are individual parcels that planted similar crops in 2017 and in a drought year. Hence, the 2017 Sentinel-1 response of a parcel is only compared with a drought year response of the same parcel. This common parcel is owned by the same farmer, at the same location, planting the same crop which creates a reliable environment for a comparative analysis. Whether drought observations - aggregated over across all crop parcels - are reflected back in common parcels, is assessed by a script that checks if the common parcel's drought response is similar to the aggregated drought response observed in Section 4.1.2. Only maize, potato and barley crops are included, as there are an insufficient amount of onion and sugar beet parcels that meet the aforementioned requirements for parcel selection.

The regional variability of C-band SAR data is analyzed by comparing Sentinel-1 backscatter time series for the three study areas. It is expected that crops in the study areas show different drought stress responses due to differences in hydrometeorological conditions, soil types and water-use policies during droughts. The different responses will also reflect on Sentinel-1 SAR responses. Furthermore, the influence of irrigation on Sentinel-1 backscatter time series is analyzed. As mentioned in Section 3.1.2, the Coevorden, Hardenberg, Tubbergen and Hof van Twente municipality areas are studied for this analysis. Coevorden and Hardenberg are located in low-Vechtstromen, while Tubbergen and Hof van Twente are located in high-Vechtstromen. Only maize and potato parcels are considered, because the difference in the number of crop parcels between the municipalities are too large to ensure a fair and reliable comparison.

# 4

## Results and Discussion

### 4.1. Seasonal crop cycle characterization using C-band Sentinel-1 SAR data

This first part of the results characterizes the seasonal cycle of maize, sugar beet, potato, onion and barley using C-band SAR data from Sentinel-1. Section 4.1.1 describes the link between the characteristic seasonal crop cycle and phenological changes. To analyze the influence of drought on C-band SAR data over agricultural parcels, the drought-induced interannual differences are described in Section 4.1.2. Then, the influence of viewing geometry and overpass time is analyzed by comparing the characteristic seasonal cycles from different orbits in Section 4.1.3. Finally, the extent to which the aggregated observations described in Section 4.1.2 are reflected in individual parcels is assessed in Section 4.1.4.

#### 4.1.1. Impact of phenological changes on C-band SAR data

In this section, an analysis is given on the influence of changes in phenology within parcels of key crops in the Netherlands on C-band SAR data from Sentinel-1. As mentioned in Section 3.3, the crop parcels in the Flevopolder during the 2017 agricultural summer season are studied in this analysis. This choice is based on the fact that ancillary ground information, in the form of field photos, are available in the Flevopolder during the 2017 season. The results of maize, sugar beet, potato, onion and barley are presented in Figure 4.1, 4.4, 4.7, 4.10 and 4.13, respectively. The figures include all Sentinel-1 observables (VV, VH and VH/VV) from the crop parcels in the Flevopolder along with precipitation data from the Lelystad KNMI weather station in the bottom row. The green-outlined bars indicate the general planting and harvest periods for the corresponding crops in the Netherlands.

#### Maize

Maize is a vertical oriented crop that is generally planted from 20 April till the start of May and harvested from mid-September till mid-October [86]. The height of the crop can vary from 1 to 4 meter above ground. The maize crops consist of a vegetative part, which includes stem and leaves; and a reproductive part, which includes the cob and the silk.

Figure 4.1 shows the Sentinel-1 backscatter from 333 maize parcels in the Flevopolder along with precipitation data. From the start of the year until the emergence, the Sentinel-1 backscatter observables are mainly dependent on the soil moisture, soil roughness and row orientation. The field photos presented in Figure 4.2 show that the maize crops have just emerged from the soil around mid-May (~DOY 135). Hence, all temporal changes before DOY 135 are attributed to changes in aforementioned soil parameters. The two backscatter peaks at DOY 110 and 135 are caused by precipitation event, observed in the precipitation data. The decrease in VV and VH backscatter before soil preparation for sowing is due to gradual smoothing of the soil [34] and decreasing soil moisture which occurs around this time of the year. At DOY 140, a minimum is observed in the VH/VV ratio, which indicates that the crops have emerged from the soil and the third leaf is unfolded for maize (BBCH 13) [14, 35]. From DOY 140 till DOY 180, a rapid increase of 5, 9 and 4 dB is observed in VV, VH and VH/VV, respectively. This coincides with the leaf development and stem elongation phase (BBCH 13 - 51) [14, 35]. The increase in VV backscatter is caused by the soil-canopy interaction (double-bounce mechanism) which cannot be distinguished from regular soil backscatter. VH backscatter increases during the vegetative stage due to the increase of leaf area and plant height, which enables an increasing amount of multiple bounces and thus higher volume scattering. The VH/VV ratio increases because VH backscatter increases relatively more than VV backscatter. The VH/VV ratio appears relatively stable compared to VV and VH backscatter because the effect of soil moisture and the soil-canopy interactions are minimized.

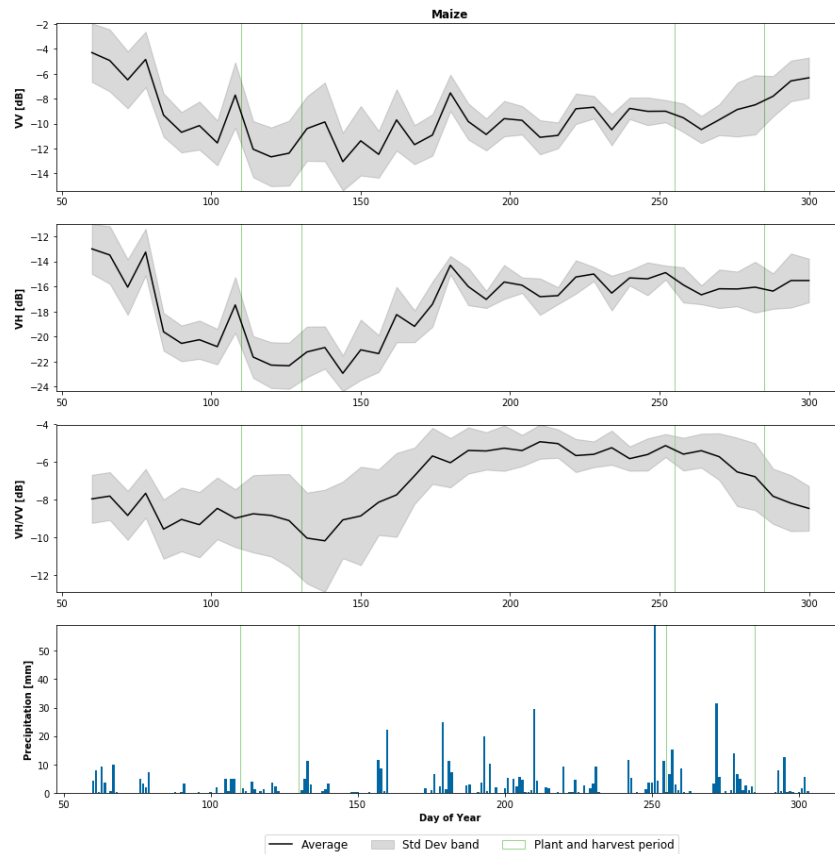


Figure 4.1: The 2017 time series of Sentinel-1 SAR data (VV, VH and VH/VV) from maize parcels in the Flevopolder. The black lines represent the mean value and the gray bands depict the standard deviation across all fields. Precipitation data is displayed in the bottom plot. The green-outlined bars correspond to the general planting and harvest periods.

After DOY 180, the rapid increase is halted for all observables. This coincides with the start of the tassel emergence phase (BBCH 51) [14, 35, 46, 50]. The field photos in Figure 4.3 showcase maize crops during this period. The backscatter stops increasing because the saturation limit of the radar signal has been reached during this stage when LAI values are 2-3 [14, 35, 46, 50]. After saturation occurs, the VH/VV ratio is mainly dependent on the VWC [14]. After DOY 210, the VH/VV ratio starts decreasing slowly, which coincided with BBCH stage 75 [35]. According to Khabbazan et al. [35] and Vreugdenhil et al. [14], this is caused by the decrease in VWC which occurs during the ripening phase until harvest (BBCH 83 - 99). The VH/VV ratio starts decreasing rapidly around DOY 270 due to harvesting. The VH/VV ratio decreases due to the increase of VV backscatter, caused by the increased contribution of soil moisture.



Figure 4.2: Maize field photo taken on the 17th of May (DOY 137) in the Flevopolder.



Figure 4.3: Maize field photo taken on the 27th of July (DOY 178) in the Flevopolder.

### Sugar beet

Sugar beet is a broad leaf plant with a two-year crop cycle. The first year consists of the vegetative phases that include leaf development, stem elongation and development of harvestable vegetative plant parts. The sugar beet crop enters the reproductive phases in the second year, which lead to seed production. However, the second year is not considered as sugar beets are harvested at the end of the first year. Sugar beets are generally planted from the end of March till the start of April and harvested from mid-September till mid-November [87].

Figure 4.4 shows the Sentinel-1 backscatter from 754 sugar beet parcels in the Flevopolder along with precipitation data. During and after the planting period, an increase of standard deviation in VV backscatter and VH/VV ratio is observed which is mainly caused by varying planting dates and row orientation [43, 44]. The two backscatter peaks around DOY 77 and 110 are caused by precipitation events as observed in the precipitation data. A steep increase in both VV and VH backscatter is observed around DOY 120 which likely indicate the emergence of the sugar beet crops from the soil. This is confirmed by the field photos in Figure 4.5 showing that the sugar beet crops have indeed emerged and the first leaves are being produced on the 17th of May (DOY 137). After DOY 135, a steep increase of 6 dB is also observed in the VH/VV ratio. The rapid increase in all SAR observables is caused by the increase in above ground biomass. During this phase, the leaves are unfolding and stems are elongating, which increases volume scattering and - to a lesser extent - soil-canopy interaction. This also causes the backscatter to be less sensitive to soil returns and thus results in a decrease in standard deviation. After DOY 170, the SAR observables stabilize. According to Haagsma [88], the VH stabilizes when the leaves of adjacent rows touch (closure). Figure 4.6 confirms this as the leaves of adjacent rows are just about to touch in the field photo of the 9th of June (DOY 160).

Furthermore, it can be noted that - unlike the maize time series - a steep decrease in the SAR observables during the harvest period is absent in the data for sugar beet parcels. This is because sugar beets are gradually harvested from mid-September till mid-December. Furthermore, the soil moisture is slowly increasing during this time of the year, which leads to increased backscatter. Hence, no sudden backscatter drop is observed in the Sentinel-1 data [35].

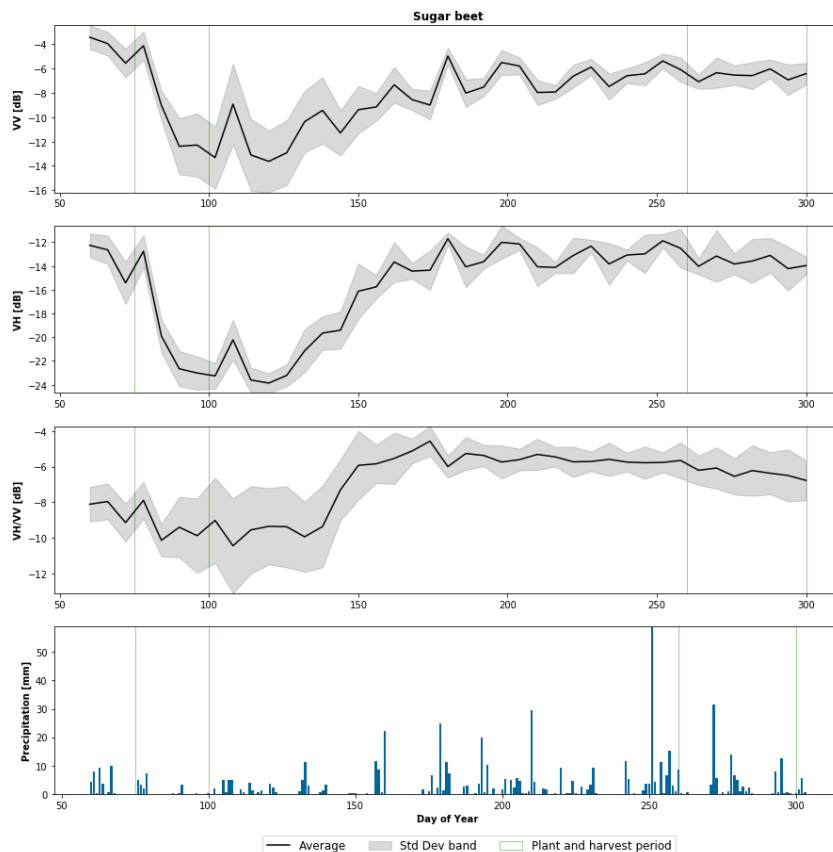


Figure 4.4: The 2017 time series of Sentinel-1 SAR data (VV, VH and VH/VV) from sugar beet parcels in the Flevopolder. The black lines represent the mean value and the gray bands depict the standard deviation across all fields. Precipitation data is displayed in the bottom plot. The green-outlined bars correspond to the general planting and harvest periods.



Figure 4.5: Sugar beet field photo taken on the 17th of May (DOY 137) in the Flevopolder.



Figure 4.6: Sugar beet field photo taken on the 9th of June (DOY 160) in the Flevopolder [89].

### Potato

Potato parcels are easily recognizable due to the deep ridges in which the potatoes are planted. The ridges can be seen in the field photos of mid-May in Figure 4.8. Potato crops are generally planted from the end of April till the beginning of May [90] and harvested in September [91].

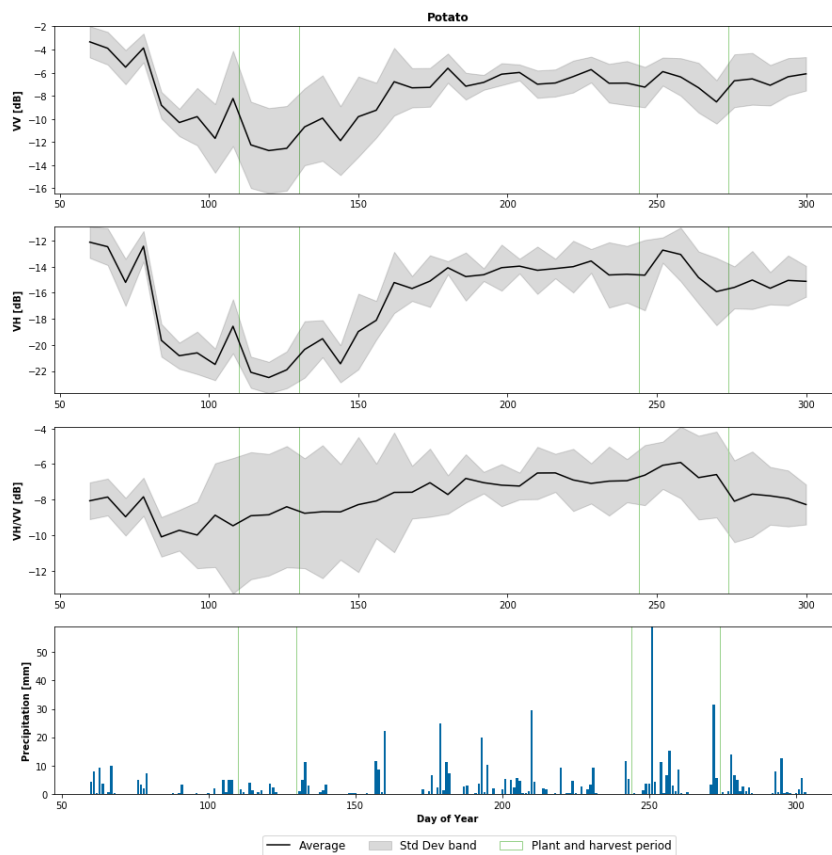


Figure 4.7: The 2017 time series of Sentinel-1 SAR data (VV, VH and VH/VV) from potato parcels in the Flevopolder. The black lines represent the mean value and the gray bands depict the standard deviation across all fields. Precipitation data is displayed in the bottom plot. The green-outlined bars correspond to the general planting and harvest periods.

Figure 4.7 shows the Sentinel-1 backscatter from 875 potato parcels in the Flevopolder along with precipitation data. Similar to the maize and sugar beet time series, the backscatter before emergence is dominated by soil moisture returns. The precipitation events around DOY 77, 110 and 140 are also observed as peaks in the VV and VH backscatter. A noticeable difference between the potato time series and the maize and sugar beet time series, is the extremely high standard deviation during planting and prior to emergence. The backscatter variation due to differences in row geometry is larger due to the deep ridges [43, 44]. The field photos in Figure 4.8 show that the crops have just emerged from the soil at 17 May (~DOY 140). Around the same time we observe a rapid increase of 7, 7.5 and 2 dB in VV, VH and VH/VV, respectively. This corresponds to the leaf development phase, formation of basal side shoots below and above surface, main stem elongation, tuber formation, inflorescence emergence and the beginning of the flowering stage (BBCH 10 - 63). Khabbazan

et al. [35] found that VV and VH backscatter stabilizes around DOY 175 when 30% of flowers have opened during the first inflorescence (BBCH 63). Figure 4.9 shows that on DOY 177, the potatoes are indeed in the flowering phase. During the harvest period, a noticeable drop in VV and VH backscatter is observed from DOY 260. This drop is caused by the destruction of the potato haulms (stalks and stems) which takes place one or two weeks before harvest [35, 92].



Figure 4.8: Potato field photo taken on the 17th of May (DOY 137) in the Flevopolder.



Figure 4.9: Potato field photo taken on the 19th of June (DOY 170) in the Flevopolder [92].

### Onion

Onion is a bulb vegetable that is generally planted at the end of March [93] and harvested in September [91]. Similar to sugar beet, the onion crop has a two year crop cycle. In the first year, the crop produces the leaves and the bulb, and the second year consists of reproductive stages. Since the onion crops are harvested at the end of the first year for their bulbs, only the first year is considered.

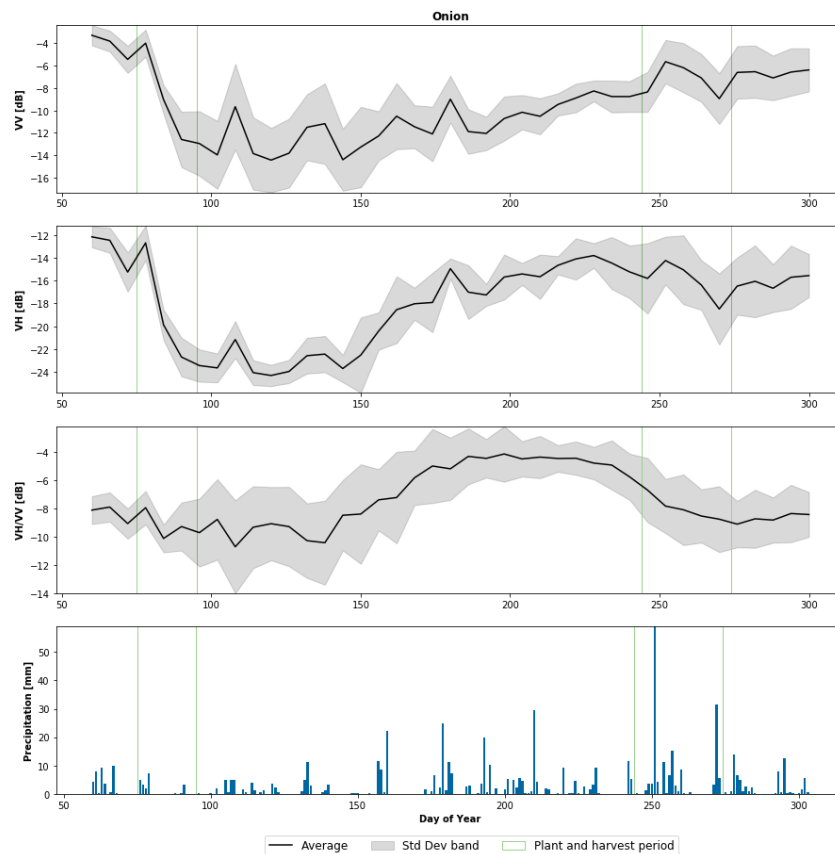


Figure 4.10: The 2017 time series of Sentinel-1 SAR data (VV, VH and VH/VV) from onion parcels in the Flevopolder. The black lines represent the mean value and the gray bands depict the standard deviation across all fields. Precipitation data is displayed in the bottom plot. The green-outlined bars correspond to the general planting and harvest periods.

Figure 4.10 shows the Sentinel-1 backscatter from 770 onion parcels in the Flevopolder along with precipitation data. The period between planting and observed increase of backscatter, due to crop growth, is relatively long for onion crops. Only ~50 days after planting, the growth results in increased volume scattering. During

this period, backscatter is dictated by soil parameters. The VH backscatter and VH/VV ratio start increasing around DOY 140 till DOY ~185 by 9 and 6 dB, respectively. Mascolo [94] found that the increase of cross-polarized backscatter coincides with the growth of the second leaf (BBCH 12) for onion crops. Figure 4.11 indeed shows that on DOY 143, the onions in the field photo were in the second leaf stage. The increase in volume scattering and thus VH backscatter and VH/VV ratio is associated with the leaf development phase of the main shoot (BBCH 10-41) [94, 95]. According to Moran et al. [95] and Mascolo [94], the backscatter stabilizes at BBCH 41 which marks the start of the harvestable vegetative plant part development phase. Figure 4.12 shows that at DOY 191, the onion crops are at the start of the bulb growth stage. The VH/VV ratio does indeed stabilize just before DOY 191. However, VH and VV backscatter keep increasing on a slower pace after DOY 191. The VH/VV ratio is relatively stable until the leaf ripening (BBCH 47) [94, 95]). During the ripening, VH backscatter and VH/VV ratio decreases as the leaves bend and dry out. However, VV backscatter keeps increasing due to the increased sensitivity to soil moisture.



Figure 4.11: Onion field photo taken on the 23rd of May (DOY 143) in the Flevopolder [96].



Figure 4.12: Onion field photo taken on the 10th of July (DOY 191) in the Flevopolder [96].

### Barley

Barley is a cereal crop with a dominant vertical orientation. It is preferred to plant barley early in the cropping season, when the weather and soil allows for it. In the Netherlands, barley is generally planted from February till mid-April. The crops are then usually harvested by the end of July on sandy soils and at the start of August for clay soils [97].

Figure 4.13 shows the Sentinel-1 backscatter from 68 barley parcels in the Flevopolder along with precipitation data. After planting, the standard deviation starts to increase in VV backscatter and VH/VV ratio, mainly because of differences in row geometry [43, 44]. Due to the vertical structure of barley, VV and VH backscatter behave different compared to other crops. After planting, around DOY 110, the VV backscatter starts to decrease, with an exception between DOY 110 and 135 that is caused by precipitation events. VV backscatter decreases by 5 dB during tillering and especially the stem elongation phase (BBCH 20 - 39). The decrease of VV is caused by attenuation by growing vertical structures in barley parcels. Similar findings are also observed in previous studies [14, 34, 35, 65]. The VH backscatter mainly depends on the soil-canopy interaction [52] and volume scattering in this stage. Throughout the tillering and stem elongation phase, the soil-canopy interaction decreases while the volume scattering opportunities increase due to growth of above ground biomass [30, 34]. The two aforementioned components mostly cancel each other out, resulting in a very slight decrease in VH backscatter. Due to the decrease of VV backscatter, the VH/VV ratio increases by ~6 dB during the tillering and stem elongation phases. The VH/VV ratio is thus a good metric for the growth of above ground biomass. During the booting phase (BBCH 40 - 49) VV backscatter reaches its minimum and the VH/VV ratio reaches its maximum around DOY 155. Then, during the heading phase (BBCH 50 - 59), both VV and VH backscatter increase. During heading phase, the contribution of the backscatter from vegetation becomes larger than the contribution of the soil [65]. VV backscatter increases because of increasing direct backscatter from the flag leaves and ears [52]. VH backscatter increases due to increasing opportunities for volume scattering. Previous studies also found the heading stage to be the turning point for co-polarized and cross-polarized backscatter [34, 35, 52, 65]. During harvest, VH backscatter and VH/VV ratio drop rapidly due to decrease of volume scattering.

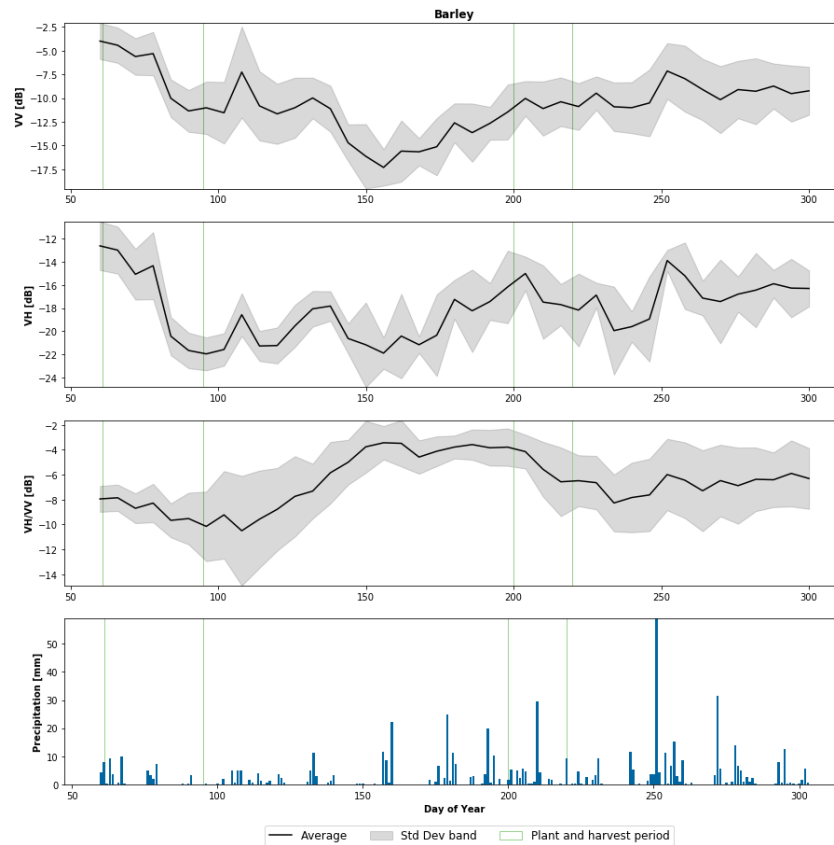


Figure 4.13: The 2017 time series of Sentinel-1 SAR data (VV, VH and VH/VV) from barley parcels in the Flevopolder. The black lines represent the mean value and the gray bands depict the standard deviation across all fields. Precipitation data is displayed in the bottom plot. The green-outlined bars correspond to the general planting and harvest periods.

#### 4.1.2. Influence of agricultural drought on the interannual variability of C-band SAR data

This section describes the influence of drought on the interannual differences between 2017, 2018 and 2019. As mentioned in Section 3.3, results from the Vechtstromen-Noord study area are presented in this section due to its vulnerability to drought. The results for Scheldestromen and the Flevopolder can be found in Appendix D. The Sentinel-1 SAR observables from maize, sugar beet, potato, onion and barley parcels are presented in Figure 4.14, 4.15, 4.16, 4.19 and 4.20, respectively. Additionally, the surface soil moisture and cumulative precipitation are shown in last two plot rows. The green outlined bars indicate the general plant and harvest periods of the corresponding crop type. The figures in this section contain Sentinel-1 backscatter data, acquired from four orbits that cover Vechtstromen-Noord. The title of the columns indicate the relative orbit number, the corresponding overpass time and incidence angle with respect to the centre of the study area. Descending orbit 37 data is used in this section for references to specific dates in the graphs. The differences between the orbits and the influence of viewing geometry is discussed in Section 4.1.3.

##### Maize

Figure 4.14 shows the Sentinel-1 backscatter from maize parcels in Vechtstromen-Noord. Before the planting period, differences between 2017 and 2018 in VV and VH backscatter are observed. This is because the VV and VH backscatter mainly depend on soil moisture and soil roughness. As leaves start to unfold and stems are elongating, VV and VH backscatter increase rapidly in both years due to increasing soil-canopy interaction and volume scattering. The observed differences are mainly caused by the differences in hydrometeorological and soil conditions. Differences in the VH/VV ratio are relatively small because the cross-pol ratio minimizes the effect of soil moisture returns. The drought onset in 2018 can be seen in the surface soil moisture and the cumulative precipitation data. The meteorological drought period started around DOY 150 and lasted until DOY 220. This likely coincides with the tasseling phase until the end of the fruit development phase (BBCH 50 - 79). After DOY 170, the impact of the drought on the VV and VH backscatter is clearly visible. During the drought period, the VV and VH backscatter values of 2018 are  $\sim 2$  dB lower than the values of 2017. This may be caused by drying of the soil, which mainly results in a reduction of VV backscatter. The VWC is reduced, which may also lead to a drop in backscatter and increased sensitivity to soil backscatter. Finally, the leaves may start to wilt if not enough water is supplied to the crop. This could lead to a decrease in volume scattering and thus backscatter, mostly VH backscatter. The VH and VV backscatter in 2018 increases and becomes

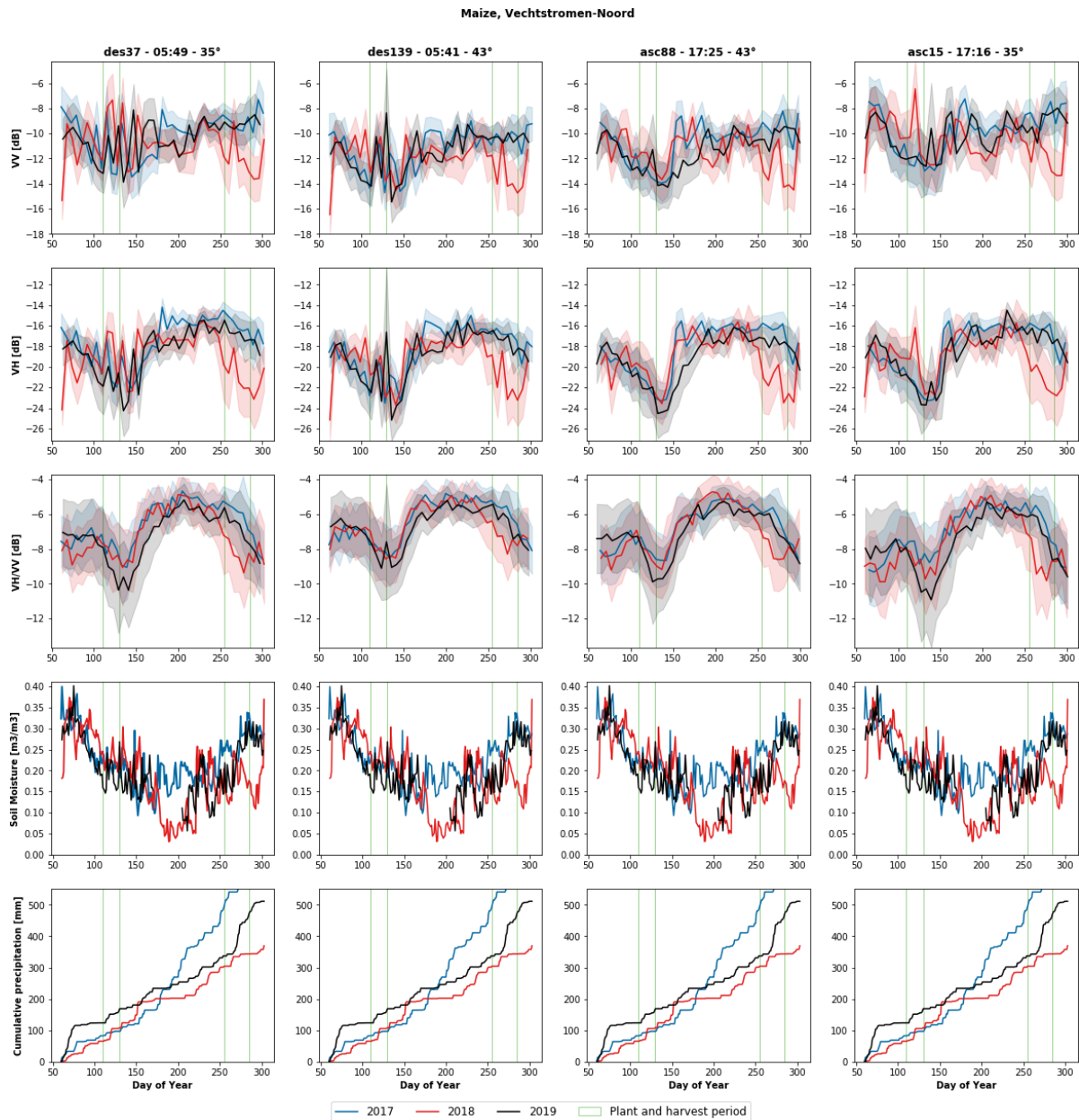


Figure 4.14: The 2017, 2018 and 2019 time series of Sentinel-1 SAR data (VV, VH and VH/VV) from maize parcels in Vechtstromen-Noord. The colored lines represent the mean value and the shaded bands depict the standard deviation across all fields. Surface soil moisture and cumulative precipitation data is displayed in the bottom two plot. The green-outlined bars correspond to the general planting and harvest periods.

similar to 2017 after precipitation events recovered the soil moisture deficit around DOY 220. When looking at the VH/VV ratio during the drought period, no large differences are observed between 2017 and 2018. After the drought in 2018, all SAR observables start decreasing. The growing season of 2018 appears to be ~30 days shorter than the growing season of 2017 when looking at the VH/VV ratio. This is because maize crops started ripening earlier and were thus also harvested earlier due to the dry conditions in 2018. Wesselink et al. [98] confirms that maize crops in 2018 were harvested very early in the Netherlands due to the drought.

The shorter 2018 season also led to a significant drop in yield of 9.1 percent compared to the average (see Figure 3.8). This is to be expected because it is likely that the drought occurred during the tasseling and flowering phase, which is the most drought sensitive stage according to Kurt Thelen [53]. This is due to a lack of synchronization between silking and shedding of the pollen during pollination. The pollen grains may not remain viable and silking might be delayed. If maize crops have tasseled and shed their pollen while blisters have not appeared yet, the crop will barren [53]. An early drop in the VH/VV ratio at the end of the season might thus be an indicator of lower expected yield.

When comparing 2019 observations with 2017 and 2018, it is noticeable that the VH/VV ratio values from the planting period until the end of stem elongation phase (DOY 130 - 180) are ~1 dB lower than the values in 2017 and 2018. This is likely because the groundwater table and the root zone soil moisture in 2019 had not recovered yet from the drought in 2018, especially in the eastern part of the Netherlands which lies on sandy soils [69]. After the drought onset in June 2018, it took 10 months for the soil moisture to recover according to their surface soil moisture data. However, the recovery is likely insufficient to restore the root zone soil moisture and groundwater level. Furthermore, no large cumulative precipitation increases are observed from DOY 70 - 105. Thus, it can be assumed that the maize crops were planted and germinated in a relatively dry soil. The aforementioned early dry period possibly resulted in an increase in largest root diameter and a decrease in leaf elongation [55]. Furthermore, Anami et al. [54] mentions that drought stress during the vegetative phase typically reduces plant and leaf sizes. A smaller leaf and plant size leads to lower volume scattering, which in turn lowers VH backscatter and the thus VH/VV ratio compared to crops from other years. The 2019 drought started around DOY 180 and resulted in a dry July month. Similar to 2018, the VV and VH backscatter values are lower during the drought. During and after the drought, the 2019 VH/VV ratio values are still slightly lower than the other years. The drought in 2019 also seems to have resulted in a shorter VH/VV ratio cycle. The 2019 maize season appears to be ~10 days shorter than the 2017 season when looking at the VH/VV ratio.

However, the lower VH/VV ratio values in 2019 did not translate to a lower yield (see Figure 3.8). While the normalized gross yield in 2019 is relatively low compared to 2017, it does not seem significantly lower than the 5-year average. Furthermore, this result shows that lower VV and VH backscatter values during a drought do not necessarily translate to lower yield. It is possible that lower yield is indicated by the drought duration, during which backscatter values decrease. The results show that a shorter VH/VV ratio cycle, due to an early drop, is a more reliable indicator for yield impact.

### **Sugar beet**

Figure 4.15 shows the Sentinel-1 backscatter from sugar beet parcels in Vechtstromen-Noord. After the planting period till DOY 140, differences between 2018 and 2017 VH and VV backscatter are mainly caused by increased soil moisture due to precipitation events. During this period, the VH/VV ratio is slightly lower in 2018 due to the high VV backscatter caused by precipitation events observed from DOY 115 till DOY 150. All SAR observables increase after DOY 140 due to the increase of above ground biomass. During this increase, the 2018 VH/VV ratio meets similar values to the 2017 VH/VV ratio. The rapid increase of backscatter stops around DOY 160 when canopy closure occurs in the sugar beet parcels. The 2018 drought begins after the closure date. Similar to the maize time series, the VV and VH backscatter during the 2018 drought period are reduced. The VV and VH backscatter values are 2.5 dB lower in the 2018 drought period compared to 2017. However, comparing the 2018 and 2017 VH/VV ratio values during and after the drought, no differences are observed.

Since the yield in 2018 is 14.1 percent lower than in 2017 and the 5-year average (see Figure 3.8), this indicates that at least the beets were affected by the drought and likely the above ground vegetation as well. The VH and VV backscatter are thus better indicators of drought stress for sugar beet crops during the drought. A large decrease in VV and VH backscatter for a long period of time can thus be good indicators for decreased crop yield.

The 2019 VH/VV ratio values between planting and the closure date are ~0.5 dB lower than 2017 VH/VV ratio values. As with maize, the lower values are likely caused by the dry soil in the early cropping season, caused by the lingering effects of the 2018 drought and the lack of precipitation from DOY 75 till 115. After the closure date, when the 2019 drought starts, the VV and VH backscatter values are clearly lower than the 2017 VV and VH values, similar to the 2018 observations. During this period, the 2019 VH/VV ratio values are still ~0.5 dB lower than the 2017 VH/VV ratio values. A possible explanation for the lower VH/VV ratio values is that the leaves were smaller in order to cope with the dry soil at the start of the 2019 cropping season. Moreover, the 2019 VH/VV backscatter trend seems to be less noisy than the 2017 and 2018 VH/VV ratio trends.

While the yield in 2019 is significantly lower than in 2017, the 2019 yield is only slightly lower than the 5-year average. Again, the lower 2019 VH/VV ratio values do not seem to indicate a significantly lower yield. It does seem that the length of the VV and VH backscatter decrease during the drought, correlates with crop yield. The 2018 backscatter decrease lasted around 60 days, while the backscatter in 2019 lasted around 35 days in the VV and VH data.

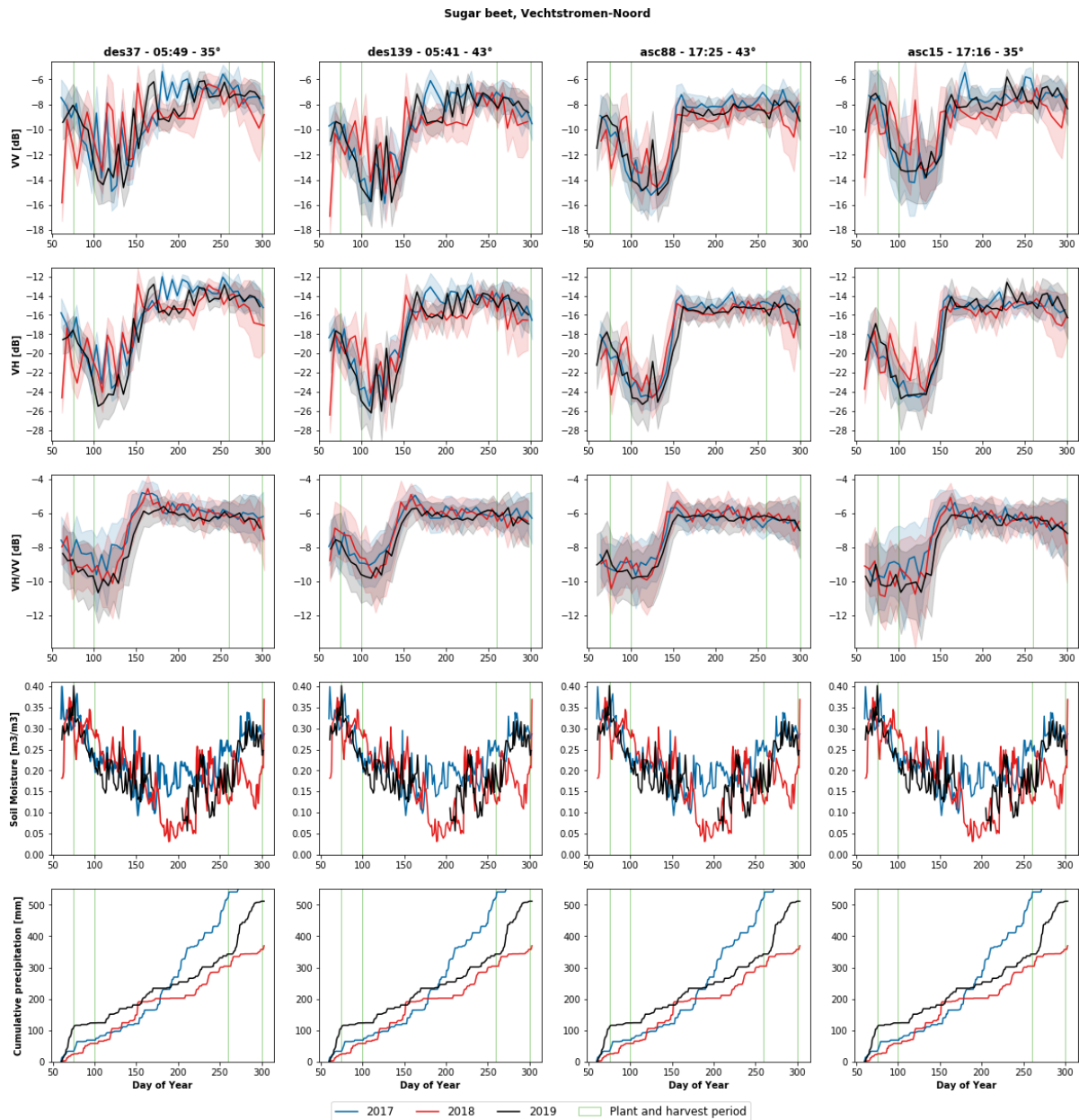


Figure 4.15: The 2017, 2018 and 2019 time series of Sentinel-1 SAR data (VV, VH and VH/VV) from sugar beet parcels in Vechtstromen-Noord. The colored lines represent the mean value and the shaded bands depict the standard deviation across all fields. Surface soil moisture and cumulative precipitation data is displayed in the bottom two plot. The green-outlined bars correspond to the general planting and harvest periods.

### Potato

Figure 4.16 shows the Sentinel-1 backscatter from potato parcels in Vechtstromen-Noord. When comparing the 2018 and 2017 VV and VH backscatter data after planting, it shows that soil moisture is responsible for most peaks in backscatter before the leaves start developing (BBCH 10). When the potato crops enter the leaf development phase, the VV and VH backscatter start to increase in both years for the same period. In both years, the VH/VV ratio is similar during the rapid backscatter increase, which stops around DOY 155 when the crops are at the beginning of the flowering stage (BBCH 63). Around this time, the precipitation events become scarce and the 2018 drought starts. Similar to the maize and sugar beet time series, the VV and VH backscatter during the 2018 drought period is lower than in 2017. However, where the differences in maize and sugar beet were around 2 and 2.5 dB, the difference for potato is only 1 dB. At the start of the drought, the VH/VV ratio in both years were relatively similar. However, from DOY 200 till DOY 220, the VH/VV ratio values in 2018 are higher than in 2017. This phenomenon is not observed for the other crops. The high VH/VV ratio values are caused by low values of VV backscatter during this period. A possible cause for the low VV backscatter values is the decrease of leaf area and increased sensitivity to soil returns due to reduced WVC and wilting leaves. Looking at the 2018 potato field photos from 28th of July (DOY 209) in Figure 4.18,

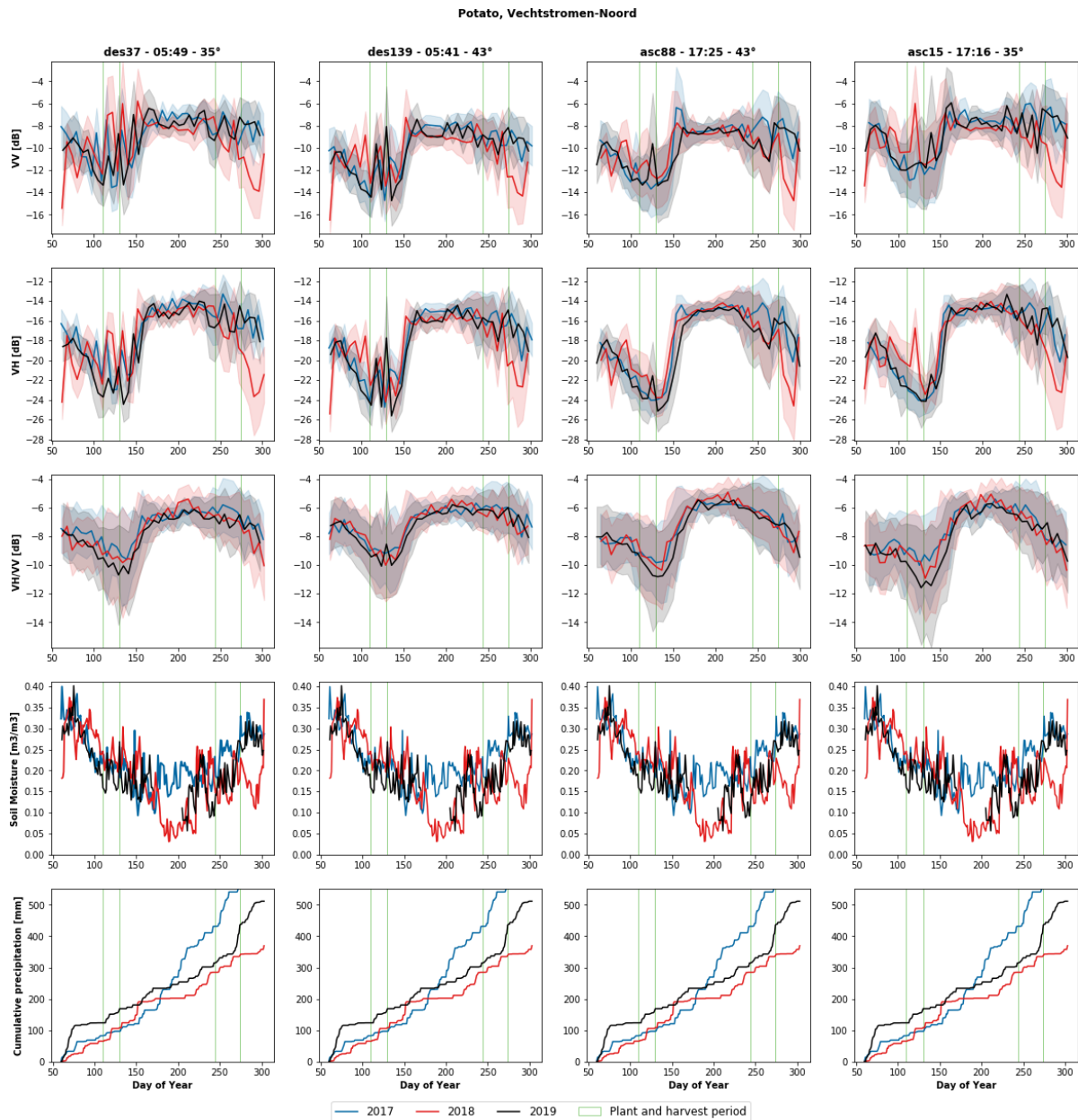


Figure 4.16: The 2017, 2018 and 2019 time series of Sentinel-1 SAR data (VV, VH and VH/VV) from potato parcels in Vechtstromen-Noord. The colored lines represent the mean value and the shaded bands depict the standard deviation across all fields. Surface soil moisture and cumulative precipitation data is displayed in the bottom two plot. The green-outlined bars correspond to the general planting and harvest periods.

dry leaves and spots with exposed dry soils are visible. Figure 4.17 shows field photos on the 14th of July (DOY 195), where no dry leaves and exposed soil can be observed.

While effects of the drought cannot be observed in the VH/VV ratio, the 2018 potato yield in Vechtstromen-Noord was severely impacted by the drought (see Figure 3.8). The potato yield in 2018 is 21.3 percent lower compared to the average. The slightly lower VV and VH backscatter values during the droughts are the only influence of the drought that can be observed from potato parcels.

Similar to the maize and sugar beet time series, the VH/VV ratio values of 2019 at the emergence is lower than the other two years. However, the 2019 VH/VV values after DOY 160 reach similar values of 2017 and 2018, unlike the maize and sugar beet time series. From DOY 160 till DOY 190, the VV and VH backscatter values are lower than 2017 due to the drought. Again, this is mainly caused by the reduced VWC and the increase of sensitivity to soil returns. Similar to 2018, the difference in VV and VH backscatter was relatively small. Large differences cannot be observed in the VH/VV ratio values. Destruction of the haulms, which is characterized by a sudden drop in VH backscatter, occurs in September in all years (DOY 244-270).

The 2019 potato yield is slightly higher than 2018, yet still significantly lower than 2017 and the 5-year average. The potato yield in 2019 is 9.2 percent lower compared to the average yield in Vechtstromen-Noord.



Figure 4.17: Potato field photo taken on the 14th of July in the Flevopolder [99].



Figure 4.18: Potato field photo taken on the 28th of July in the Flevopolder [99].

### Onion

Figure 4.19 shows the Sentinel-1 backscatter from onion parcels in Vechtstromen-Noord. Similar to time series of other crops, no large differences in the SAR observables are observed between 2018 and 2017 before the drought. The 2018 drought likely occurred during the stem elongation phase and the start of the bulb development phase until the leaves start bending. The 2018 VH backscatter during the early part of the drought (DOY 170-190) is slightly lower than in 2017. However, two peaks are observed in the 2017 VH backscatter which are likely caused by an increase in surface soil moisture due to precipitation events. During this period, the exposed soil fraction is still high so soil returns are still visible in the backscatter data. The 2018 temporal trend of the VH/VV ratio during the drought is relatively similar to 2017. In 2018, all SAR observables start to decrease around DOY 210. When looking at the VH/VV ratio, which best reflects the structure of the crop, the 2018 season was ~10 days shorter than the 2017 season. This is likely because the onions ripened faster and entered senescence earlier.

Onions that experience drought stress from the start of the bulb formation stage, generally result in decreased final bulb weight [62] and thus in a decrease in yield. This decrease is seen in the normalized gross yield data, shown in Figure 3.8. The 2018 onion yield is 23.1 percent lower than the average.

Similar to the maize and sugar beet time series, the 2019 VH/VV ratio values are lower than 2017 and 2018. The 2019 VH/VV ratio values are ~1 dB lower during the emergence, leaf development, bulb development stage. Again, this is likely caused by the soil moisture and the groundwater table which had not yet recovered from the 2018 drought. Combined with little precipitation for a short period in the early season, this led to onion crops being planted into a relatively dry soil and thus a decreased above ground biomass overall compared to other years. The 2019 VH/VV ratio values become similar to 2017 VH/VV ratio values during ripening and harvest.

The 2019 onion yield is 7.4 percent lower compared to the average in Vechtstromen-Noord. However, when comparing the onion yield of 2019 with 2017, no significant decrease is observed. Hence, the lower VH/VV ratio values before ripening did not translate into lower yield for onion crops.

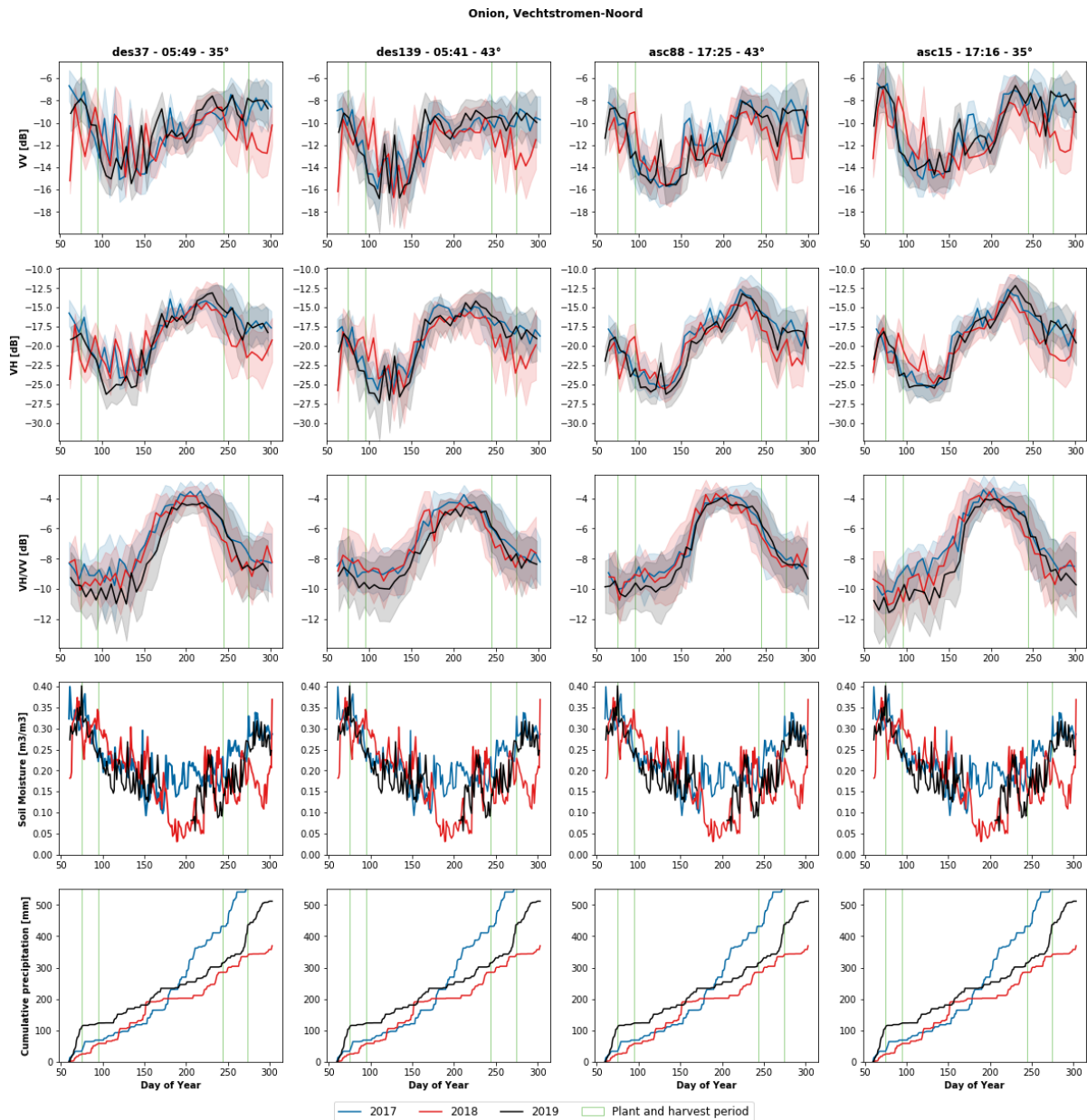


Figure 4.19: The 2017, 2018 and 2019 time series of Sentinel-1 SAR data (VV, VH and VH/VV) from onion parcels in Vechtstromen-Noord. The colored lines represent the mean value and the shaded bands depict the standard deviation across all fields. Surface soil moisture and cumulative precipitation data is displayed in the bottom two plot. The green-outlined bars correspond to the general planting and harvest periods.

### Barley

Figure 4.20 shows the Sentinel-1 backscatter from barley parcels in Vechtstromen-Noord. The VV backscatter in 2018 and 2017 decreases after planting until the development of the flag (leaves around DOY 160), due to attenuation by the growing vertical structures in the parcels. During this time, the impact of precipitation events are clearly visible in the form of backscatter peaks. The VH backscatter is relatively stable and the effects of precipitation are clearly visible before DOY 160. The VH/VV ratio, which reflects the above ground biomass well, increases in both years from  $\sim -9$  dB till  $-4$  dB after tillering until the development of flag leaves at DOY 160. After DOY 160, the VV and VH backscatter increase in both years because the contribution of the vegetation becomes dominant over the contribution of the soil during the heading phase. During this period, the VH/VV ratio in 2017 is stable, whereas in 2018 the VH/VV ratio slowly decreases. After DOY 180, a rapid decrease in all SAR observables is seen. The VH backscatter and VH/VV ratio in 2017 drop around DOY 205. Similar findings were found in Harfenmeister et al. [65]. High temperatures, solar radiation and less precipitation leads to faster development of the barley crops [64, 65]. The development of the barley crops in 2018 was thus sped up by the drought, which led to a faster ripening and an early harvest.

As can be seen in Figure 3.8 the faster development of barley crops in 2018 did not lead to a lower normalized gross yield in Vechtstromen-Noord than 2017 or the 5-year average. A possible reason could be that

summer barley crops in the Netherlands are planted and harvested early, relative to other crops. The 2018 drought started after the heading stage and thus very late in the growing cycle of the barley crops. Hence, the drought occurred too late in the season for the yield to be impacted.

In 2019, the VV and VH backscatter values were low after planting due to the lack of precipitation from DOY 75 till 110. Then, VV and VH backscatter increases with large peaks due to precipitation events. From DOY 140 till 160, both VH and VV backscatter decreased due to attenuation of radar signal by growth of above ground biomass. The 2019 VH/VV ratio does not have lower values unlike the time series of maize, sugar beet and onion. The 2019 VH/VV ratio follows the same pattern as 2017 and 2018 till DOY 160. After DOY 160 till DOY 190, the VV and VH backscatter increase because the vegetation backscatter becomes dominant after the heading phase. During this period, the VH/VV ratio decreases. After DOY 190, large peaks can be observed in VV and VH backscatter, indicating that soil contribution has increased. This can be due to crops drying out or the crops being harvested. After DOY 190, the VH/VV ratio rapidly decreases, except for peaks at DOY 210 and 220 which are caused by a large increase of soil moisture.

Similar to 2018, the normalized gross yield shown in Figure 3.8 did not show a decrease in 2019 compared to 2017 and the average. This is also likely due to the drought starting too late in the growing cycle of the barley crops to negatively impact the yield.

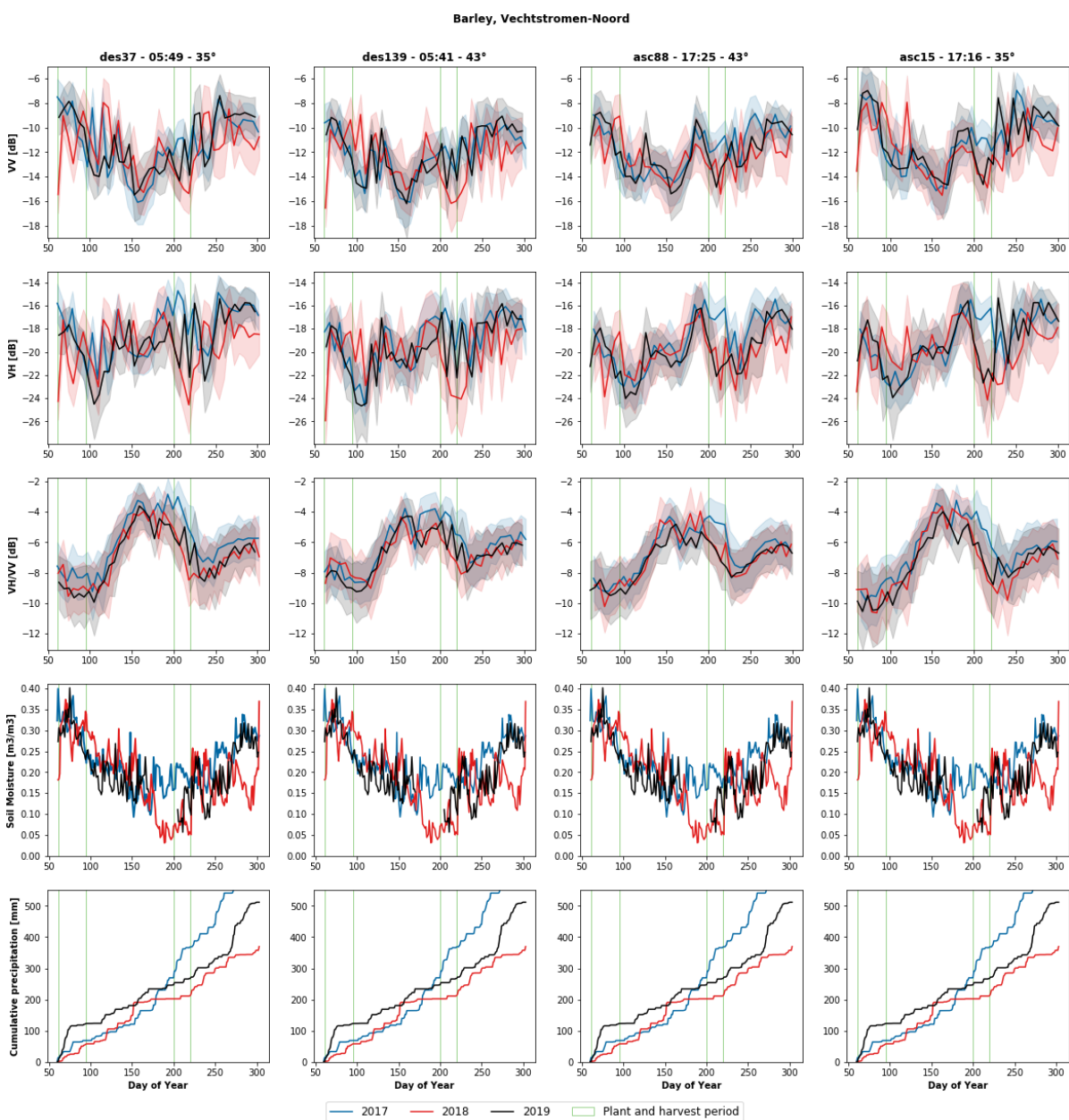


Figure 4.20: The 2017, 2018 and 2019 time series of Sentinel-1 SAR data (VV, VH and VH/VV) from barley parcels in Vechtstromen-Noord. The colored lines represent the mean value and the shaded bands depict the standard deviation across all fields. Surface soil moisture and cumulative precipitation data is displayed in the bottom two plot. The green-outlined bars correspond to the general planting and harvest periods.

### 4.1.3. Influence of Sentinel-1 viewing geometry and overpass time

To analyze the influence of the incidence angle and the local passage time on C-band SAR data from Sentinel-1, data acquired from different relative orbit covering Vechtstromen-Noord are compared. This section refers to figures presented in Section 4.1.2. The orbits that cover Vechtstromen-Noord are descending orbit 37, descending orbit 139, ascending orbit 88 and ascending orbit 15. The corresponding overpass time and incidence angle with respect to the centre of the study area for the aforementioned relative orbits are indicated as column titles in the figures.

Influences of the incidence angle on the backscatter can be observed for most crops. Looking at the backscatter from the maize parcels in Figure 4.14, it can be seen that both VV and VH backscatter during emergence is slightly lower in descending orbit 139 and ascending orbit 88. This is in accordance with the incidence angle differences between the relative orbits. Relative orbit 139 and 88 have an incidence angle of  $43^\circ$  while relative orbit 37 and 15 have an incidence angle of  $35^\circ$ , with respect to the center of Vechtstromen-Noord. For example, in 2018, the lowest point in VH backscatter has a value of -22.5, -24, -23.5, -22.5 for relative orbits 37, 139, 88 and 15, respectively. The same is observed in VV backscatter. However, the difference in VV backscatter is generally larger than in VH backscatter which results in high VH/VV ratio for larger incidence angles. The lowest point in the 2019 VH/VV ratio has a value of -10.5, -9, -10, -11 for relative orbits 37, 139, 88 and 15, respectively.

Another difference between the orbits is the magnitude of VV and VH backscatter decrease during the 2018 and 2019 droughts, described in Section 4.1.2. For sugar beet and potatoes, this phenomenon is more prominent in the descending orbits, which can be observed in Figure 4.15 and 4.16). The ascending orbits show little to no difference, relative to the descending orbits. A possible cause is the different local times at which the satellite passes the region of interest. The descending orbits pass Vechtstromen around 05:45 and the ascending orbits pass around 17:20. The VWC is dynamic and has a daily cycle. Generally, crops have high VWC around 05:45 compared to 17:20 [100, 101]. A possible explanation is that crops use their water during the day and the VWC will be at a low point at the end of the afternoon. Hence, the VWC will be relatively low for both normal and dry years, which reduces the observed differences caused by the drought in the ascending orbits. During the evening and at night, water is absorbed by the plant. Hence, the differences in VWC between a dry year and a normal year become apparent during the morning pass because the plant can only absorb limited water in a dry year. Another possibility is that the differences in backscatter between the dry and normal years are caused by difference in surface canopy water content due to dew. Vermunt et al. [102] used a truck-mounted L-band scatterometer to monitor diurnal variations from maize parcels. They concluded that the diurnal backscatter cycle mostly depends on internal and surface water content when the plant is nearing maximum biomass. Thus, dew formation may be reduced in the dry years, which results in lower VV and VH backscatter values. Since dew is most prominent around 06:00, only descending orbits are able to capture the interannual differences caused by dew.

The influence of the local overpass time can also be found in the Sentinel-1 backscatter from onion parcels in Figure 4.19. After VV and especially VH backscatter become relatively stable around DOY 160, VV and VH backscatter rapidly increase in the ascending orbits around DOY 200 in the studied years. The descending orbits show no change around DOY 200 in 2017. In 2018, a small increase is observed only in descending orbit 37. A small increase in VV and VH backscatter is observed around DOY 200 in 2019. However, the rapid backscatter increases observed around DOY 200 in the ascending orbits do not reflect in the VH/VV ratio. This suggests that the observations are likely caused by soil moisture and soil-canopy interaction.

Overall, the influence of the incidence angle is found to be limited to the general offset of the backscatter values. Hence, influence of the incidence angle on the drought-induced interannual variability of Sentinel-1 derived C-band SAR data is found to be negligible. On the other hand, the influence of the overpass time is found to have a great influence on interannual variability, especially for sugar beet and potato crops. The overpass time influences the magnitude of decrease in VV and VH backscatter that is caused by a drop in VWC.

### 4.1.4. The extent to which drought observations aggregated across all parcels are reflected in individual parcels

The influence of drought is clearly observed in the results presented in Section 4.1.2. However, whether drought observations aggregated across all parcels are reflected in individual parcels is unknown. Hence, this section presents an assessment on the extent to which drought observations made in Section 4.1.2 are reflected in individual parcels.

To rule out differences in soil type, water board's policies regarding droughts and farmers' decision-making, only common parcels are analyzed. Common parcels are individual parcels in which the same crops were planted in 2017 and in one of the drought years. Hence, the 2017 Sentinel-1 SAR response of a parcel is only compared with a drought year response of the same parcel. This common parcel is owned by the same farmer, at the same location, planting the same crop which creates a reliable environment for a comparison study. Whether a common parcel has a similar response to the aggregated response is assessed by a script that compares the average backscatter in 2017 and a drought year during a given period. Table 4.1 gives an overview of the aggregated observation that were analyzed. This section includes maize, potato and barley crops in the Vechtstromen-Noord area. Onion and sugar beet parcels are not included in this analysis, as there are insufficient amount of onion and sugar beet parcels that meet the requirements for parcel selection.

Table 4.1: The drought-induced interannual variability observations that are analyzed in this section.

crop	year	observation description
maize	2018a	early drop in VH/VV ratio at the end of the season
	2018b	lower VH backscatter values during the drought
	2019	lower VH/VV ratio values from emergence until harvest
potato	2018	lower VH backscatter values during the drought
	2019	lower VH backscatter values during the drought
barley	2018	early drop in VH/VV ratio at the end of the season
	2019	early drop in VH/VV ratio at the end of the season

### Maize

The aggregated drought response in 2018 is an early drop in the VH/VV ratio at the end of the season compared to 2017, due to early ripening and harvest. To assess if a common parcel has a similar response to the aggregated response, a script is used to compare the average VH/VV ratio from the onset of the drought until harvest for each common parcel. If the average backscatter of 2018 is lower than in 2017 for that parcel in this period, it is assumed that the common parcel shows the same response as the average response. Figure 4.21 shows the 2017 and 2018 VH/VV response of a common parcel. This is a very clear example of a parcel that is impacted by the drought, of which the VH/VV ratio decreases during the drought. The average VH/VV ratio value within the analysis period is clearly lower in 2018 and thus satisfies the condition of the script. Another aggregated drought response in 2018 that is studied, is decreased VH backscatter values during the drought.

The aggregated VH/VV ratio response in 2019 starts at lower values during emergence and stays lower than the 2017 VH/VV ratio values for a large duration of the cropping season. The script for the individual parcels in 2019 compares the average VH/VV ratio from the emergence of the crop until harvest. If the average is lower in 2019, it is assumed that the common parcel shows the same response as the aggregated response.

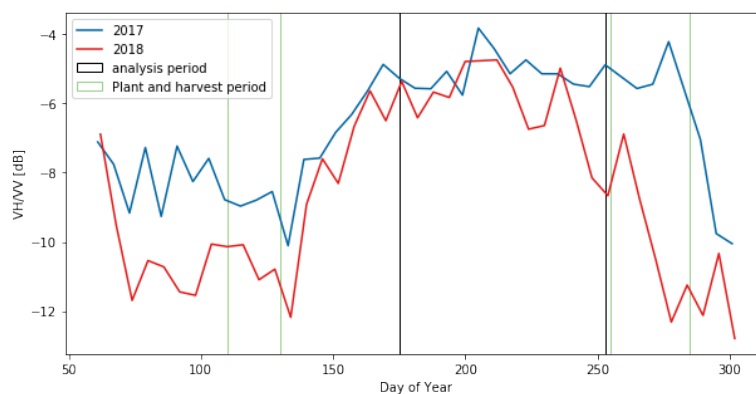


Figure 4.21: Sentinel-1 VH/VV ratio from a maize parcel in 2017 and 2018.

The results are presented in Table 4.2. The extent to which drought observations aggregated across all parcels are reflected in individual parcels is represented by a percentage of common parcels that satisfy the condition described in the script. It is expected that in a non-drought year about 50% of the parcels would satisfy the condition, which in this case is lower average VH/VV ratio values in a certain period. In order to conclude that the common parcel's Sentinel-1 response was similar to the aggregated response, the percentage of common parcels that satisfies the condition should be significantly higher than 50%. For both observations in 2018,

most of the parcels satisfied the conditions. Around 78% of the parcels in 2018 had low VH/VV ratio values after the drought onset across both descending orbits compared to 2017. Furthermore, approximately 94% of the individual parcels had low VH backscatter values during the drought compared to 2017. In 2019, approximately 91% of the parcels had low VH/VV ratio values after emergence compared to 2017.

Table 4.2: Individual parcel analysis results for maize parcels in Vechtstromen-Noord.

orbit nr.	2018a [% of parcels]	2018b [% of parcels]	2019 [% of parcels]
des37	1560/2036 (76.7%)	1900/2035 (93%)	1156/1267 (91.2%)
des139	1611/2036 (79.1%)	1911/2036 (94%)	1150/1267 (90.8%)

### Potato

The aggregated drought response during the 2018 drought is that VH backscatter values of potato parcels are significantly lower in descending orbits. To find the percentage of common parcels with similar responses, a script is used to compare the average VH backscatter during the 2018 drought. If the average is lower in 2018, it is assumed that the common parcel shows the same response as the aggregated response. The aggregated drought response during the 2019 drought is similar to 2018, where VH backscatter values are lower. Hence, a similar script is used to assess whether common parcels have a similar response to the aggregated response in 2019.

The results are presented in Table 4.3. In 2018, a majority of the common parcels show a drought response similar to the aggregated response, especially in descending orbit 139. The results are interesting because in both 2018 and 2019, the script checks for the average VH backscatter value during the drought. Hence, the condition applied to the script was similar and can be directly compared as both droughts mainly occurred in the same period of the cropping season. It can be concluded that the aggregated 2019 drought responses were observed more often in individual parcels than the aggregated 2018 drought responses.

Table 4.3: Individual parcel analysis results for potato parcels in Vechtstromen-Noord.

orbit nr.	2018 [% of parcels]	2019 [% of parcels]
des37	17/25 (68%)	24/24 (100%)
des139	20/25 (80%)	24/24 (100%)

### Barley

The aggregated drought response during the 2018 drought is the VH/VV ratio of barley parcels rapidly decreases after DOY 170 while in 2017 the VH/VV backscatter rapidly decreases around DOY 225. To find the percentage of common parcels that have similar responses, a script is used that compares the average VH/VV backscatter values from DOY 170 until DOY 200. If the average backscatter is lower in 2018, it is assumed that the common parcel shows the same response as the average response. The aggregated drought response during the 2019 drought is similar to 2018 where VH/VV backscatter rapidly decreases after DOY 170. Hence, a similar script is used to assess whether common parcels show similar response in 2019.

Table 4.4: Individual parcel analysis results for barley parcels in Vechtstromen-Noord.

orbit nr.	2018 [% of parcels]	2019 [% of parcels]
des37	56/62 (90.3%)	76/83 (91.6%)
des139	53/62 (85.5%)	73/83 (89.0%)

The results of the individual parcel analysis is presented in Table 4.4. In 2018 and 2019, most of the common parcels had a drought response similar to the aggregated response, especially in descending orbit 37. Similar to potato, the results are directly comparable in 2018 and 2019, same exact VH/VV ratio response was shown. Even though the average drop in 2018 VH/VV ratio is larger in Vechtstromen-Noord, as can be seen in Figure 4.20, this does not translate to more common parcels showing the same response in 2018. A possible cause is the difference in the studied number of parcels. Compared to the total amount of barley parcels in Vechtstromen-Noord, the studied parcels in this section is relatively low.

Overall, it can be concluded that the aggregated observations made in Section 4.1.2 are generally reflected in individual parcels. This gives a promising outlook on the use of Sentinel-1 SAR data on the detection of crop drought stress for farmers and their parcels.

## 4.2. Regional variability of agricultural drought C-band Sentinel-1 SAR data

The second part of the results discusses the regional variability and possible causes for the spatial differences of C-band SAR data of crops. Section 4.2.1 compares the C-band SAR backscatter from all study areas for the studied crops. Then, four municipalities within the Vechtstromen waterboard are analyzed to determine if influences of irrigation are detectable in Section 4.2.2.

### 4.2.1. Drought-induced differences between the study areas

In this section, the regional variability of C-band SAR data is analyzed by comparing the study areas. It is expected that crops in different study areas show different drought stress responses due to differences in hydrometeorological conditions, soil types and water-use policies during droughts. The different crop responses then lead to different Sentinel-1 SAR responses.

For this analysis, data of one orbit per study area is displayed to include all study areas. Descending orbits are used since these are more likely to capture differences in VWC as discussed in Section 4.1.3. The orbits were chosen with the aim of reducing geometrical differences while comparing the data. This is achieved by choosing an orbit combination that minimizes the difference in incidence angle. Furthermore, high incidence angles ( $>43^\circ$ ) are avoided because they result in a longer pathway in the canopy and thus increase the effect of saturation. Saturation may decrease the observed effects of drought stress on plants which is unfavorable. The chosen orbits are descending orbit 139, 110 and 37 for Vechtstromen-Noord, Scheldestromen and Flevopolder, respectively. The results for maize, sugar beet, potatoes, onions and barley are presented in Figure 4.22, 4.23, 4.24, 4.25 and 4.26, respectively. Similar to the figures in the previous section, surface soil moisture and cumulative precipitation data is provided in the bottom two rows. Furthermore, the average number of parcels is shown in the titles.

#### Maize

Figure 4.22 shows the Sentinel-1 backscatter from maize parcels in the study areas. When focusing on the differences in VH/VV ratio after stabilization, it is noticeable that the 2019 values in Vechtstromen-Noord are extremely low compared to 2017 and 2018. In Scheldestromen, and to a lesser extent in the Flevopolder, the 2019 VH/VV backscatter is mostly similar to 2018. A likely cause is the soil type in Vechtstromen-Noord, which is dominated by sand. Scheldestromen's and Flevopolder's soil type consists mostly of clay which has greater ability to retain water compared to sand. This means that after the 2018 drought, areas with a sandy soil had a harder time recharging the groundwater, which leads to these areas being impacted heavier in 2019. Furthermore, it can be seen that lack of precipitation events from DOY 70 until 110 leads to the largest drop in surface soil moisture in Vechtstromen-Noord. Surface soil moisture levels during planting were lower in Vechtstromen-Noord than in other study areas. As mentioned Section 4.1.2, early dry periods for maize crops could lead to an increase in largest root diameter and a decrease in leaf elongation [55]. This results in a decrease in VH and thus VH/VV backscatter. In addition, the cumulative precipitation shows a dry period in the mid-season for Vechtstromen-Noord. This period is shorter for Scheldestromen and non-existent for the Flevopolder, which could explain the decreased VH/VV ratio values in 2019.

Another distinct difference between the study areas is the rapid decrease in the VH/VV ratio due to harvest at the end of the cropping season. Compared to 2017, the VH/VV ratio in 2018 starts dropping approximately 40, 25, 10 days earlier in Vechtstromen-Noord, Scheldestromen and Flevopolder, respectively. This order is also in accordance with the normalized gross yield data. The normalized gross yield changed with -9.07, -1.28 and 2.62 percent compared to the 5-year average. For 2019, the VH/VV ratio rapidly declines approximately 15 and 10 days earlier than in 2017 in Vechtstromen-Noord and Scheldestromen, respectively. In the Flevopolder, no early decline is observed for the 2019 VH/VV ratio.

The influence of incidence angle on VH/VV ratio values during emergence, which is discussed in Section 4.1.3, can also be observed here, especially in 2019. During emergence, Vechtstromen-Noord has the highest VH/VV values in all years followed by Flevopolder. Scheldestromen shows the lowest values during emergence. This is in accordance with the incidence angles of the chosen orbit numbers, which are approximately  $43^\circ$ ,  $38^\circ$  and  $41^\circ$  for Vechtstromen-Noord, Scheldestromen and Flevopolder, respectively.

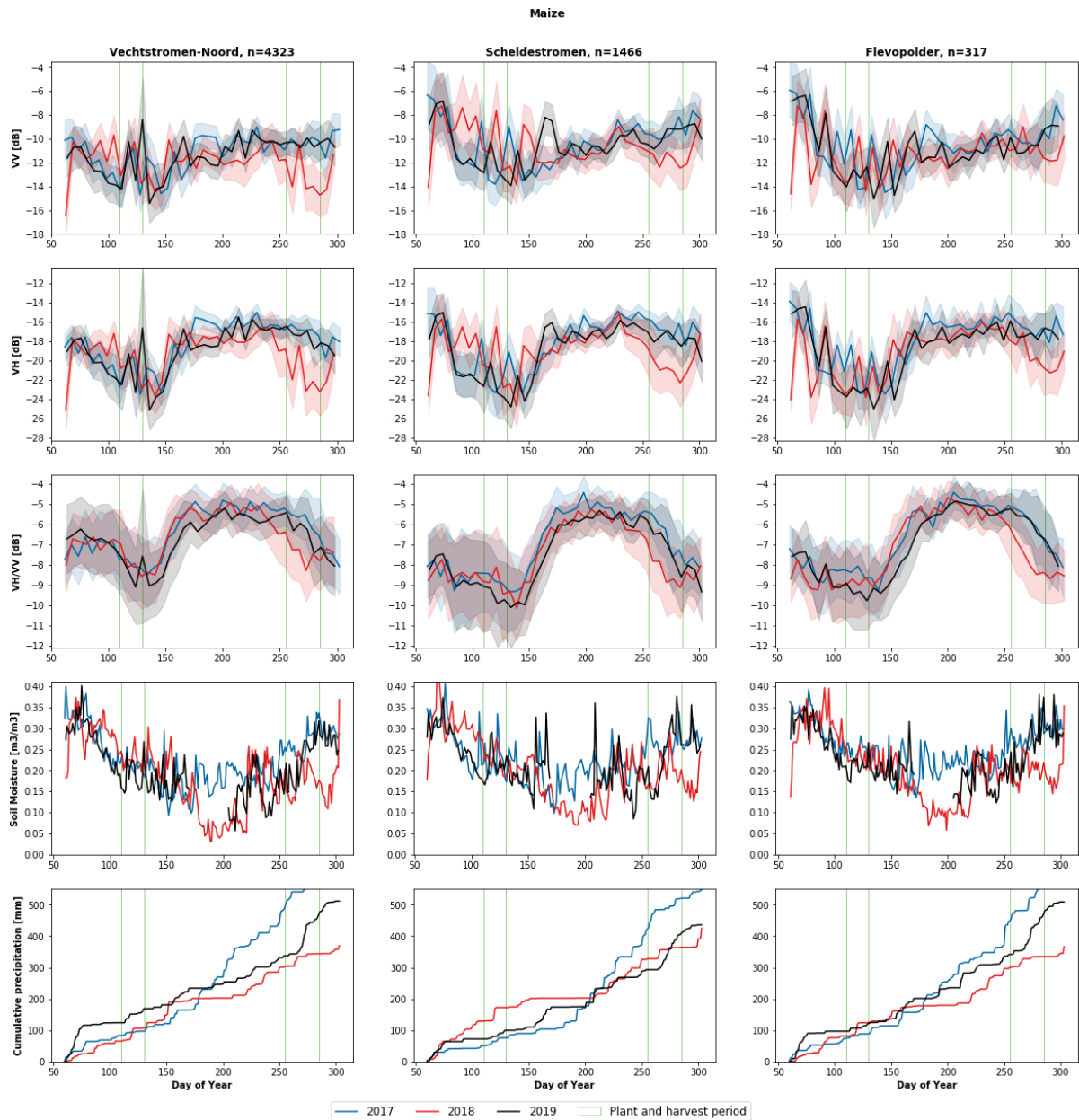


Figure 4.22: The 2017, 2018 and 2019 time series of Sentinel-1 SAR data (VV, VH and VH/VV) from maize parcels in all study areas. The colored lines represent the mean value and the shaded bands depict the standard deviation across all fields. Surface soil moisture and cumulative precipitation data is displayed in the bottom two plot. The green-outlined bars correspond to the general planting and harvest periods.

## Sugarbeet

Figure 4.23 shows the Sentinel-1 backscatter from sugar beet parcels in the study areas. The first remarkable observation is that the 2018 VV and VH backscatter values around DOY 150 are relatively low in Scheldestromen. However, the higher backscatter values in Vechtstromen-Noord and the Flevopolder are likely caused by precipitation events and their time of occurrence. Precipitation events occurred in all study areas around DOY 150. However, it is possible that the precipitation event in Scheldestromen occurred after the satellite had passed.

Furthermore, the phenomenon that is mentioned in Section 4.1.2, where VV and VH backscatter decreases during the mid-season droughts of 2018, is visible for all areas. This observation is more prominent in Vechtstromen-Noord, less in Scheldestromen and least in the Flevopolder. On top of that, the impact of the drought lasts longer in Vechtstromen-Noord, followed by Scheldestromen and the Flevopolder. This order in VH/VV ratio drop is also in accordance with the yield data in which the normalized gross yield in 2018 changed with -14.08, -11.44 and 3.99 percent compared to the 5-year average (see Figure 3.8).

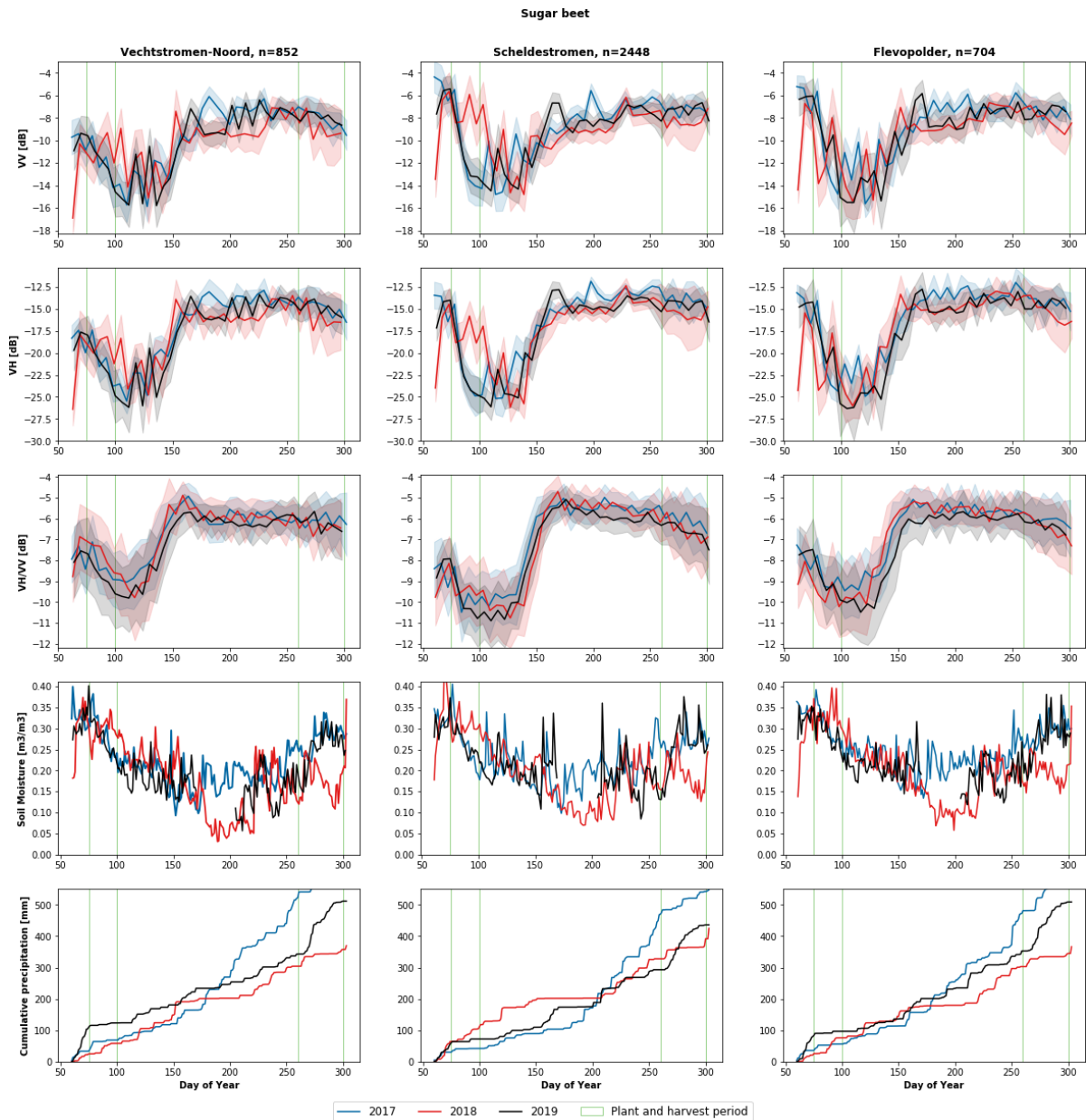


Figure 4.23: The 2017, 2018 and 2019 time series of Sentinel-1 SAR data (VV, VH and VH/VV) from sugar beet parcels in all study areas. The colored lines represent the mean value and the shaded bands depict the standard deviation across all fields. Surface soil moisture and cumulative precipitation data is displayed in the bottom two plot. The green-outlined bars correspond to the general planting and harvest periods.

A remarkable observation is that the emergence in the Flevopolder occurs later in 2019, when looking at the VH/VV ratio. This is likely not due to dry soil, since sugar beets in other areas were also planted in dry soils. Hence, it can be assumed that the sugar beets were planted later in the season in the Flevopolder.

Another difference is seen in 2019 around DOY 200. In Vechtstromen-Noord, the three precipitation events from DOY 190 till 230, observed in the cumulative precipitation and the soil moisture data, can be clearly distinguished in the VV and VH backscatter data. However, the heavy precipitation event in Scheldestromen around DOY 205 cannot be observed in the VV and VH backscatter, while crops in both areas were in the same stage. A possibility is that, even though the precipitation and the soil moisture data were acquired from a different location, the precipitation event was very local and did not affect a majority of the sugar beet crop parcels. Overall, no clear influence of the drought is observed in the VH/VV ratio time series in all three study areas.

### Potato

Figure 4.24 shows the Sentinel-1 backscatter from all potato parcels in the study areas. Similar to the sugar beet time series, a difference between the 2018 VH backscatter values around DOY 150 can be observed in which the values in Scheldestromen are lower. Again, this is likely caused by the timing or intensity of precipitation events around DOY 150 in Scheldestromen.

Another difference observed in the Sentinel-1 response of potato crops is the drop in VV and VH backscatter during the 2018 drought compared to 2017. This decrease in backscatter during the 2018 drought is observed in all study areas. However, it is clearest in Scheldestromen and Vechtstromen-Noord. Also, Scheldestromen and Vechtstromen-Noord were heavily impacted, based on the normalized gross yield data in Figure 3.8. The normalized gross yield decreased by 21.31, 25.00 and 10.52 in Vechtstromen-Noord, Scheldestromen and Flevopolder, respectively. Similar to the sugar beet time series, no clear influence of the drought is observed in the VH/VV ratio time series in all three study areas.

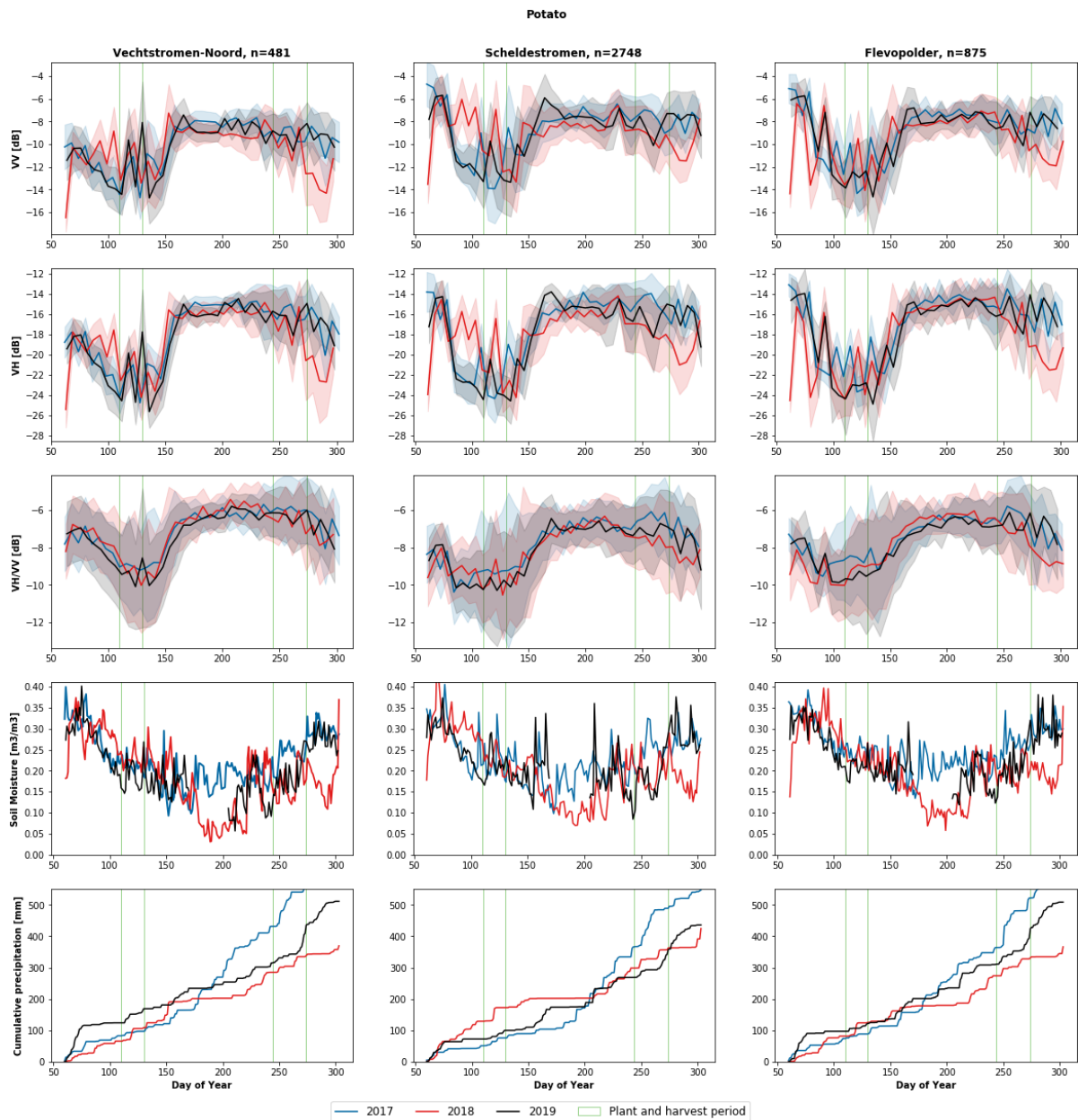


Figure 4.24: The 2017, 2018 and 2019 time series of Sentinel-1 SAR data (VV, VH and VH/VV) from potato parcels in all study areas. The colored lines represent the mean value and the shaded bands depict the standard deviation across all fields. Surface soil moisture and cumulative precipitation data is displayed in the bottom two plot. The green-outlined bars correspond to the general planting and harvest periods.

### Onion

Figure 4.25 shows the Sentinel-1 backscatter from onion parcels in the study areas. It is expected that Schelde-stromen would be the most impacted area when looking at the yield data in Figure 3.8. The normalized gross yield dropped by 23.12, 71.28 and 31.19 percent compared to the 5-year average in Vechtstromen-Noord, Scheldestromen and the Flevopolder, respectively. Scheldestromen may have been impacted the heaviest due to the lack of available fresh water for irrigation because of the increased salt intrusion in the drought period [68]. The effects of the drought are clearly observed in the VH backscatter and VH/VV ratio trend of 2018 during and after the drought period. Lower values of VH backscatter and VH/VV ratio are observed and the rapid decrease due to harvest or drying occurs sooner compared to other years. The latter is also observed for the other two areas to a lesser extent. The reason why regional variabilities are more pronounced for onions compared to other crops, is because onions are relatively more sensitive to droughts compared to the other crops. Hence, precipitation deficits and water management decisions are clearly observed provided that they are extreme enough.

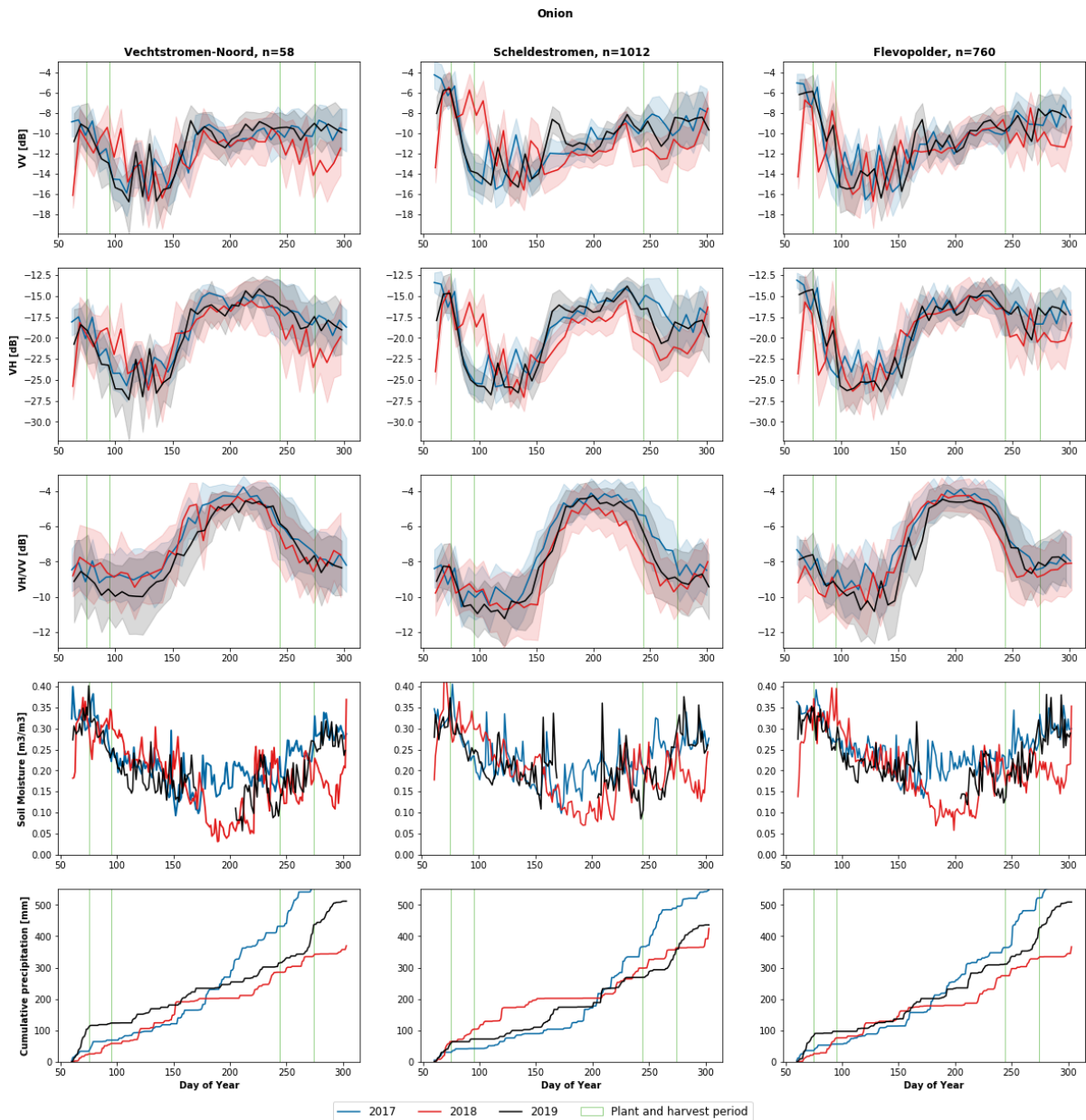


Figure 4.25: The 2017, 2018 and 2019 time series of Sentinel-1 SAR data (VV, VH and VH/VV) from onion parcels in all study areas. The colored lines represent the mean value and the shaded bands depict the standard deviation across all fields. Surface soil moisture and cumulative precipitation data is displayed in the bottom two plot. The green-outlined bars correspond to the general planting and harvest periods.

Furthermore, the 2019 VH/VV ratio data clearly displays that the root zone soil moisture in Vechtstromen-Noord had not been restored properly yet [69]. The values during and after planting until DOY 190 are ex-

tremely low compared to 2017 and 2018. This is not observed for Scheldestromen since it is situated below sea level and the soil mostly consists of clay. Therefore, 2019 VH/VV ratio does not show signs of drought early in the season for most crops.

Lastly, the effects of incidence angle are clearly observed in the VH/VV backscatter from onion parcels during emergence. During this phase, Vechtstromen-Noord has the highest VH/VV values in all years followed by Flevopolder. Scheldestromen shows the lowest values during emergence. This is in accordance with the incidence angles for the chosen orbit numbers, which is equal to  $43^\circ$ ,  $38^\circ$  and  $41^\circ$  for Vechtstromen-Noord, Scheldestromen and Flevopolder, respectively.

### Barley

Figure 4.26 shows the Sentinel-1 backscatter from barley parcels in the study areas. In Vechtstromen-Noord, the 2018 and 2019 VH/VV ratio starts diverging from the 2017 VH/VV on DOY 160. After DOY 160, the VH/VV ratio values of 2018 and 2019 are significantly lower than 2017. In Scheldestromen and the Flevopolder, this observation occurs around DOY 190. Since high temperatures, solar radiation and less precipitation lead to

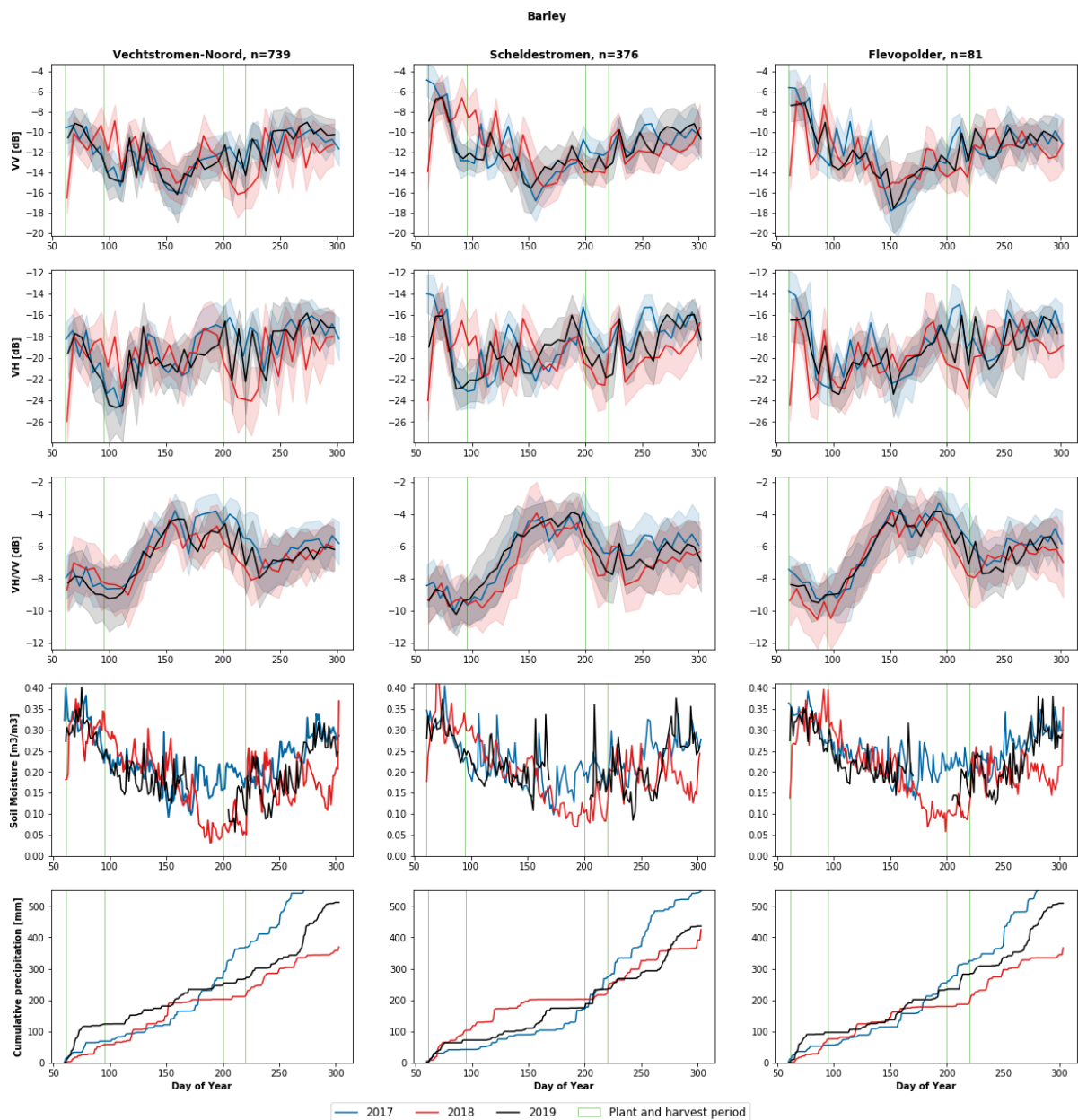


Figure 4.26: The 2017, 2018 and 2019 time series of Sentinel-1 SAR data (VV, VH and VH/VV) from barley parcels in all study areas. The colored lines represent the mean value and the shaded bands depict the standard deviation across all fields. Surface soil moisture and cumulative precipitation data is displayed in the bottom two plot. The green-outlined bars correspond to the general planting and harvest periods.

faster development of barley crops [64, 65], it can be assumed that the barley crops in Vechtstromen-Noord were impacted more heavily. However, no drop in normalized gross yield is observed in Figure 3.8. A possible explanation could be that the onset of the droughts was late in the barley cropping season since barley is planted and harvested relatively early.

Another difference between the areas is that the 2019 VH/VV trend in Scheldestromen is relatively stable compared to the noisy trend of Vechtstromen-Noord and Flevopolder. Furthermore, it seems like the barley in Scheldestromen had a slow start in 2018 when looking at the VV and the VH/VV backscatter. This could be because the barley was planted later in the season.

#### 4.2.2. Influence of irrigation on the regional variability of C-band SAR data

In this section, an analysis is given on the ability to detect the effects of irrigation or water management practices during drought on C-band SAR data from Sentinel-1. As mentioned in Section 3.1.2, the study areas in this analysis are the Coevorden, Hardenberg, Tubbergen and Hof van Twente municipality areas. Coevorden and Hardenberg are located in low-Vechtstromen while Tubbergen and Hof van Twente are located in high-Vechtstromen. Only maize and potato parcels are considered because the difference in the number of parcels between the municipalities for crops are too large to ensure a fair comparison. The Sentinel-1 backscatter from maize and potato in descending orbit 37 are presented in Figure 4.28 and 4.29, respectively. The response from maize and potato parcels in all municipalities in 2017 is extremely similar, which confirms the fact that soil and meteorological influences are mostly identical in the municipalities up until the start of the harvest. Hence, it can be assumed that any observed difference between the municipalities in high-Vechtstromen (red municipalities) and low-Vechtstromen (blue municipalities) is mainly caused by a difference in irrigation. The consideration to irrigate or not, is not only related to water availability but also to economic profitability of the crop. In the agricultural field, irrigation with surface water is preferred due to the higher temperature and the low costs compared to irrigation with groundwater. The cost of surface water irrigation is lower because the energy consumption is lower. Since the economic value of silage maize is relatively low, maize parcels are likely only irrigated with surface water. However, potatoes are only allowed to be irrigated with groundwater due to an increased risk of plant diseases when irrigating with surface water.

##### Maize

The 2018 VH/VV ratio of the red municipalities and blue municipalities starts deviating from 2017 after DOY 230. It seems that the crop season was shorter for both blue and red municipalities and that harvest was initiated earlier in 2018. However, the VH/VV ratio in the red municipalities starts decreasing earlier and faster at the end of the season compared to the VH/VV ratio in the blue municipalities. A possible explanation is that more maize parcels the red municipalities were impacted heavily by the drought due to the ban on open wa-

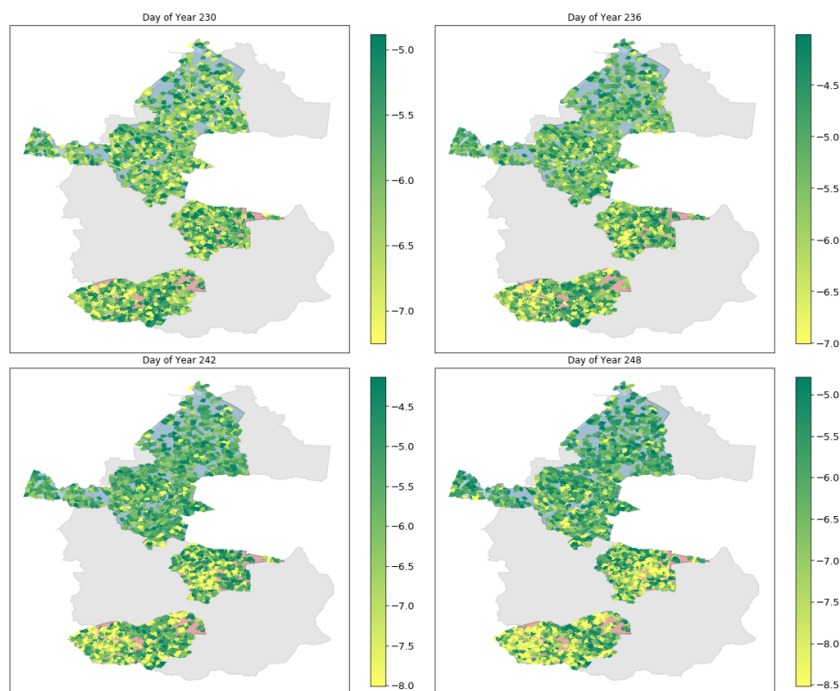


Figure 4.27: VH/VV ratio values of maize parcels in the Coevorden, Hardenberg, Tubbergen and Hof van Twente municipalities.

ter irrigation, which resulted in an earlier ripening and senescence and thus an early harvest. Both Coevorden and Hardenberg have extremely similar VH/VV ratio signatures. The same can be concluded for Tubbergen and Hof van Twente. This can also be seen in Figure 4.27 where VH/VV ratio values of maize parcels are mapped. The top-left map, which shows the VH/VV ratio on DOY 230, shows regional variability between the blue and the red municipalities. This difference increases with each subsequent SAR acquisition, resulting in a distinct difference which supports the assumption that there is a clear distinction between the red and blue municipalities with regards to irrigation policy. Furthermore, it can also be observed that after DOY 230, the standard deviation of VH/VV backscatter in the red municipalities is significantly higher than the blue municipalities. This is possibly because farmers in the red municipalities were only allowed to irrigate from groundwater. Not all farmers are willing to irrigate silage maize with groundwater since groundwater irrigation is costly. This may lead to an increase in the backscatter variation across the parcels. Also, the VH and VV backscatter is significantly lower in the red municipalities during the harvest period around DOY 260.

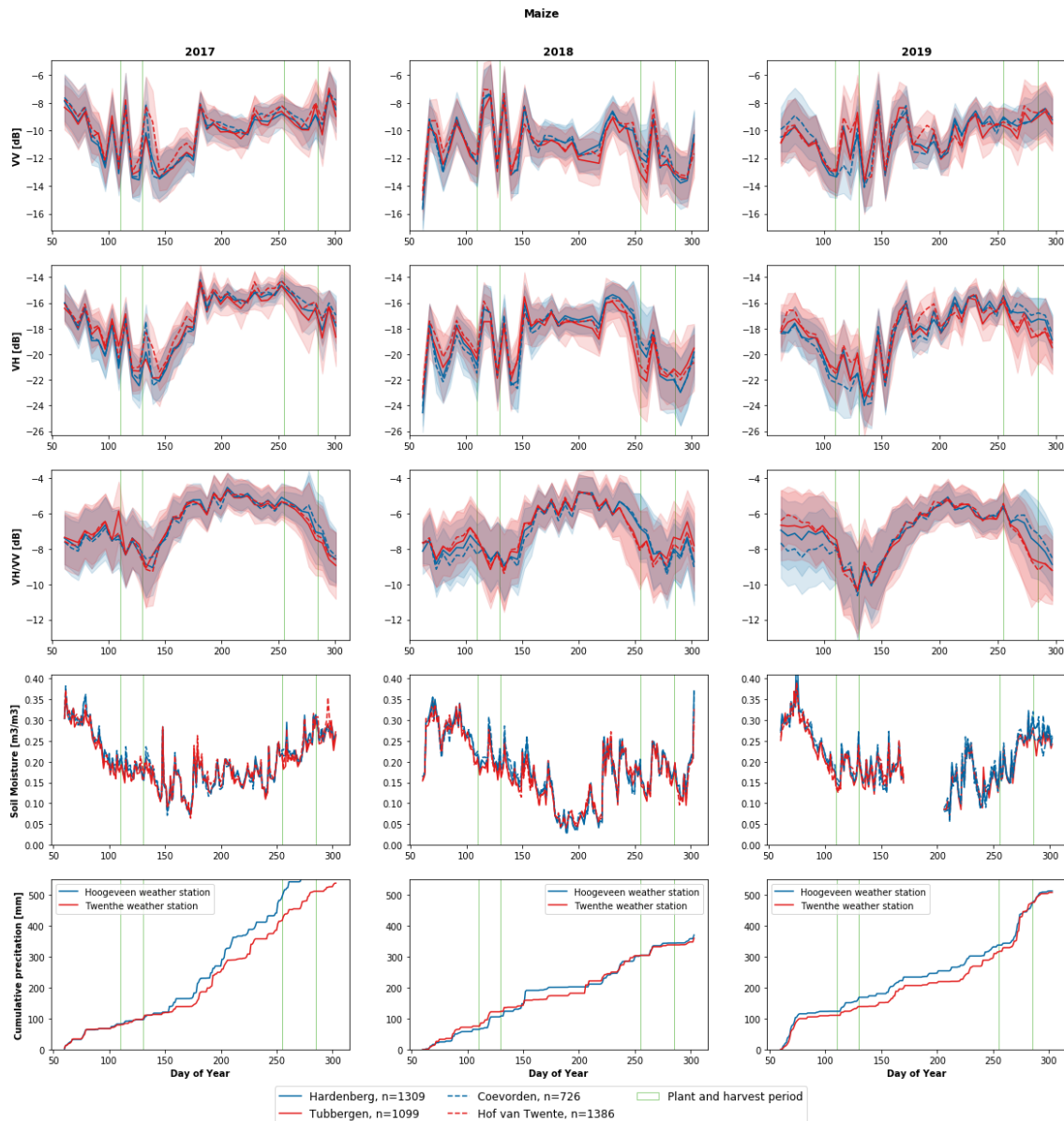


Figure 4.28: The 2017, 2018 and 2019 time series of Sentinel-1 SAR data (VV, VH and VH/VV) from maize parcels in the Coevorden, Hardenberg, Tubbergen and Hof van Twente municipalities. The colored lines represent the mean value and the shaded bands depict the standard deviation across all fields. Surface soil moisture and cumulative precipitation data is displayed in the bottom two plots. The green-outlined bars correspond to the general planting and harvest periods.

In 2019, the differences between the blue and red municipalities are extremely small until the harvest period, especially when looking at the VH/VV ratio. The VH/VV ratio in the red municipalities starts to decrease around DOY 260 while in the blue municipalities, the VH/VV ratio starts to decrease around DOY 275. Just like in 2018, the VH/VV ratio in the red municipalities starts decreasing earlier in the end of the season compared

to the VH/VV ratio in the blue municipalities. Furthermore, the standard deviation of the VH/VV ratio during harvesting is higher in the red municipalities, similar to 2018.

### Potato

The VH backscatter and VH/VV ratio response of potato parcels in 2018 start to diverge around DOY 210 when the drought nears its end. The potato results show that the Hof van Twente municipality show similar values to the blue municipalities before harvest and that the VH/VV backscatter values in Tubbergen decrease before harvest. Hence, unlike the maize time series, the VH/VV ratio responses in the red municipalities do not overlap in 2018 and 2019. A systematic differences between the VH/VV ratio in the blue and red municipalities is not expected as potatoes have to be irrigated with groundwater and all municipalities were allowed to irrigate with groundwater. It is thus expected that potato parcels in the red municipalities do not show a systematic lower or higher backscatter than potato parcels in the blue ones during droughts. At the same time, the standard deviation of the VH/VV ratio in the red municipalities starts to increase rapidly as well, resulting in an extreme difference of standard deviation between the blue and red municipalities in both orbits. A possible cause is the relatively low numbers of parcels in Tubbergen and especially Hof van Twente. The differences between the red municipalities and the blue municipalities in 2019 are similar but smaller than in 2018.

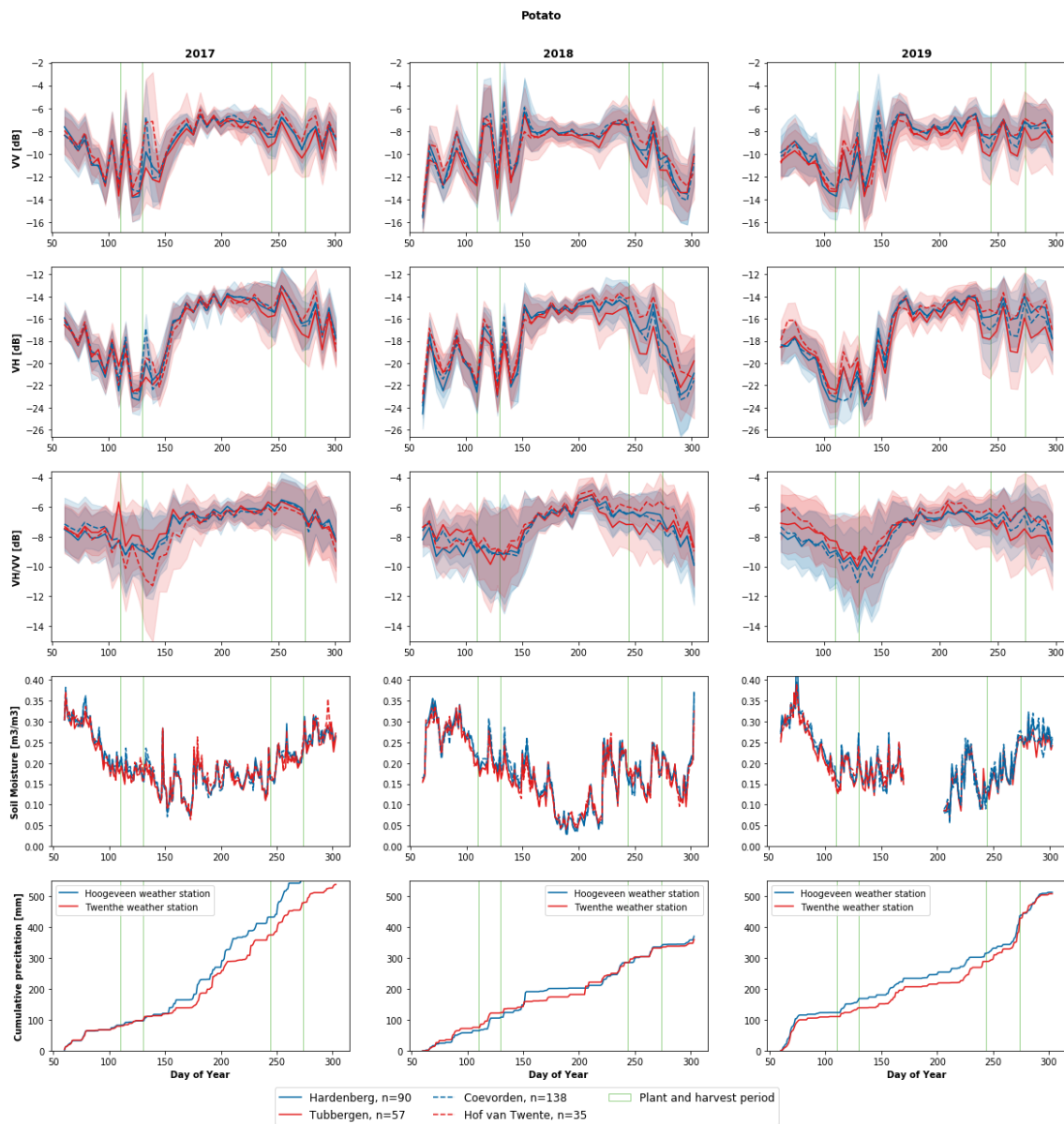


Figure 4.29: The 2017, 2018 and 2019 time series of Sentinel-1 SAR data (VV, VH and VH/VV) from potato parcels in the Coevorden, Hardenberg, Tubbergen and Hof van Twente municipalities. The colored lines represent the mean value and the shaded bands depict the standard deviation across all fields. Surface soil moisture and cumulative precipitation data is displayed in the bottom two plots. The green-outlined bars correspond to the general planting and harvest periods.

# 5

## Conclusions and Recommendations

### 5.1. Conclusions

The goal of this research was to assess the influence of drought on C-band Sentinel-1 SAR data over crop parcels in the Netherlands. To achieve this goal, research questions were posed in Section 1.3 to provide a systematic approach to ensure a robust assessment. The answers to the posed research questions and the conclusions of this research are stated below.

#### **How are phenological changes of key crops in the Netherlands reflected in C-band Sentinel-1 SAR data?**

The influence of phenological changes on SAR backscatter depends massively on the crop type. Generally, backscatter from crop parcels is low before emergence and very sensitive to changes in soil moisture. After emergence, VH backscatter and VH/VV ratio increase rapidly during leaf development and stem elongation phases. Saturation then occurs, which halts the increase and stabilizes the backscatter. During the ripening and the senescence phases, the VH and VH/VV backscatter generally decreases slowly. Lastly, the VH/VV ratio decreases rapidly during harvesting. Barley crops are the exception in terms of VV and VH backscatter, of which backscatter in both polarizations decrease during leaf development and stem elongation phases due to increasing attenuation of the soil backscatter caused by the vertical structure of the barley crops. After the heading phase, VV and VH backscatter increase because backscatter from vegetation becomes dominant over the contribution of the soil.

#### **How is drought reflected in the interannual variability of C-band Sentinel-1 SAR data?**

The results in Section 4.1.2 show that for maize, sugar beet and potato, the VV and VH backscatter is 2.5, 2 and 1 dB lower during the drought period of 2018 and 2019 compared to 2017, respectively. This observation is absent in the results for onion and barley. The lower VV and VH backscatter during drought may be caused by dry soil, reduction of VWC and changes in leaf geometry. Additional ancillary data and modelling is necessary in order to appoint the main causes of backscatter reduction during drought.

Furthermore, it was found that the seasonal VH/VV ratio cycle for maize, onion and barley is shorter in a drought year and shortest in 2018. This is caused by faster crop development and thus an earlier harvest due to dry circumstances. The VH/VV ratio cycle in 2018 was 30, 10 and 20 days shorter compared to 2017 for maize, onion and barley, respectively. However, VH/VV ratio trends for sugar beet and potato did not show significant difference in 2018 compared to 2017.

At last, the VH/VV ratio values are significantly lower during the vegetative stages in 2019 compared to the other years. This is observable for potato and onion and especially for maize and sugar beet. This is likely caused by insufficiently restored root zone soil moisture and groundwater due to lingering effects of the 2018 drought. Planting and germinating the crops in dry soil likely leads to smaller leaves and thus lower VH backscatter values.

#### **What is the influence of viewing geometry and overpass time on C-band Sentinel-1 SAR data?**

Overall, the influence of incidence angle is found to be limited to the general offset of the backscatter values. Hence, the influence of the incidence angle on the drought-induced interannual variability of Sentinel-1 backscatter time series is found to be negligible. On the other hand, the overpass time is found to have significant influence on drought-induced interannual variability. The magnitude of the drop in VV and VH backscatter during drought periods was larger in descending orbits, which pass the Netherlands around 05:45, especially for sugar beet and potato crops. A possible cause for this is that differences in VWC are more apparent in the morning due to the water management of the crops. Another possibility is that the dif-

ferences in backscatter between the dry and normal years are caused by difference in surface canopy water content due to dew formation on the leaves in the morning.

#### **Are the drought observations aggregated across all parcels reflected in individual parcels?**

Aggregated drought responses in Section 4.1.2 are also observed for a majority of the individual parcels. Around 78% of the individual maize parcels had a shorter VH/VV ratio cycle in 2018 and 94% of the individual parcels had lower VH backscatter values during the 2018 drought, compared with 2017. For potato, the percentage of individual parcels that had lower VH backscatter values during the drought period compared to 2017 was between 68% and 80% in 2018 and 100% in 2019. For barley, around 90% of the individual parcels in 2018 and 2019 showed shorter VH/VV ratio cycle compared to 2017. This gives a promising outlook on the use of dense C-band SAR data for the detection of crop drought stress and drought stress monitoring for farmers and decision-makers.

#### **What is the drought-induced regional variability of C-band Sentinel-1 SAR data?**

The regional variability was assessed by comparing the Sentinel-1 backscatter time series in the study areas. Due to many factors, including soil type, hydrometeorological conditions and irrigation policies, being dissimilar between the study areas, appointing the cause of observed regional variability is difficult.

Generally, drought responses were most extreme in Vechtstromen-Noord. This is to be expected since this area is most vulnerable to droughts due to its sandy soil. For maize, the VH/VV ratio in 2018 starts dropping approximately 40, 25, 10 days earlier than 2017 at the end of the season in Vechtstromen-Noord, Scheldestromen and Flevopolder, respectively. This is in accordance with the yield data. For sugar beets, the drop in VV and VH backscatter is largest in magnitude and duration in Vechtstromen-Noord compared to other study areas. Also, Vechtstromen-Noord had a harder time recharging groundwater as a response to the 2018 drought, which leads to this area being impacted heavier at the start of 2019. In turn, this led to lower VH/VV ratio values for maize, sugar beet and onion in this area.

However, onion crops in 2018 were impacted most in Scheldestromen according to yield data. This clearly translated into lower VH backscatter and VH/VV ratio values during and after the drought period.

#### **Is the influence of irrigation during drought reflected in C-band Sentinel-1 SAR data?**

The influence of irrigation during drought on Sentinel-1 backscatter time series was analyzed for maize and potato crops. In the maize time series, the influence of irrigation was clearly observed in the VH/VV ratio values during harvest. An early harvest is observed in areas in which farmers were not allowed to irrigate with open water, compared to areas in which farmers were allowed to irrigate with open water. No distinct difference was observed in the VV and VH backscatter during the drought period. No distinct systematic differences were found between the two types of areas in the potato time series. This was expected as potato crops are generally irrigated with groundwater.

Overall, the usage of Sentinel-1 SAR data for drought monitoring purposes showed tremendous potential. Sentinel-1 SAR data is not affected by cloud cover and thus reliably provides backscatter data with a return period of 6 days without combining data from different orbits. The influences of drought are clearly observed in Sentinel-1 SAR data aggregated across multiple crop parcels, especially descending orbits. Drought responses are also observed for a majority of the individual parcels. This gives a promising outlook on future development and use of commercial products that use dense C-band SAR data for prediction and decision-making purposes. Especially for crops for which VV and VH backscatter significantly reduces during a drought period and therefore allows for real-time drought detection.

A disadvantage of using SAR data for drought detection is that the response is complex and hard to interpret for farmers, policy-makers and others with little to no knowledge of SAR remote sensing. Furthermore, it is difficult to validate and interpret the data without ancillary data such as precipitation and soil moisture because there is no reliable way to distinguish between the causes of temporal changes. Also, observed drought responses do not necessarily lead to a reduction in gross yield. Moreover, the drought responses vary greatly for different crop types.

## **5.2. Recommendations**

This research intends to serve as a foundation for investigating agricultural drought detection using microwave remote sensing. Naturally, further research needs to be done in order to have a better understanding of the opportunities and the limitations of using SAR data for drought monitoring purposes. Further research topics and general remarks are summed up below.

**Case study with ground-truth data**

This research performed aggregated analyses which deal with a lack of ancillary data. Hence, a smaller and controlled case study involving several parcels of different crops will be useful to validate the findings of this research and find new drought related responses. It is desirable to cooperate with farmers since they are able to provide frequent ancillary data such as field photos. In addition, local temperature, soil moisture and precipitation measurements (combined with field photos) will make validation easier.

**Combine data from different early morning passes**

This study showed that data from descending orbits of Sentinel-1, that pass the Netherlands around 05:45, are especially useful for agricultural drought monitoring purposes. Furthermore, the influence of incidence angle on the SAR response during drought was found to be negligible. Combining data from early morning passes whenever possible increases the temporal resolution.

**Investigate drought response of different crop types**

Maize, sugar beet, potato, onion and barley were studied in this research. Further research needs to be done on other crop types such as soy, rapeseed, and other vegetable crops to better understand the limitations and benefits of using SAR for agricultural drought monitoring purposes.

**Compare SAR response with different optical indices such as NDVI**

Optical sensors are also used for agricultural drought monitoring. Hence, a (case) study which compares the response of SAR with the response of an optical index during drought will showcase the benefits and drawbacks of SAR. An analysis on whether SAR can detect drought earlier than NDVI will also be interesting since SAR is sensitive to VWC and the NDVI is mostly an indicator of greenness. During a drought, changes in VWC occur earlier than changes to greenness.

**Investigate relation between interannual differences and yield**

This research showed that drought observation in SAR data, such as reduced VH backscatter and VH/VV ratio do not necessarily translate to lower yield. The magnitude and the period length of the drought observations are likely important factors with regards to yield. Additional research needs to be done on this relation to find the best indicator for decreased gross yield.

**Agricultural drought influence on other bands such as S-band or L-band**

This research used data acquired by Sentinel-1 which is C-band SAR data. SARs operating at other bands, such as S-band and L-band, have different properties regarding penetration depth and the interaction with crops. Hence, additional research using data from a satellite with suitable spatio-temporal resolution operating at a different band such as ALOS-2 (L-band) will be useful. Planned missions of interest include NISAR (L-band and S-band) and ROSE-L (L-band).

# Bibliography

- [1] H. Charles J. Godfray, John R. Beddington, Ian R. Crute, Lawrence Haddad, David Lawrence, James F. Muir, Jules Pretty, Sherman Robinson, Sandy M. Thomas, and Camilla Toulmin. Food security: the challenge of feeding 9 billion people. *Science*, 327(5967):812–818, 2010. ISSN 0036-8075. doi: 10.1126/science.1185383. URL <https://science.sciencemag.org/content/327/5967/812>. American Association for the Advancement of Science.
- [2] Josef Schmidhuber and Francesco N. Tubiello. Global food security under climate change. *Proceedings of the National Academy of Sciences*, 104(50):19703–19708, 2007. ISSN 0027-8424. doi: 10.1073/pnas.0701976104. URL <https://www.pnas.org/content/104/50/19703>.
- [3] Nikos Alexandratos and Jelle Bruinsma. World Agriculture towards 2030/2050: the 2012 revision, June 2012. ESA Working paper No. 12-03. Rome, FAO.
- [4] Yinpeng Li, Wei Ye, Meng Wang, and Xiaodong Yan. Climate change and drought: a risk assessment of crop-yield impacts. *Climate Research*, 39(1):31–46, May 2009. ISSN 0936-577X, 1616-1572. doi: 10.3354/cr00797. URL <https://www.int-res.com/abstracts/cr/v39/n1/p31-46/>.
- [5] Petr Hlavinka, Miroslav Trnka, Daniela Semerádová, Martin Dubrovský, Zdeněk Žalud, and Martin Možný. Effect of drought on yield variability of key crops in Czech Republic. *Agricultural and Forest Meteorology*, 149(3):431–442, March 2009. ISSN 0168-1923. doi: 10.1016/j.agrformet.2008.09.004. URL <http://www.sciencedirect.com/science/article/pii/S0168192308002487>.
- [6] Seyed Yahya Salehi-Lisar and Hamideh Bakhshayeshan-Agdam. Drought Stress in Plants: Causes, Consequences, and Tolerance. In Mohammad Anwar Hossain, Shabir Hussain Wani, Soumen Bhattacharjee, David J Burritt, and Lam-Son Phan Tran, editors, *Drought Stress Tolerance in Plants, Vol 1: Physiology and Biochemistry*, pages 1–16. Springer International Publishing, Cham, 2016. ISBN 978-3-319-28899-4. doi: 10.1007/978-3-319-28899-4\_1. URL [https://doi.org/10.1007/978-3-319-28899-4\\_1](https://doi.org/10.1007/978-3-319-28899-4_1).
- [7] A. Lopez-Nicolas, M. Pulido-Velazquez, and H. Macian-Sorribes. Economic risk assessment of drought impacts on irrigated agriculture. *Journal of Hydrology*, 550:580–589, July 2017. ISSN 0022-1694. doi: 10.1016/j.jhydrol.2017.05.004. URL <http://www.sciencedirect.com/science/article/pii/S0022169417302822>.
- [8] Jie Zhang, Pietro Elia Campana, Tian Yao, Yang Zhang, Anders Lundblad, Forrest Melton, and Jinyue Yan. The water-food-energy nexus optimization approach to combat agricultural drought: a case study in the United States. *Applied Energy*, 227:449–464, October 2018. ISSN 0306-2619. doi: 10.1016/j.apenergy.2017.07.036. URL <http://www.sciencedirect.com/science/article/pii/S030626191730908X>.
- [9] Joo Heon Lee and Chang Joo Kim. A multimodel assessment of the climate change effect on the drought severity–duration–frequency relationship. *Hydrological Processes*, 27(19):2800–2813, 2013. ISSN 1099-1085. doi: 10.1002/hyp.9390. URL <https://onlinelibrary.wiley.com/doi/abs/10.1002/hyp.9390>.
- [10] Justin Sheffield and Eric F. Wood. Projected changes in drought occurrence under future global warming from multi-model, multi-scenario, IPCC AR4 simulations. *Climate Dynamics*, 31(1):79–105, July 2008. ISSN 1432-0894. doi: 10.1007/s00382-007-0340-z. URL <https://doi.org/10.1007/s00382-007-0340-z>.
- [11] Rasmus Houborg and Matthew F. McCabe. Daily Retrieval of NDVI and LAI at 3 m Resolution via the Fusion of CubeSat, Landsat, and MODIS Data. *Remote Sensing*, 10(6):890, June 2018. doi: 10.3390/rs10060890. URL <https://www.mdpi.com/2072-4292/10/6/890>.
- [12] Bin Wang, Atsuo Ono, Kanako MURAMATSU, and Noboru FUJIWARA. *Automated Detection and Removal of Clouds and Their Shadows from Landsat TM Images*. 1999.

- [13] Tamme van der Wal, Bauke Abma, Antidio Viguria, Emanuel Prévinaire, Pablo Zarco-Tejada, Philippe Serruys, Eric Valkengoed, and Paul Voet. FieldCopter: unmanned aerial systems for crop monitoring services. July 2013.
- [14] Mariette Vreugdenhil, Wolfgang Wagner, Bernhard Bauer-Marschallinger, Isabella Pfeil, Irene Teubner, Christoph Rüdiger, and Peter Strauss. Sensitivity of Sentinel-1 Backscatter to Vegetation Dynamics: An Austrian Case Study. *Remote Sensing*, 10(9):1396, September 2018. doi: 10.3390/rs10091396. URL <https://www.mdpi.com/2072-4292/10/9/1396>.
- [15] Heather McNairn and Jiali Shang. A Review of Multitemporal Synthetic Aperture Radar (SAR) for Crop Monitoring. In Yifang Ban, editor, *Multitemporal Remote Sensing: Methods and Applications*, Remote Sensing and Digital Image Processing, pages 317–340. Springer International Publishing, Cham, 2016. ISBN 978-3-319-47037-5. doi: 10.1007/978-3-319-47037-5\_15. URL [https://doi.org/10.1007/978-3-319-47037-5\\_15](https://doi.org/10.1007/978-3-319-47037-5_15).
- [16] Ramon Torres, Paul Snoeij, Dirk Geudtner, David Bibby, Malcolm Davidson, Evert Attema, Pierre Potin, Björn Rommen, Nicolas Floury, Mike Brown, Ignacio Navas Traver, Patrick Deghaye, Berthyl Duesmann, Betlem Rosich, Nuno Miranda, Claudio Bruno, Michelangelo L'Abbate, Renato Croci, Andrea Pietropaolo, Markus Huchler, and Friedhelm Rostan. GMES Sentinel-1 mission. *Remote Sensing of Environment*, 120:9–24, May 2012. ISSN 00344257. doi: 10.1016/j.rse.2011.05.028. URL <https://linkinghub.elsevier.com/retrieve/pii/S0034425712000600>.
- [17] ESA. Observation Scenario Sentinel-1. URL <https://sentinel.esa.int/web/sentinel/missions/sentinel-1/observation-scenario>. accessed on 4 February 2020.
- [18] Mark Dolman, Gerben Jukema, and Pascal Ramaekers. De Nederlandse landbouwexport 2018 in breder perspectief. Technical Report 2019-001, Wageningen Economic Research, Wageningen, 2019. URL <https://doi.org/10.18174/468099>.
- [19] CBS. GDP, output and expenditures; changes, Quarterly National Accounts. URL <https://opendata.cbs.nl/statline/#/CBS/en/dataset/84106ENG/table?ts=1599577906474>. accessed on 5 December 2019.
- [20] Vittal Hari, Oldrich Rakovec, Yannis Markonis, Martin Hanel, and Rohini Kumar. Increased future occurrences of the exceptional 2018–2019 Central European drought under global warming. *Scientific Reports*, 10(1):12207, August 2020. ISSN 2045-2322. doi: 10.1038/s41598-020-68872-9. URL <https://www.nature.com/articles/s41598-020-68872-9>. Number: 1 Publisher: Nature Publishing Group.
- [21] CBS. Arable crops; production, to region. URL <https://opendata.cbs.nl/#/CBS/en/dataset/7100eng/table?ts=1599577672463>. accessed on 22 May 2020.
- [22] Wolfgang Wagner, Guido Lemoine, and Helmut Rott. A Method for Estimating Soil Moisture from ERS Scatterometer and Soil Data. *Remote Sensing of Environment*, 70(2):191–207, November 1999. ISSN 00344257. doi: 10.1016/S0034-4257(99)00036-X. URL <https://linkinghub.elsevier.com/retrieve/pii/S003442579900036X>.
- [23] Yann H. Kerr, Philippe Waldteufel, Philippe Richaume, Jean Pierre Wigneron, Paolo Ferrazzoli, Ali Mahmoodi, Ahmad Al Bitar, François Cabot, Claire Gruhier, Silvia Enache Juglea, Delphine Leroux, Arnaud Mialon, and Steven Delwart. The SMOS Soil Moisture Retrieval Algorithm. *IEEE Transactions on Geoscience and Remote Sensing*, 50(5):1384–1403, May 2012. ISSN 0196-2892, 1558-0644. doi: 10.1109/TGRS.2012.2184548. URL <http://ieeexplore.ieee.org/document/6161633/>.
- [24] Robert M. Parinussa, Thomas R. H. Holmes, Niko Wanders, Wouter A. Dorigo, and Richard A. M. de Jeu. A Preliminary Study toward Consistent Soil Moisture from AMSR2. *Journal of Hydrometeorology*, 16(2):932–947, April 2015. ISSN 1525-755X, 1525-7541. doi: 10.1175/JHM-D-13-0200.1. URL <http://journals.ametsoc.org/doi/10.1175/JHM-D-13-0200.1>.
- [25] R. van der Schalie, R.M. Parinussa, L.J. Renzullo, A.I.J.M. van Dijk, C.-H. Su, and R.A.M. de Jeu. SMOS soil moisture retrievals using the land parameter retrieval model: Evaluation over the Murrumbidgee Catchment, southeast Australia. *Remote Sensing of Environment*, 163:70–79, June 2015. ISSN

00344257. doi: 10.1016/j.rse.2015.03.006. URL <https://linkinghub.elsevier.com/retrieve/pii/S0034425715001029>.
- [26] Yi Y. Liu, Richard A. M. de Jeu, Matthew F. McCabe, Jason P. Evans, and Albert I. J. M. van Dijk. Global long-term passive microwave satellite-based retrievals of vegetation optical depth: LONG-TERM VEGETATION OPTICAL DEPTH. *Geophysical Research Letters*, 38(18):n/a–n/a, September 2011. ISSN 00948276. doi: 10.1029/2011GL048684. URL <http://doi.wiley.com/10.1029/2011GL048684>.
- [27] Matthew O. Jones, Lucas A. Jones, John S. Kimball, and Kyle C. McDonald. Satellite passive microwave remote sensing for monitoring global land surface phenology. *Remote Sensing of Environment*, 115(4): 1102–1114, April 2011. ISSN 00344257. doi: 10.1016/j.rse.2010.12.015. URL <https://linkinghub.elsevier.com/retrieve/pii/S0034425710003615>.
- [28] Kaighin Alexander McColl, Dara Entekhabi, and María Piles. Uncertainty Analysis of Soil Moisture and Vegetation Indices Using Aquarius Scatterometer Observations. *IEEE Transactions on Geoscience and Remote Sensing*, 52(7):4259–4272, July 2014. ISSN 1558-0644. doi: 10.1109/TGRS.2013.2280701.
- [29] Mariette Vreugdenhil, Wouter A. Dorigo, Wolfgang Wagner, Richard A. M. de Jeu, Sebastian Hahn, and Margreet J. E. van Marle. Analyzing the Vegetation Parameterization in the TU-Wien ASCAT Soil Moisture Retrieval. *IEEE Transactions on Geoscience and Remote Sensing*, 54(6):3513–3531, June 2016. ISSN 0196-2892, 1558-0644. doi: 10.1109/TGRS.2016.2519842. URL <http://ieeexplore.ieee.org/document/7410033/>.
- [30] Grant Wiseman, Heather McNairn, Saeid Homayouni, and Jiali Shang. RADARSAT-2 Polarimetric SAR Response to Crop Biomass for Agricultural Production Monitoring. *IEEE Journal of Selected Topics in Applied Earth Observations and Remote Sensing*, 7(11):4461–4471, November 2014. ISSN 2151-1535. doi: 10.1109/JSTARS.2014.2322311. Conference Name: IEEE Journal of Selected Topics in Applied Earth Observations and Remote Sensing.
- [31] Fan Wu, Chao Wang, Hong Zhang, Bo Zhang, and Yixian Tang. Rice Crop Monitoring in South China With RADARSAT-2 Quad-Polarization SAR Data. *IEEE Geoscience and Remote Sensing Letters*, 8(2): 196–200, March 2011. ISSN 1558-0571. doi: 10.1109/LGRS.2010.2055830. Conference Name: IEEE Geoscience and Remote Sensing Letters.
- [32] Chen Liu, Jiali Shang, Paris W. Vachon, and Heather McNairn. Multiyear Crop Monitoring Using Polarimetric RADARSAT-2 Data. *IEEE Transactions on Geoscience and Remote Sensing*, 51(4): 2227–2240, April 2013. ISSN 1558-0644. doi: 10.1109/TGRS.2012.2208649. Conference Name: IEEE Transactions on Geoscience and Remote Sensing.
- [33] Yuza Suga and Tomohisa Konishi. Rice crop monitoring using X, C and L band SAR data. page 710410, Cardiff, Wales, United Kingdom, October 2008. doi: 10.1117/12.800051. URL <http://proceedings.spiedigitallibrary.org/proceeding.aspx?doi=10.1117/12.800051>.
- [34] Amanda Veloso, Stéphane Mermoz, Alexandre Bouvet, Thuy Le Toan, Milena Planells, Jean-François Dejoux, and Eric Ceschia. Understanding the temporal behavior of crops using Sentinel-1 and Sentinel-2-like data for agricultural applications. *Remote Sensing of Environment*, 199:415–426, September 2017. ISSN 0034-4257. doi: 10.1016/j.rse.2017.07.015. URL <http://www.sciencedirect.com/science/article/pii/S0034425717303309>.
- [35] Saeed Khabbazan, Paul Vermunt, Susan Steele-Dunne, Lexy Ratering Arntz, Caterina Marinetti, Dirk van der Valk, Lorenzo Iannini, Ramses Molijn, Kees Westerdijk, and Corné van der Sande. Crop Monitoring Using Sentinel-1 Data: A Case Study from The Netherlands. *Remote Sensing*, 11(16):1887, January 2019. doi: 10.3390/rs11161887. URL <https://www.mdpi.com/2072-4292/11/16/1887>.
- [36] Ali Nasrallah, Nicolas Baghdadi, Mohammad El Hajj, Talal Darwish, Hatem Belhouchette, Ghaleb Faour, Salem Darwich, and Mario Mhawej. Sentinel-1 Data for Winter Wheat Phenology Monitoring and Mapping. *Remote Sensing*, 11(19):2228, January 2019. doi: 10.3390/rs11192228. URL <https://www.mdpi.com/2072-4292/11/19/2228>.
- [37] Rudiyanto, Budiman Minasny, Ramisah M. Shah, Norhidayah Che Soh, Chusnul Arif, and Budi Indra Setiawan. Automated Near-Real-Time Mapping and Monitoring of Rice Extent, Cropping Patterns, and Growth Stages in Southeast Asia Using Sentinel-1 Time Series on a Google Earth Engine Platform. *Remote Sensing*, 11(14):1666, January 2019. doi: 10.3390/rs11141666. URL <https://www.mdpi.com/2072-4292/11/14/1666>.

- [38] ESA. Acquisition Modes Sentinel-1, . URL <https://sentinel.esa.int/web/sentinel/user-guides/sentinel-1-sar/acquisition-modes>. accessed on 24 November 2020.
- [39] ESA. Data Products Sentinel-1, . URL <https://sentinel.esa.int/web/sentinel/missions/sentinel-1/data-products>. accessed on 24 November 2020.
- [40] A. Freeman and S.L. Durden. A three-component scattering model for polarimetric SAR data. *IEEE Transactions on Geoscience and Remote Sensing*, 36(3):963–973, May 1998. ISSN 1558-0644. doi: 10.1109/36.673687. Conference Name: IEEE Transactions on Geoscience and Remote Sensing.
- [41] Sybrand van Beijma, Alexis Comber, and Alistair Lamb. Use of airborne polarimetric SAR, optical and elevation data for mapping and monitoring of salt marsh vegetation habitats. page 92430N, Amsterdam, Netherlands, October 2014. doi: 10.1117/12.2066487. URL <http://proceedings.spiedigitallibrary.org/proceeding.aspx?doi=10.1117/12.2066487>.
- [42] M. Craig Dobson and Fawwaz T. Ulaby. Mapping soil moisture distribution with imaging radar. *Principles and applications of imaging radar, manual of remote sensing*, 2:407–433, 1998.
- [43] Jack F. Paris. Radar Backscattering Properties of Corn And Soybeans at Frequencies of 1.6, 4.75, And 13.3 GHz. *IEEE Transactions on Geoscience and Remote Sensing*, GE-21(3):392–400, July 1983. ISSN 0196-2892. doi: 10.1109/TGRS.1983.350472. URL <http://ieeexplore.ieee.org/document/4157424/>.
- [44] Lingli Zhao, Jie Yang, Pingxiang Li, Xin Huang, Lei Shi, and Liangpei Zhang. Characterization of the coherent scattering induced by ridging patterns in agriculture by the use of polarimetric SAR imagery. *International Journal of Remote Sensing*, 38(12):3502–3518, June 2017. ISSN 0143-1161. doi: 10.1080/01431161.2017.1297545. URL <https://doi.org/10.1080/01431161.2017.1297545>. Publisher: Taylor & Francis \_eprint: <https://doi.org/10.1080/01431161.2017.1297545>.
- [45] Heather McNairn, Jiali Shang, Xianfeng Jiao, and Catherine Champagne. The Contribution of ALOS PALSAR Multipolarization and Polarimetric Data to Crop Classification. *IEEE Transactions on Geoscience and Remote Sensing*, 47(12):3981–3992, December 2009. ISSN 1558-0644. doi: 10.1109/TGRS.2009.2026052.
- [46] PAOLO Ferrazzoli, Simonetta Paloscia, Paolo Pampaloni, GIOVANNI Schiavon, DOMENICO Solimini, and Peter Coppo. Sensitivity of microwave measurements to vegetation biomass and soil moisture content: A case study. *IEEE Transactions on Geoscience and Remote Sensing*, 30(4):750–756, 1992.
- [47] Susan C. Steele-Dunne, Heather McNairn, Alejandro Monsivais-Huertero, Jasmeet Judge, Pang-Wei Liu, and Kostas Papathanassiou. Radar Remote Sensing of Agricultural Canopies: A Review. *IEEE Journal of Selected Topics in Applied Earth Observations and Remote Sensing*, 10(5):2249–2273, May 2017. ISSN 1939-1404, 2151-1535. doi: 10.1109/JSTARS.2016.2639043.
- [48] Francesco Mattia, Thuy Le Toan, Ghislain Picard, Francesco I. Posa, Angelo D’Alessio, Claudia Notarnicola, Anna Maria Gatti, Michele Rinaldi, Giuseppe Satalino, and Guido Pasquariello. Multitemporal C-band radar measurements on wheat fields. *IEEE Transactions on Geoscience and Remote Sensing*, 41(7):1551–1560, 2003.
- [49] Pete Mouginis. Introduction to Radar Remote Sensing, 2017. URL [http://satftp.soest.hawaii.edu/space/hawaii/vfts/kilauea/radar\\_ex/page2.html](http://satftp.soest.hawaii.edu/space/hawaii/vfts/kilauea/radar_ex/page2.html). accessed on 19 July 2020.
- [50] Xianfeng Jiao, Heather McNairn, Jiali Shang, Elizabeth Pattey, Jianguo Liu, and Catherine Champagne. The sensitivity of RADARSAT-2 polarimetric SAR data to corn and soybean leaf area index. *Canadian Journal of Remote Sensing*, 37(1):69–81, 2011.
- [51] H McNairn and B Brisco. The application of C-band polarimetric SAR for agriculture: a review. *Canadian Journal of Remote Sensing*, 30(3):18, 2004.
- [52] S.C.M. Brown, S. Quegan, K. Morrison, J.C. Bennett, and G. Cookmartin. High-resolution measurements of scattering in wheat canopies-implications for crop parameter retrieval. *IEEE Transactions on Geoscience and Remote Sensing*, 41(7):1602–1610, July 2003. ISSN 0196-2892. doi: 10.1109/TGRS.2003.814132. URL <http://ieeexplore.ieee.org/document/1221815/>.

- [53] Kurt Thelen. Assessing drought stress effects on corn yield, June 2007. URL [https://www.canr.msu.edu/news/assessing\\_drought\\_stress\\_effects\\_on\\_corn\\_yield](https://www.canr.msu.edu/news/assessing_drought_stress_effects_on_corn_yield). Michigan State University Extension.
- [54] Sylvester Anami, Marc De Block, Jesse Machuka, and Mieke Van Lijsebettens. Molecular Improvement of Tropical Maize for Drought Stress Tolerance in Sub-Saharan Africa. *Critical Reviews in Plant Sciences*, 28(1-2):16–35, March 2009. ISSN 0735-2689, 1549-7836. doi: 10.1080/07352680802665305. URL <http://www.tandfonline.com/doi/abs/10.1080/07352680802665305>.
- [55] Urs Schmidhalter, Michel Evequoz, Karl-Heinz Camp, and Christoph Studer. Sequence of drought response of maize seedlings in drying soil. *Physiologia Plantarum*, 104(2):159–168, October 1998. ISSN 0031-9317, 1399-3054. doi: 10.1034/j.1399-3054.1998.1040203.x. URL <http://doi.wiley.com/10.1034/j.1399-3054.1998.1040203.x>.
- [56] M. Abdollahian-Noghabi and R. J. Froud-Williams. Effect of moisture stress and re-watering on growth and dry matter partitioning in three cultivars of sugar beet. *Aspects of Applied Biology (United Kingdom)*, 1998.
- [57] Barbara Shaw, T H Thomas, and D T Cooke. Responses of sugar beet (*Beta vulgaris* L.) to drought and nutrient deficiency stress. page 8.
- [58] Kay F. Brown, A. B. Messemer, R. J. Dunham, and P. V. Biscoe. Effect of drought on growth and water use of sugar beet. *The Journal of Agricultural Science*, 109(3):421–435, December 1987. ISSN 0021-8596, 1469-5146. doi: 10.1017/S0021859600081636. URL [https://www.cambridge.org/core/product/identifier/S0021859600081636/type/journal\\_article](https://www.cambridge.org/core/product/identifier/S0021859600081636/type/journal_article).
- [59] Fahed Albiski, Safaa Najla, Rabab Sanoubar, Nour Alkabani, and Ramzi Murshed. In vitro screening of potato lines for drought tolerance. *Physiology and Molecular Biology of Plants*, 18(4):315–321, October 2012. ISSN 0974-0430. doi: 10.1007/s12298-012-0127-5. URL <https://doi.org/10.1007/s12298-012-0127-5>.
- [60] Luisa Dalla Costa, G. Delle Vedove, G. Gianquinto, R. Giovanardi, and A. Peressotti. Yield, water use efficiency and nitrogen uptake in potato: influence of drought stress. *Potato Research*, 40(1):19–34, March 1997. ISSN 0014-3065, 1871-4528. doi: 10.1007/BF02407559. URL <http://link.springer.com/10.1007/BF02407559>.
- [61] Jude E. Obidiegwu, Glenn J. Bryan, Hamlyn G. Jones, and Ankush Prashar. Coping with drought: stress and adaptive responses in potato and perspectives for improvement. *Frontiers in Plant Science*, 6, 2015. ISSN 1664-462X. doi: 10.3389/fpls.2015.00542. URL <https://www.frontiersin.org/articles/10.3389/fpls.2015.00542/full>. Publisher: Frontiers.
- [62] B. R. de Lis, I. Ponce, J. B. Cavagnaro, and R. M. Tizio. Studies of Water Requirements of Horticultural Crops: II. Influence of Drought at Different Growth Stages of Onion1. *Agronomy Journal*, 59(6): 573–576, 1967. ISSN 1435-0645. doi: 10.2134/agronj1967.00021962005900060025x. URL <https://access.onlinelibrary.wiley.com/doi/abs/10.2134/agronj1967.00021962005900060025x>.  
\_eprint:  
<https://access.onlinelibrary.wiley.com/doi/pdf/10.2134/agronj1967.00021962005900060025x>.
- [63] R. M. Bhatt, N. K. Rao, and R. Veere Gowda. Response of bulb onion (*Allium cepa* L.) to water stress: photosynthesis, stomatal conductance and osmotic adjustment. *Indian Journal of Horticulture*, 63(3): 276–280, 2006. ISBN: 0972-8538 Publisher: The Horticultural Society of India.
- [64] Nezar H. Samarah. Effects of drought stress on growth and yield of barley. *Agronomy for Sustainable Development*, 25(1):145–149, 2005. URL <https://hal.archives-ouvertes.fr/hal-00886257>. Publisher: Springer Verlag/EDP Sciences/INRA.
- [65] Katharina Harfenmeister, Daniel Spengler, and Cornelia Weltzien. Analyzing Temporal and Spatial Characteristics of Crop Parameters Using Sentinel-1 Backscatter Data. *Remote Sensing*, 11(13):1569, January 2019. doi: 10.3390/rs11131569. URL <https://www.mdpi.com/2072-4292/11/13/1569>. Number: 13 Publisher: Multidisciplinary Digital Publishing Institute.
- [66] KNMI. Klimatologie - Daggegevens van het weer in Nederland. URL <http://projects.knmi.nl/klimatologie/daggegevens/selectie.cgi>. accessed on 17 December 2019.

- [67] Joop Kroes, Iwan Supit, Jos van Dam, Paul van Walsum, and Martin Mulder. Impact of capillary rise and recirculation on simulated crop yields. *Hydrology and Earth System Sciences*, 22(5):2937–2952, May 2018. ISSN 1607-7938. doi: 10.5194/hess-22-2937-2018. URL <https://www.hydrology-earth-syst-sci.net/22/2937/2018/>.
- [68] Karel van Hussen, Ilse van de Velde, Rianne Läkamp, and Susanne van der Kooij. Economische schade door droogte in 2018, February 2019. Ecorys.
- [69] VanderSat. Recovery from the 2018 drought in the Netherlands, March 2019. URL <http://vandersat.com/blog/recovery-from-the-2018-drought-in-the-netherlands/>. accessed on 29 September 2020.
- [70] Hans Gels and Linda van der Toorn. Extreme droogte 2018: ‘Vechtstromen snakt (nog steeds) naar water’. accessed on 2 August 2020.
- [71] ESRI. ArcGIS Hub. URL [https://hub.arcgis.com/search?owner=Esri\\_NL\\_Content](https://hub.arcgis.com/search?owner=Esri_NL_Content). accessed on 15 December 2020.
- [72] PDOK. Dataset: Basisregistratie Gewaspercelen (BRP). URL <https://www.pdok.nl/introductie/-/article/basisregistratie-gewaspercelen-brp->. accessed on 23 January 2020.
- [73] Henning Skriver, Francesco Mattia, Giuseppe Satalino, Anna Balenzano, Valentijn R. N. Pauwels, Niko E. C. Verhoest, and Malcolm Davidson. Crop Classification Using Short-Revisit Multitemporal SAR Data. *IEEE Journal of Selected Topics in Applied Earth Observations and Remote Sensing*, 4(2):423–431, June 2011. ISSN 2151-1535. doi: 10.1109/JSTARS.2011.2106198.
- [74] Nataliia Kussul, Guido Lemoine, Francisco Javier Gallego, Sergii V. Skakun, Mykola Lavreniuk, and Andrii Yu. Shelestov. Parcel-Based Crop Classification in Ukraine Using Landsat-8 Data and Sentinel-1A Data. *IEEE Journal of Selected Topics in Applied Earth Observations and Remote Sensing*, 9(6):2500–2508, June 2016. ISSN 2151-1535. doi: 10.1109/JSTARS.2016.2560141.
- [75] Lu Xu, Hong Zhang, Chao Wang, Bo Zhang, and Meng Liu. Crop Classification Based on Temporal Information Using Sentinel-1 SAR Time-Series Data. *Remote Sensing*, 11(1):53, January 2019. doi: 10.3390/rs11010053. URL <https://www.mdpi.com/2072-4292/11/1/53>.
- [76] Kristof Van Tricht, Anne Gobin, Sven Gilliams, and Isabelle Piccard. Synergistic Use of Radar Sentinel-1 and Optical Sentinel-2 Imagery for Crop Mapping: A Case Study for Belgium. *Remote Sensing*, 10(10):1642, October 2018. doi: 10.3390/rs10101642. URL <https://www.mdpi.com/2072-4292/10/10/1642>.
- [77] Uwe Meier. *Growth stages of mono- and dicotyledonous plants*. Blackwell Wissenschafts-Verlag, 1997. ISBN 3-8263-3152-4.
- [78] KNMI. Maandsommen neerslag, normalen, anomalieën. URL <https://www.knmi.nl/nederland-nu/klimatologie/geografische-overzichten/archief/maand/rd>. accessed on 24 November 2020.
- [79] VanderSat. Detailed soil moisture data. URL <https://vandersat.com/technology/soil-moisture/>. accessed on 23 January 2020.
- [80] VanderSat. VanderSat Data Products, 2020. URL [https://docs.vandersat.com/VanderSat\\_Data\\_Products.html](https://docs.vandersat.com/VanderSat_Data_Products.html). accessed on 16 December 2020.
- [81] Richard A. M. de Jeu, Thomas R. H. Holmes, Robert M. Parinussa, and Manfred Owe. A spatially coherent global soil moisture product with improved temporal resolution. *Journal of Hydrology*, 516: 284–296, August 2014. ISSN 0022-1694. doi: 10.1016/j.jhydrol.2014.02.015. URL <http://www.sciencedirect.com/science/article/pii/S0022169414001139>.
- [82] Richard Adrianus Maria De Jeu, Anna Helena Alida De Nijs, and Michel Hendricus Wilibrord VAN KLINK. Method and system for improving the resolution of sensor data, December 2017. URL <https://patents.google.com/patent/WO2017216186A1/en>.
- [83] Sinergise Laboratory. EO Browser | Sentinel Hub. URL <https://www.sentinel-hub.com/explore/eobrowser>. accessed on 23 January 2020.

- [84] Google Earth Engine. Sentinel-1 Algorithms. URL <https://developers.google.com/earth-engine/guides/sentinel1?hl=nl>.
- [85] Vineet Kumar, Manuel Huber, Björn Rommen, and Susan Steele-Dunne. SandboxNL: Parcel based Rapid Crop Monitoring using Sentinel-1 SAR and Google Earth Engine in The Netherlands. *Earth System Science Data*, 2020.
- [86] CSAR. De Aanbevelende Rassenlijst Akkerbouw en Veehouderij 2020, 2019. Commissie Samenstelling Aanbevelende Rassenlijst.
- [87] Suikerbieten - Akkerbouwbedrijf Mts. Hoogterp. URL <http://www.mtshoogterp.nl/suikerbieten.php>. accessed on 28 October 2020.
- [88] M. Haagsma. *Crop monitoring with Radar: Correlation between SAR polarimetric response and vegetation indices*. PhD thesis, Delft University of Technology, Delft, 2015. Master's Thesis.
- [89] Harry Schreuder. Suikerbieten - Gewasgroei 2017, 2017. URL <https://www.harrysfarm.nl/gewasgroei-2017-suikerbieten/>. accessed on 30 October 2020.
- [90] Pootaardappelen - Akkerbouwbedrijf Mts. Hoogterp. URL <http://www.mtshoogterp.nl/pootaardappelen.php>. accessed on 28 October 2020.
- [91] Het Kleine Loo. Akkerbouw in de 4 seizoenen. URL 2009.
- [92] Harry Schreuder. Aardappelen - Gewasgroei 2017, 2017. URL <https://www.harrysfarm.nl/gewasgroei-2017-aardappelen/>. accessed on 30 October 2020.
- [93] Zaaiuien - Akkerbouwbedrijf Mts. Hoogterp. URL <http://www.mtshoogterp.nl/zaaiuien.php>. accessed on 28 October 2020.
- [94] Lucio Mascolo. *Polarimetric SAR for the monitoring of agricultural crops*. PhD thesis, Università degli Studi di Cagliari, April 2015. URL <https://iris.unica.it/handle/11584/266604?mode=full.1140#.XfIbsehKg2w>.
- [95] M. Susan Moran, Luis Alonso, Jose F. Moreno, Maria Pilar Cendrero Mateo, D. Fernando de la Cruz, and Amelia Montoro. A RADARSAT-2 Quad-Polarized Time Series for Monitoring Crop and Soil Conditions in Barrax, Spain. *IEEE Transactions on Geoscience and Remote Sensing*, 50(4):1057–1070, April 2012. ISSN 0196-2892, 1558-0644. doi: 10.1109/TGRS.2011.2166080. URL <http://ieeexplore.ieee.org/document/6034522/>.
- [96] Harry Schreuder. Zaaiuien - Gewasgroei 2017, 2017. URL <https://www.harrysfarm.nl/gewasgroei-2017-zaaiuien/>. accessed on 30 October 2020.
- [97] RGT planet. Hoogste opbrengst in de zomergerst. URL <https://www.barenbrug.nl/akkerbouw/producten/zomergerst>. accessed on 28 October 2020.
- [98] Marie Wesselink, Brigitte Kroonen, and Janjo de Haan. Toekomst van de maisteelt op zandgrond : Overzicht van huidige situatie en mogelijke maatregelen om de maisteelt te verduurzamen. Technical report, Stichting Wageningen Research, Wageningen Plant Research, Business unit Open Teelten, Wageningen, June 2019. URL <https://research.wur.nl/en/publications/b105cee7-4dea-4fb8-aa57-fbd0aa34c2ee>.
- [99] Schreuder. Aardappelen - Gewasgroei 2018, 2018. URL <https://www.harrysfarm.nl/gewasgroei-2018-aardappelen/>. accessed on 30 October 2020.
- [100] T. van Emmerik, S. C. Steele-Dunne, J. Judge, and N. van de Giesen. Impact of Diurnal Variation in Vegetation Water Content on Radar Backscatter From Maize During Water Stress. *IEEE Transactions on Geoscience and Remote Sensing*, 53(7):3855–3869, July 2015. ISSN 1558-0644. doi: 10.1109/TGRS.2014.2386142. Conference Name: IEEE Transactions on Geoscience and Remote Sensing.
- [101] B Brisco, R Brown, J Koehler, G Sofko, and M Mckibben. The diurnal pattern of microwave backscattering by wheat. *Remote Sensing of Environment*, 34(1):37–47, October 1990. ISSN 00344257. doi: 10.1016/0034-4257(90)90082-W. URL <https://linkinghub.elsevier.com/retrieve/pii/003442579090082W>.

- [102] P. C. Vermunt, S. Khabbazan, S. C. Steele-Dunne, J. Judge, A. Monsivais-Huertero, L. Guerriero, and P.-W. Liu. Response of Subdaily L-Band Backscatter to Internal and Surface Canopy Water Dynamics. *IEEE Transactions on Geoscience and Remote Sensing*, pages 1–16, 2020. ISSN 1558-0644. doi: 10.1109/TGRS.2020.3035881. Conference Name: IEEE Transactions on Geoscience and Remote Sensing.

# A

## BBCH stage tables

### A.1. Maize

Table A.1: Maize BBCH stages and corresponding SAR backscatter responses [77].

Principal Growth Stage	Growth Stage Name	Sub growth Stage	Sub Growth Stage	SAR Backscatter Response		
0	Germination	0	Dry Seed	Soil backscatter dominates		
		1	Beginning of seed imbibition			
		3	Seed imbibition complete			
		5	Radicle emerged from caryopsis			
		6	Radicle elongated, root hairs and/or side roots visible			
		7	Coleptile emerged from caryopsis			
		9	Emergence: coleoptile penetrates soil surface			
		1	Leaf Development	10	First leaf through coleoptile	
				11	First leaf unfolded	
12	2nd leaves unfolded					
13	3rd leaves unfolded			VH/VV backscatter starts increasing rapidly due to volume scattering caused by the leaves [14, 35]		
-	Stage continues					
19	9 or more leaves unfolded					
3	Stem elongation	30	Beginning of stem elongation	Rapid increase VH/VV backscatter slows down [14]		
		31	first node detectable			
		32	2 nodes detectable			
		33	3 nodes detectable			
		3.	continue			
		39	9 or more nodes detectable			
5	Inflorescence emergence, heading	51	Beginning of tassel emergence: tassel detectable at top of stem	Saturation of VV, VH and VH/VV backscatter [14, 35, 46, 50]. VH/VV backscatter now dependent on VWC [14].		
		53	Tip of tassel visible			
		55	Middle of tassel emergence: middle of tassel begins to separate			
		59	End of tassel emergence: tassel fully emerged and separated			
6	Flowering, anthesis	61	Male: stamens in middle of tassel visible, Female: tip of ear emerging from leaf sheath			
		63	Male: beginning of pollen shedding, Female: tips of stigmata visible			
		65	Male: upper and lower parts of tassel in flower, Female: stigmata fully emerged			
		67	Male: flowering completed, Female: stigmata drying			
		69	End of flowering: stigmata completely dry			
7	Development of fruit	71	Beginning of grain development: kernels at blister stage, about 16% dry matter			
		73	early milk			

		75	Kernels in middle of cob yellowish-white (variety-dependent), content milky, about 40% dry matter	VH/VV backscatter starts slowly declining [35]
		79	Nearly all kernels have reached final size	
8	Ripening	83	Early dough: kernel content soft, about 45% dry matter	
		85	Dough stage: kernels yellowish to yellow (variety dependent), about 55% dry matter	
		87	Physiological maturity: black dot/layer visible at base of kernels, about 60% dry matter	
		89	Fully ripe: kernels hard and shiny, about 65% dry matter	
9	Senescence	92	Leaves and shoots beginning to dicolour	
		97	Plant dead and collapsing	
		99	Harvested product	

## A.2. Sugar beet

Table A.2: Sugar beet BBCH stages and corresponding SAR backscatter responses [77].

Principal Growth Stage	Growth Stage Name	Sub growth Stage	Sub Growth Stage	SAR Backscatter Response
0	Germination	0	Dry Seed	Soil backscatter dominates
		1	Beginning of seed imbibition	
		3	Seed imbibition complete	
		5	Radicle emerged from seed	
		7	Shoot emerged from seed	
		9	Emergence: shoot penetrates soil surface	
1	Leaf Development	10	First leaf visible	VH and VH/VV starts increasing [35]
		11	First pair of leaves visible, not yet unfolded	
		12	2 leaves unfolded	
		14	4 leaves unfolded	
		15	5 leaves unfolded	
		-	Stage continues	
		19	9 or more leaves unfolded	
3	Stem elongation	30	rosette growth (crop cover)	Saturation of the VH/VV backscatter signal [35]
		31	crop cover 10% of ground	
		32	crop cover 20% of ground	
		33	crop cover 30% of ground	
		3.	continue	
		39	crop cover 90% of ground	
4	Development of harvestable vegetative plant parts Beet root	49	Beet root has reached harvestable size	
5	Inflorescence emergence, heading	51	Beginning of tassel emergence: tassel detectable at top of stem	
		53	Tip of tassel visible	
		55	Middle of tassel emergence: middle of tassel begins to separate	
		59	End of tassel emergence: tassel fully emerged and separated	
6	Flowering, anthesis	61	Male: stamens in middle of tassel visible, Female: tip of ear emerging from leaf sheath	
		63	Male: beginning of pollen shedding, Female: tips of stigmata visible	
		65	Male: upper and lower parts of tassel in flower, Female: stigmata fully emerged	
		67	Male: flowering completed, Female: stigmata drying	
		69	End of flowering: stigmata completely dry	
7	Development of fruit	71	Beginning of grain development: kernels at blister stage, about 16% dry matter	
		73	early milk	
		75	Kernels in middle of cob yellowish-white (variety-dependent), content milky, about 40% dry matter	
		79	Nearly all kernels have reached final size	
8	Ripening	83	Early dough: kernel content soft, about 45% dry matter	
		85	Dough stage: kernels yellowish to yellow (variety dependent), about 55% dry matter	
		87	Physiological maturity: black dot/layer visible at base of kernels, about 60% dry matter	
		89	Fully ripe: kernels hard and shiny, about 65% dry matter	
9	Senescence	92	Leaves and shoots beginning to discolour	
		97	Plant dead and collapsing	
		99	Harvested product	

## A.3. Potato

Table A.3: Potato BBCH stages and corresponding SAR backscatter responses [77].

Principal Growth Stage	Growth Stage Name	Sub growth Stage	Sub Growth Stage	SAR Backscatter Response	
0	Germination	0	Dry Seed	Soil backscatter dominates and high inter-parcel standard deviation due to row geometry [35]	
		1	Beginning of seed imbibition		
		3	Seed imbibition complete		
		5	Radicle emerged from caryopsis		
		7	Hypocotyl with cotyledons breaking		
		8	Hypocotyl with cotyledons growing towards soil surface		
1	Leaf Development	9	Emergence: cotyledons penetrates soil surface		
		10	First leaf through coleoptile		
		11	1st leaf of main stem unfolded (>3 cm)		Rapid VH and VV backscatter increase [35]
		12	2nd leaf (>3 cm) clearly visible		
		13	3rd leaf (>3 cm)		
2	Formation of basal side shoots below and above soil surface (main stem)	-	Stage continues		
		19	9 or more leaves unfolded		
		21	First basal side shoot visible		
		22	2nd basal side shoot visible		
		23	3rd basal side shoot visible		
3	Main stem elongation (crop cover)	2.	continue		
		29	9 or more basal side shoots visible		
		31	Beginning of crop cover: 10% of plants meet between rows		
		32	20% of plants meet between rows		
		33	30% of plants meet between rows		
		34	40% of plants meet between rows		
		35	50% of plants meet between rows		
		36	60% of plants meet between rows		
4	Tuber formation	37	70% of plants meet between rows		
		38	80% of plants meet between rows		
		39	Crop cover complete: about 90% of plants meet between rows		
		40	Tuber initiation: swelling of first stolon tips to twice the diameter of subtending stolon		
		41	10% of total final tuber mass reached		
		42	20% of total final tuber mass reached		
		43	30% of total final tuber mass reached		
		44	40% of total final tuber mass reached		
		45	50% of total final tuber mass reached		
		46	60% of total final tuber mass reached		
		47	70% of total final tuber mass reached		
5	Inflorescence (cyme) emergence	48	Maximum of total tuber mass reached, tubers detach easily from stolons, skin set not yet complete (skin easily removable with thumb)		
		49	Skin set complete: (skin at apical end of tuber not removable with thumb) 95% of tubers in this stage		
		51	First individual buds (1–2 mm) of first inflorescence visible (main stem)		
6	Flowering	55	Buds of first inflorescence extended to 5 mm		
		59	First flower petals of first inflorescence visible		
		60	First open flowers in population		
		61	Beginning of flowering: 10% of flowers in the first inflorescence open (main stem)		
		62	20% of flowers in the first inflorescence open		
		63	30% of flowers in the first inflorescence open		VH and VV stabilizes [35]
		64	40% of flowers in the first inflorescence open		
65	Full flowering: 50% of flowers in the first inflorescence open				

		66	60% of flowers in the first inflorescence open	
		67	70% of flowers in the first inflorescence open	
		68	80% of flowers in the first inflorescence open	
		69	End of flowering in the first inflorescence	
7	Development of fruit	70	First berries visible	
		71	10% of berries in the first fructification have reached full size(main stem)	Inter-parcel variation starts increasing until BBCH 90 because reduction in vegetation water content increases sensitivity of the backscatter to the underlying soil layer [35]
		72	20% of berries in the first fructification have reached full size	
		73	30% of berries in the first fructification have reached full size	
		7.	. Stages continue	
8	Ripening of fruit and seed	81	Berries in the first fructification still green, seed light-coloured (main stem)	
		85	Berries in the first fructification ochre-coloured or brownish	
		89	Berries in the first fructification shrivelled, seed dark	
9	Senescence	91	Beginning of leaf yellowing	
		93	Most of the leaves yellowish	
		95	50% of the leaves brownish	
		97	Leaves and stem dead, stems bleached and dry	
		99	Harvested product	

## A.4. Onion

Table A.4: Onion BBCH stages and corresponding SAR backscatter responses [77].

Principal Growth Stage	Growth Stage Name	Sub growth Stage	Sub Growth Stage	SAR Backscatter Response	
0	Germination	0	Dry Seed	Soil backscatter dominates	
		1	Beginning of seed imbibition		
		3	Seed imbibition complete		
		5	Radicle emerged from caryopsis		
		7	Cotyledon breaking through seed coat		
		9	Emergence: Cotyledon breaking through soil surface		
		10	Cotyledon visible as hook		
		11	Hook stage: hooked Cotyledon green		
		12	Whip stage: Cotyledon has whip-like form		
1	Leaf Development (Main shoot)	10	Advanced whip stage: whip begins to die off	Start rapid increase of HH and HV backscatter [94]	
		11	First leaf (>3 cm) clearly visible		
		12	2nd leaf (>3 cm) clearly visible		
		13	3rd leaf (>3 cm)		
		-	Stage continues		
		19	9 or more leaves clearly visible		
4	Development of harvestable vegetative plant parts	41	Leaf bases begin to thicken or extend	HH and HV stop increasing [94, 95]	
		43	30% of the expected bulb or shaft diameter reached		
		45	50% of the expected bulb or shaft diameter reached		
		47	Bolting begins; 10% of the plants leaves bent over		HV starts decreasing [94]
		48	Leaves bent over in 50% of plants		
		49	Leaves dead, bulb top dry, growth complete		
5	Inflorescence emergence	51	Onion bulb begins to elongate		
		53	30% of the expected length of flower stem reached		
		55	Flower stem at full length; sheath closed		
		57	Sheath burst open		
		59	First flower petals visible; flowers still closed		
6	Flowering, anthesis	60	First flowers open (sporadically)		
		61	Beginning of flowering: 10% of flowers open		
		62	20% of flowers open		
		63	30% of flowers open		
		64	40% of flowers open		
		65	Full flowering: 50% of flowers open		
		67	Flowering finishing: 70% of petals fallen or dry		
		69	End of flowering		
7	Development of fruit	71	First capsules formed		
		72	20% of capsules formed		
		73	30% of capsules formed		
		74	40% of capsules formed		
		75	50% of capsules formed		
		76	60% of capsules formed		
		77	70% of capsules formed		
		78	80% of capsules formed		
		79	Capsule development completed; seeds pale		
8	Ripening	81	Beginning of ripening: 10% of capsules ripe		
		85	First capsule bursting		
		89	Fully ripe: seeds black and hard		
9	Senescence	92	Leaves and shoots beginning to discolour		
		95	50% of leaves yellow or dead		
		97	Plants or above ground part dead		
		99	Harvested Product		

## A.5. Barley

Table A.5: Barley BBCH stages and corresponding SAR backscatter responses [77].

Principal Growth Stage	Growth Stage Name	Sub growth Stage	Sub Growth Stage	SAR Backscatter Response
0	Germination	0	Dry Seed	Soil backscatter dominates
		1	Beginning of seed imbibition	
		3	Seed imbibition complete	
		5	Radicle emerged from caryopsis	
		6	Radicle elongated, root hairs and/or side roots visible	
		7	Coleptile emerged from caryopsis	
		9	Emergence: coleoptile penetrates soil surface	
1	Leaf Development	10	First leaf through coleoptile	
		11	First leaf unfolded (>3 cm)	
		12	2nd leaf (>3 cm) clearly visible	
		13	3rd leaf (>3 cm)	
		-	Stage continues	
2	Tillering	19	9 or more leaves unfolded	soil backscatter still dominant [65]
		20	No tillers	
		21	[34]	
		22	2 tillers detectable	
		23	3 tillers detectable	
		2.	continue	
3	Stem elongation	29	end of tillering	
		30	Beginning of stem elongation	
		31	first node at least 1 cm above tillering node	
		32	2nd node at least 2 cm above node 1	
		33	3rd node at least 2 cm above node 2	
		3.	continue	
4	Booting	37	Flag leaf just visible, still rolled	maximum VH/VV ratio [35, 65]. VV starts backscatter increasing [35, 52, 65]
		39	Flag leaf stage: flag leaf fully unrolled, ligule just visible	
		41	Early boot stage: flag leaf sheath extending	
		43	Mid boot stage: flag leaf sheath just visibly swollen	
		45	Late boot stage: flag leaf sheath swollen	
5	Inflorescence emergence, heading	47	Flag leaf sheath opening	VH backscatter increase [34, 35, 48, 65]
		49	First awns visible (in awned forms only)	
		51	Beginning of heading: tip of inflorescence emerged from sheath & VV	
		52	20% of inflorescence emerged	
		53	30% of inflorescence emerged	
		54	40% of inflorescence emerged	
		55	Middle of heading: half of inflorescence emerged	
56	60% of inflorescence emerged			
6	Flowering, anthesis	57	70% of inflorescence emerged	
		5	80% of inflorescence emerged	
		59	End of heading: inflorescence fully emerged	
7	Development of fruit	61	Beginning of flowering: first anthers visible	
		65	Full flowering: 50% of anthers mature	
		69	End of flowering: all spikelets have completed flowering but some dehydrated anthers may remain	
8	Ripening	71	Watery ripe: first grains have reached half their final size	VV & VH backscatter start decreasing again [65]
		73	Early milk	
		75	Medium milk: grain content milky, grains reached final size, still green	
		77	Late milk	
8	Ripening	83	Early dough	VV & VH backscatter start decreasing again [65]
		85	Soft dough: grain content soft but dry. Fingernail impression not held	

		87	Hard dough: grain content solid. Fingernail impression held	
		89	Fully ripe: grain hard, difficult to divide with thumbnail	
9	Senescence	92	Over-ripe: grain very hard, cannot be dented by thumbnail	Start decrease VH/VV backscatter due to decrease in VWC [34]
		93	Grains loosening in day-time	
		97	Plant dead and collapsing	
		99	Harvested product	

# B

## Field photo archive

The author wishes to acknowledge the Flevoland 2017 field campaign participants who contributed to the field data collection.

### Flevoland-2017 Maize Parcels PvD-M2



Figure B.1: Field photo archive of maize parcel PvD-M2 in the Flevopolder in 2017.

### Flevoland-2017 Sugar Beet Parcels DB 2.1/1.1



Figure B.2: Field photo archive of sugar beet parcel DB2.1/1.1 in the Flevopolder in 2017.

### Flevoland-2017 Potato Parcels DB-A1/A2

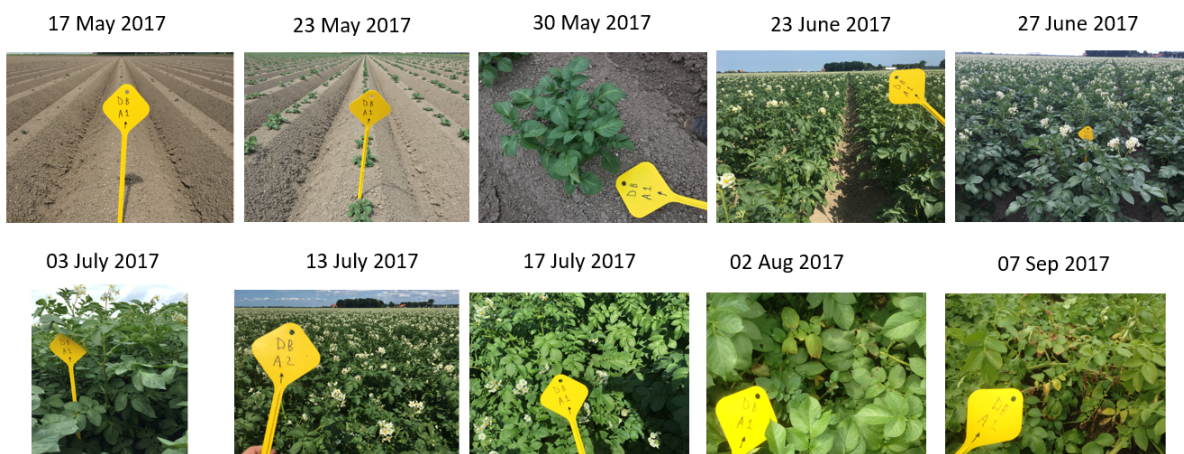


Figure B.3: Field photo archive of potato parcel DB-A1/A2 in the Flevopolder in 2017.

# C

## Python: Post-Processing Code

---

```
def SAR_std(S1):
    SAR = pd.read_csv(S1)

    #transpose to end up with parcels on columns and measurements on rows
    SAR = SAR.transpose()

    #create separate dataframes for VH, VV and CR
    ind_CR_mean = np.arange(5, len(SAR)-3, 8) #indices which contain cross-ratio (VH/VV)
        measurements
    ind_CR_std = np.arange(6, len(SAR)-3, 8) #indices which contain cross-ratio (VH/VV)
        measurements

    ind_VH_mean = np.arange(7, len(SAR)-3, 8) #indices which contain VH measurements
    ind_VH_std = np.arange(8, len(SAR)-3, 8) #indices which contain VH measurements

    ind_VV_mean = np.arange(9, len(SAR)-3, 8) #indices which contain VV measurements
    ind_VV_std = np.arange(10, len(SAR)-3, 8) #indices which contain VV measurements
    VH_mean = SAR.iloc[ind_VH_mean, :]
    VH_std = SAR.iloc[ind_VH_std, :]

    VV_mean = SAR.iloc[ind_VV_mean, :]
    VV_std = SAR.iloc[ind_VV_std, :]

    CR_mean = SAR.iloc[ind_CR_mean, :]
    CR_std = SAR.iloc[ind_CR_std, :]

    #removing rows and columns that only contain NaN values
    VH_mean = VH_mean.dropna(how='all')
    VV_mean = VV_mean.dropna(how='all')
    CR_mean = CR_mean.dropna(how='all')

    VH_mean = VH_mean.dropna(how='all', axis=1)
    VV_mean = VV_mean.dropna(how='all', axis=1)
    CR_mean = CR_mean.dropna(how='all', axis=1)

    VH_std = VH_std.dropna(how='all')
    VV_std = VV_std.dropna(how='all')
    CR_std = CR_std.dropna(how='all')

    VH_std = VH_std.dropna(how='all', axis=1)
    VV_std = VV_std.dropna(how='all', axis=1)
    CR_std = CR_std.dropna(how='all', axis=1)

    VH_mean = VH_mean.T.reset_index(drop=True).T
    VV_mean = VV_mean.T.reset_index(drop=True).T
    CR_mean = CR_mean.T.reset_index(drop=True).T
```

---

```

VH_std = VH_std.T.reset_index(drop=True).T
VV_std = VV_std.T.reset_index(drop=True).T
CR_std = CR_std.T.reset_index(drop=True).T

#extracting dates from the index column and replace the current index column with dates
dates = []
for i in range(len(VH_mean)):
    split = (str(VH_mean.index[i]).split("SDV_")[-1])
    dates.append(split.split("T")[0])

dates = pd.to_datetime(dates, format='%Y%m%d', errors='ignore')
VH_mean.index = dates
VV_mean.index = dates
CR_mean.index = dates
VH_std.index = dates
VV_std.index = dates
CR_std.index = dates

#converting linear values to logarithmic values (dB)
VH_mean = VH_mean.applymap(np.log10) * 10
VV_mean = VV_mean.applymap(np.log10) * 10
CR_mean = CR_mean.applymap(np.log10) * 10
VH_std = VH_std.applymap(np.log10) * 10
VV_std = VV_std.applymap(np.log10) * 10
CR_std = CR_std.applymap(np.log10) * 10

CR_mean = CR_mean.sort_index()
VH_mean = VH_mean.sort_index()
VV_mean = VV_mean.sort_index()

CR_std = CR_std.sort_index()
VH_std = VH_std.sort_index()
VV_std = VV_std.sort_index()

DOY = []
for i in range(len(VH_mean)):
    strptime = datetime.datetime.strptime(str(VH_mean.index[i]), "%Y-%m-%d %H:%M:%S")
    DOY.append(strptime.timetuple().tm_yday)

VH_mean.index = DOY
VV_mean.index = DOY
CR_mean.index = DOY
VH_std.index = DOY
VV_std.index = DOY
CR_std.index = DOY

#combining rows in order to get 1 value per date
VH_mean = VH_mean.groupby(VH_mean.index).sum()
VV_mean = VV_mean.groupby(VV_mean.index).sum()
CR_mean = CR_mean.groupby(CR_mean.index).sum()
VH_std = VH_std.groupby(VH_std.index).sum()
VV_std = VV_std.groupby(VV_std.index).sum()
CR_std = CR_std.groupby(CR_std.index).sum()

#adding interparcel mean per acquisition day
VH_mean['mean'] = VH_mean.mean(axis=1)
VV_mean['mean'] = VV_mean.mean(axis=1)
CR_mean['mean'] = CR_mean.mean(axis=1)
VH_std['mean'] = VH_std.mean(axis=1)
VV_std['mean'] = VV_std.mean(axis=1)
CR_std['mean'] = CR_std.mean(axis=1)
return VH_mean, VH_std, VV_mean, VV_std, CR_mean, CR_std

```

---

# D

## Scheldestromen and the Flevopolder results

## D.1. Scheldestromen

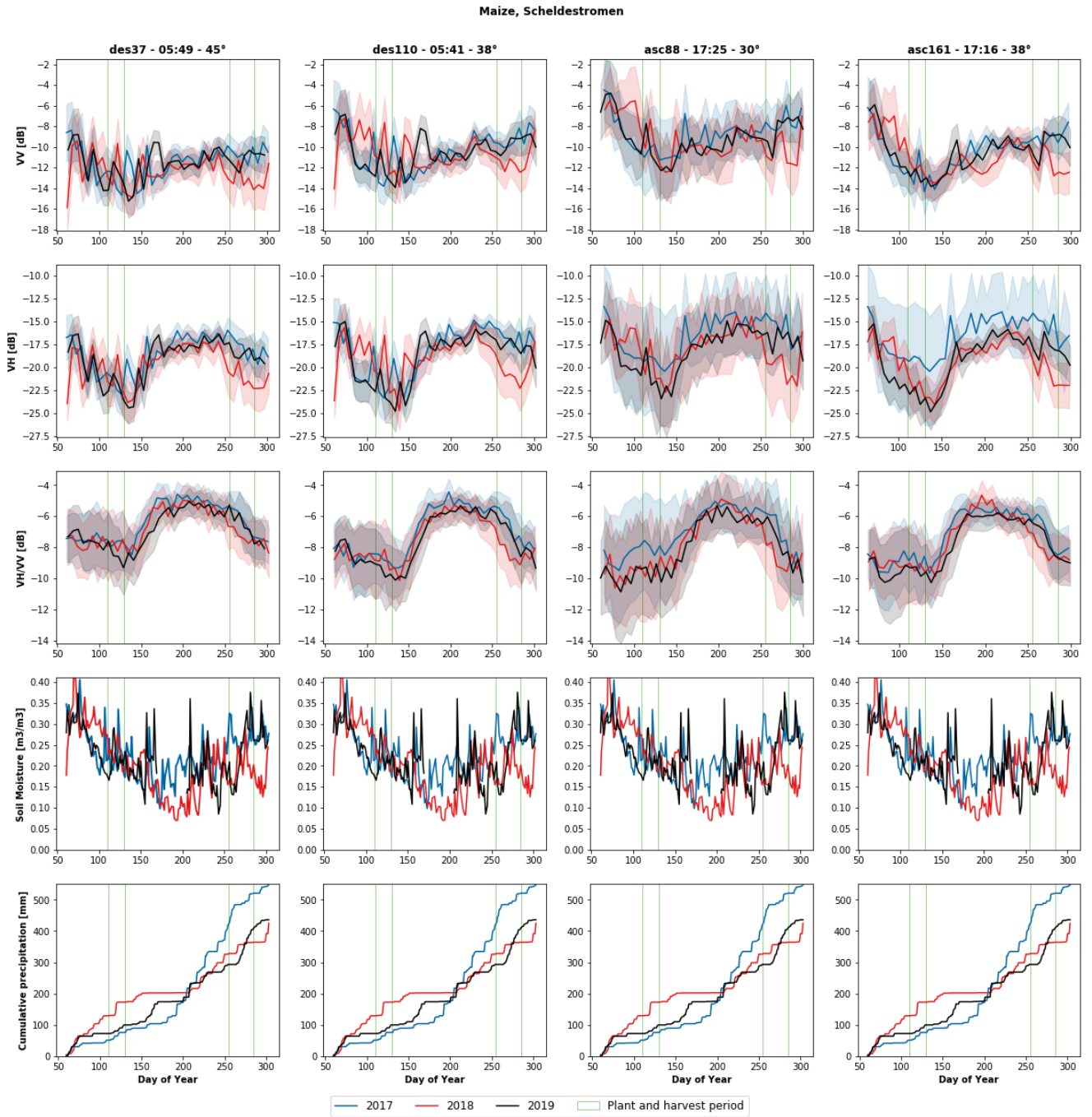


Figure D.1: 2017, 2018 and 2019 Sentinel-1 backscatter data for maize parcels, soil moisture and cumulative precipitation in Scheldestromen.

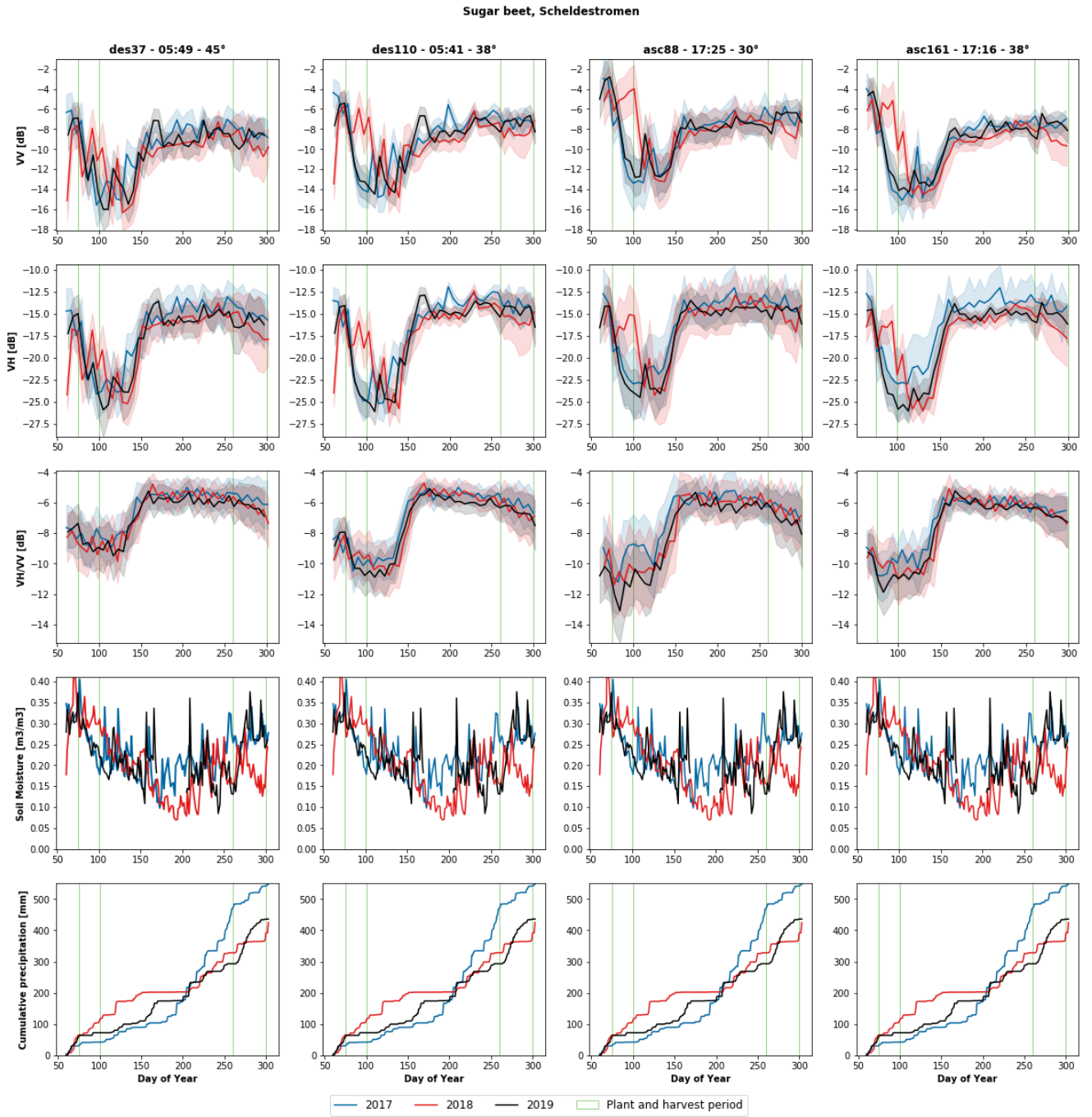


Figure D.2: 2017, 2018 and 2019 Sentinel-1 backscatter data for sugar beet parcels, soil moisture and cumulative precipitation in Scheldestromen.

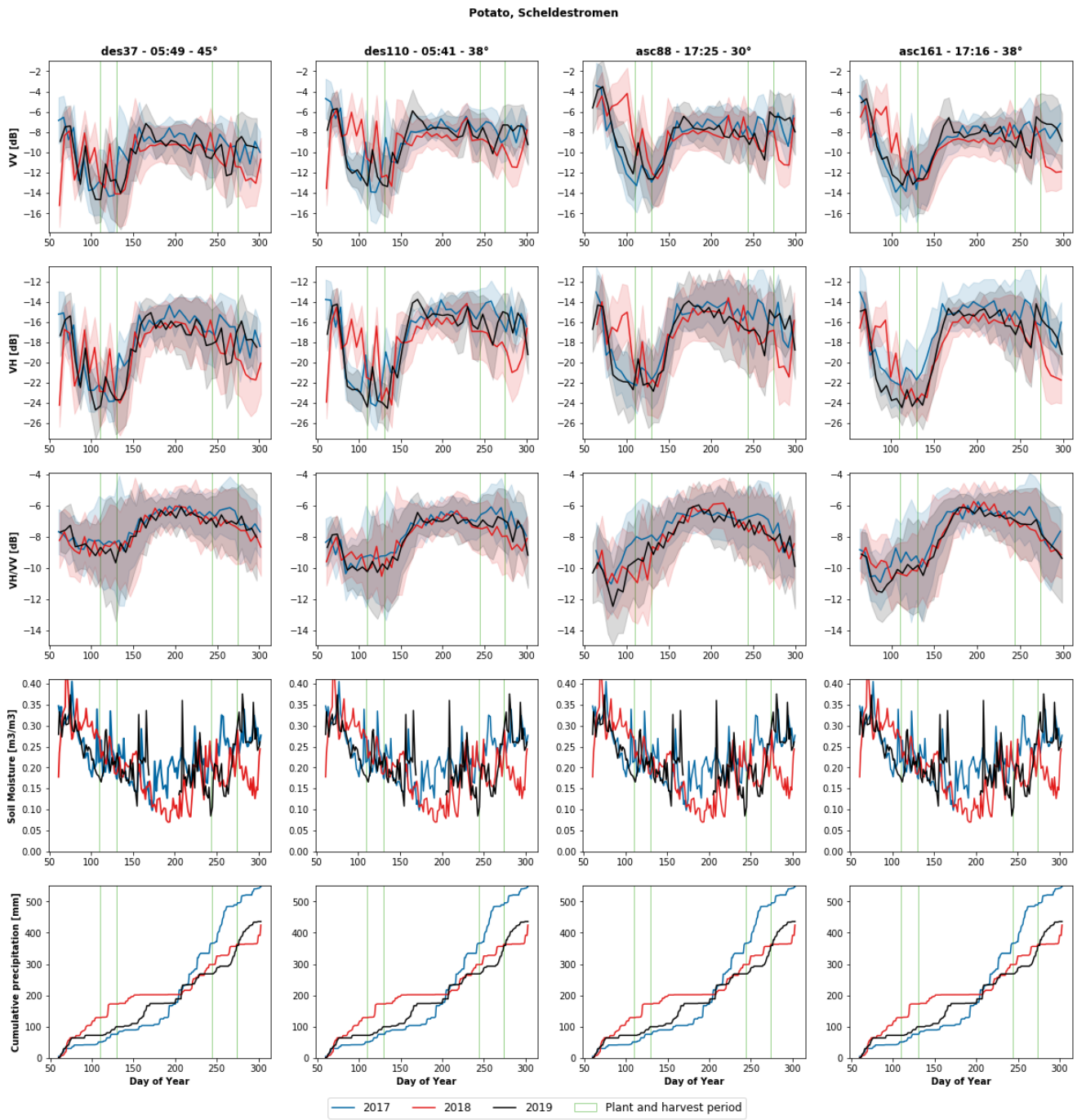


Figure D.3: 2017, 2018 and 2019 Sentinel-1 backscatter data for potato parcels, soil moisture and cumulative precipitation in Scheldestromen.

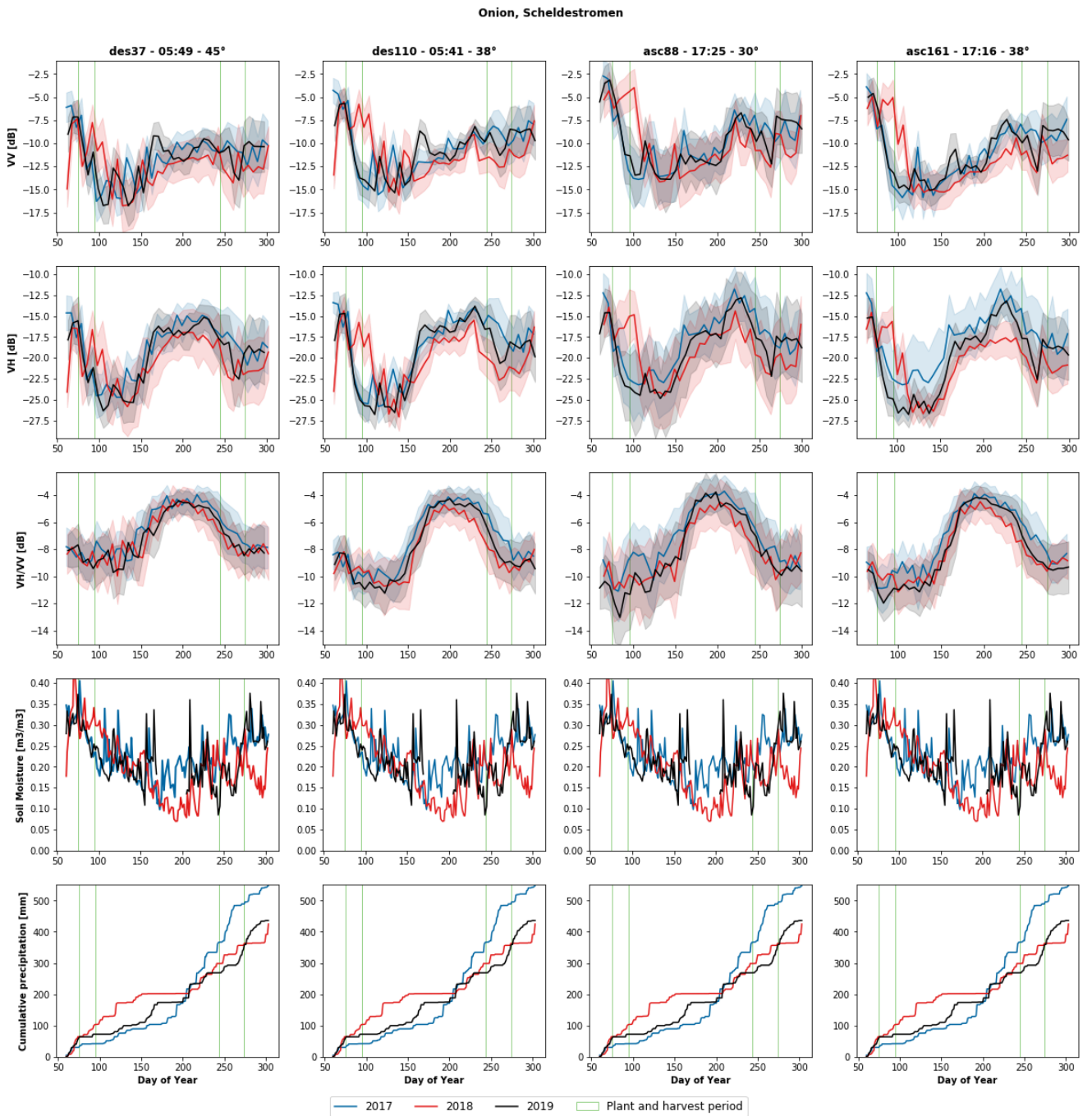


Figure D.4: 2017, 2018 and 2019 Sentinel-1 backscatter data for onion parcels, soil moisture and cumulative precipitation in Scheldestromen.

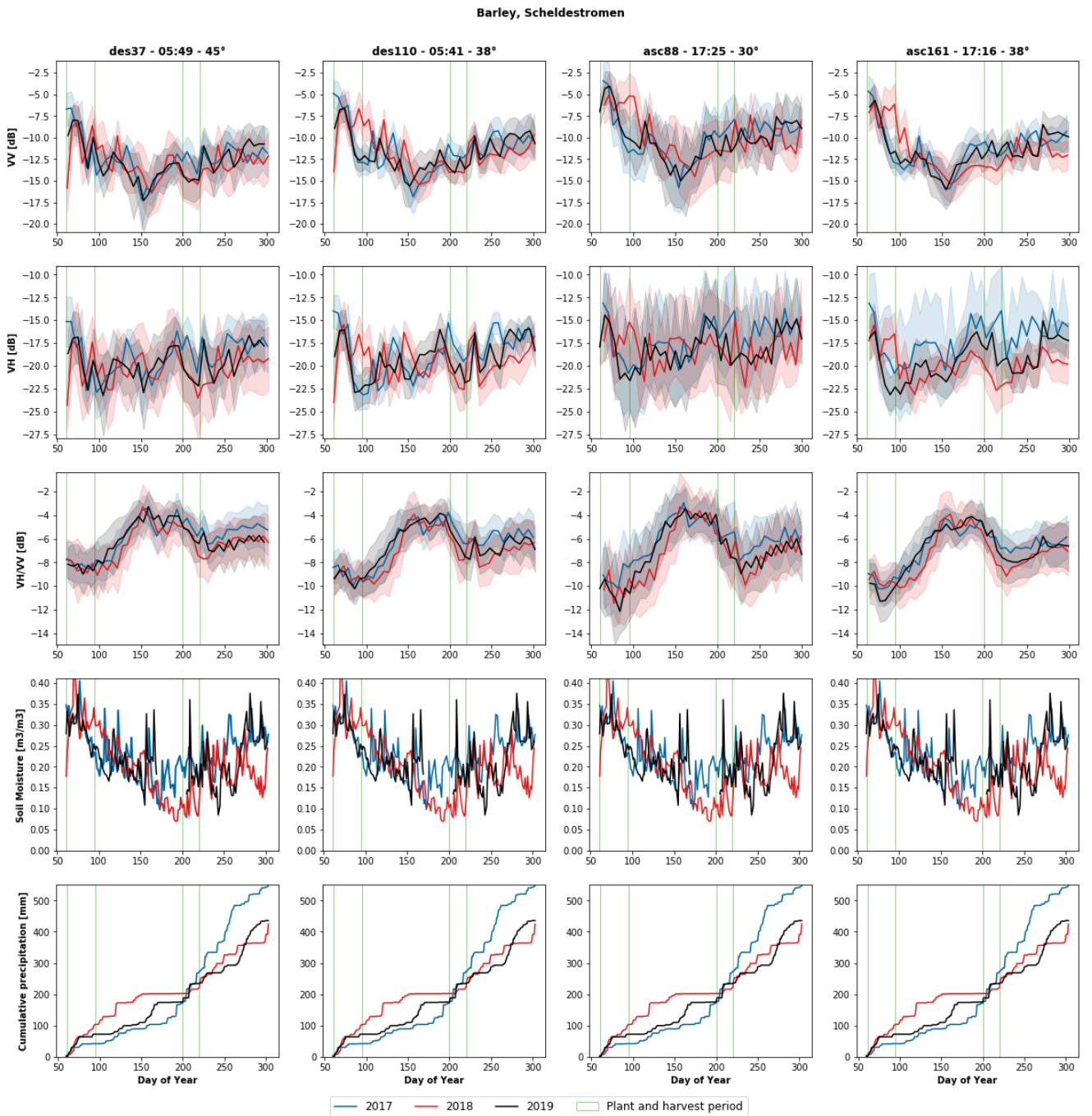


Figure D.5: 2017, 2018 and 2019 Sentinel-1 backscatter data for barley parcels, soil moisture and cumulative precipitation in Scheldestromen.

## D.2. Flevopolder

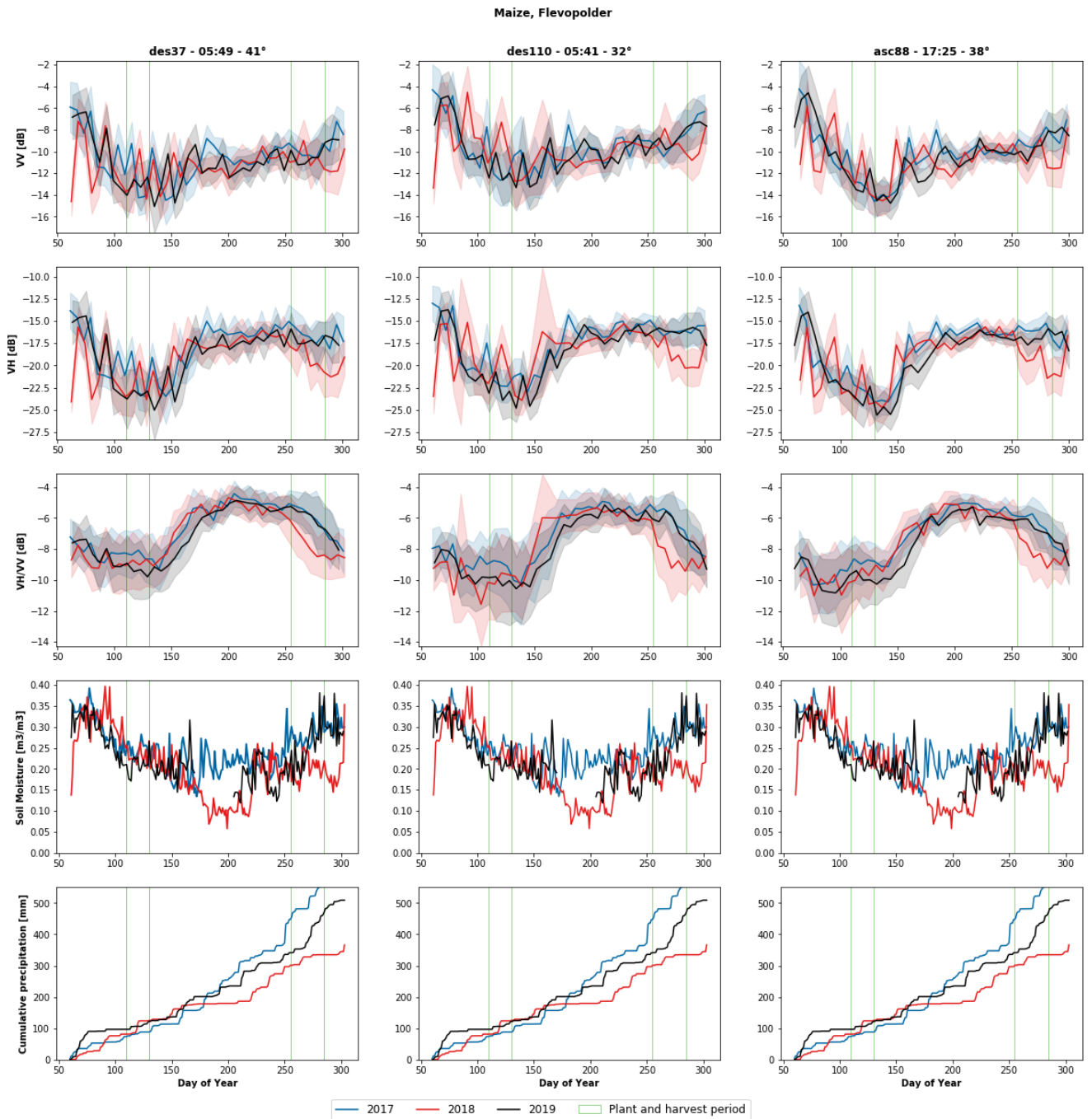


Figure D.6: 2017, 2018 and 2019 Sentinel-1 backscatter data for maize parcels, soil moisture and cumulative precipitation in the Flevopolder.

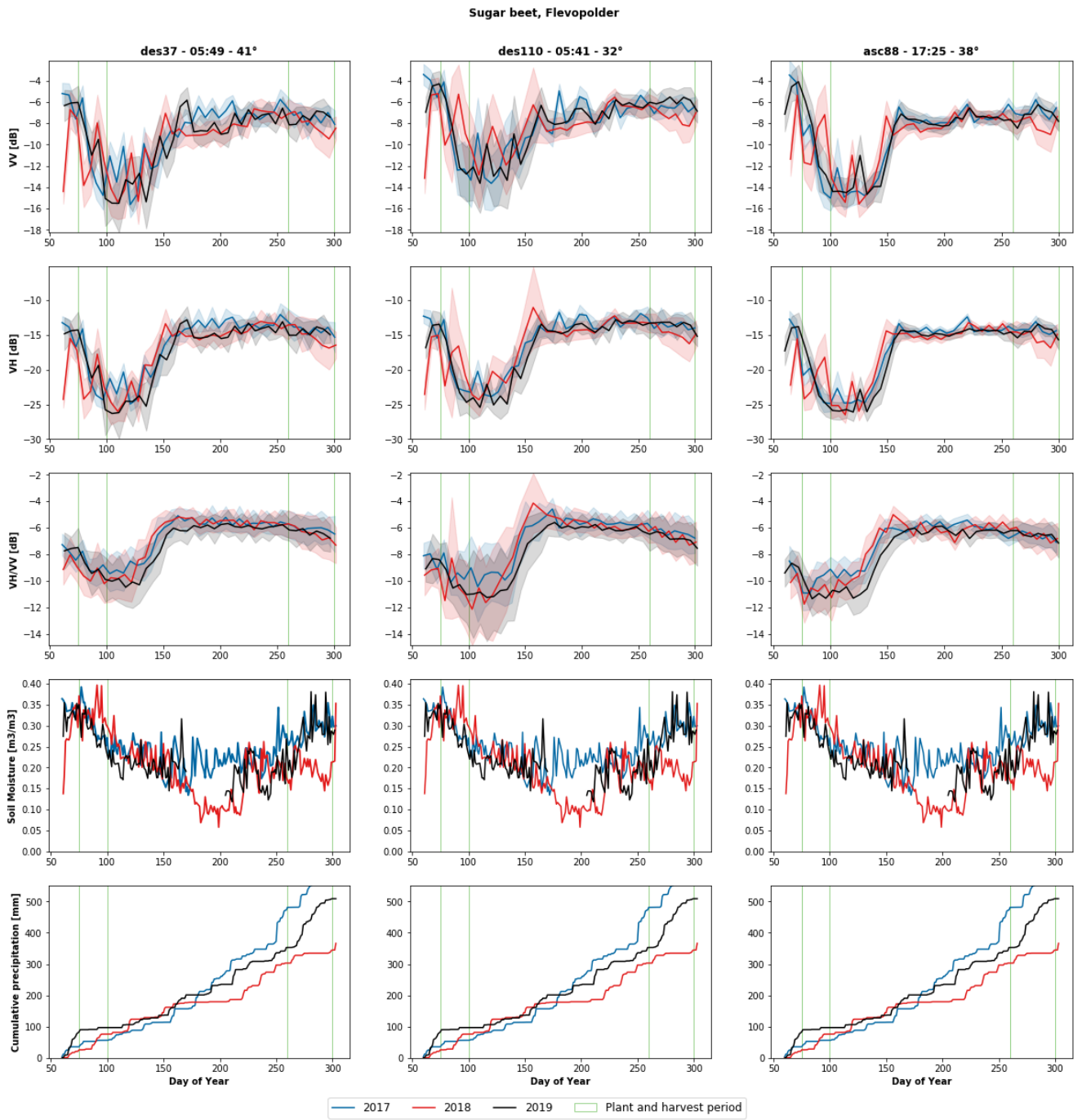


Figure D.7: 2017, 2018 and 2019 Sentinel-1 backscatter data for sugar beet parcels, soil moisture and cumulative precipitation in the Flevopolder.

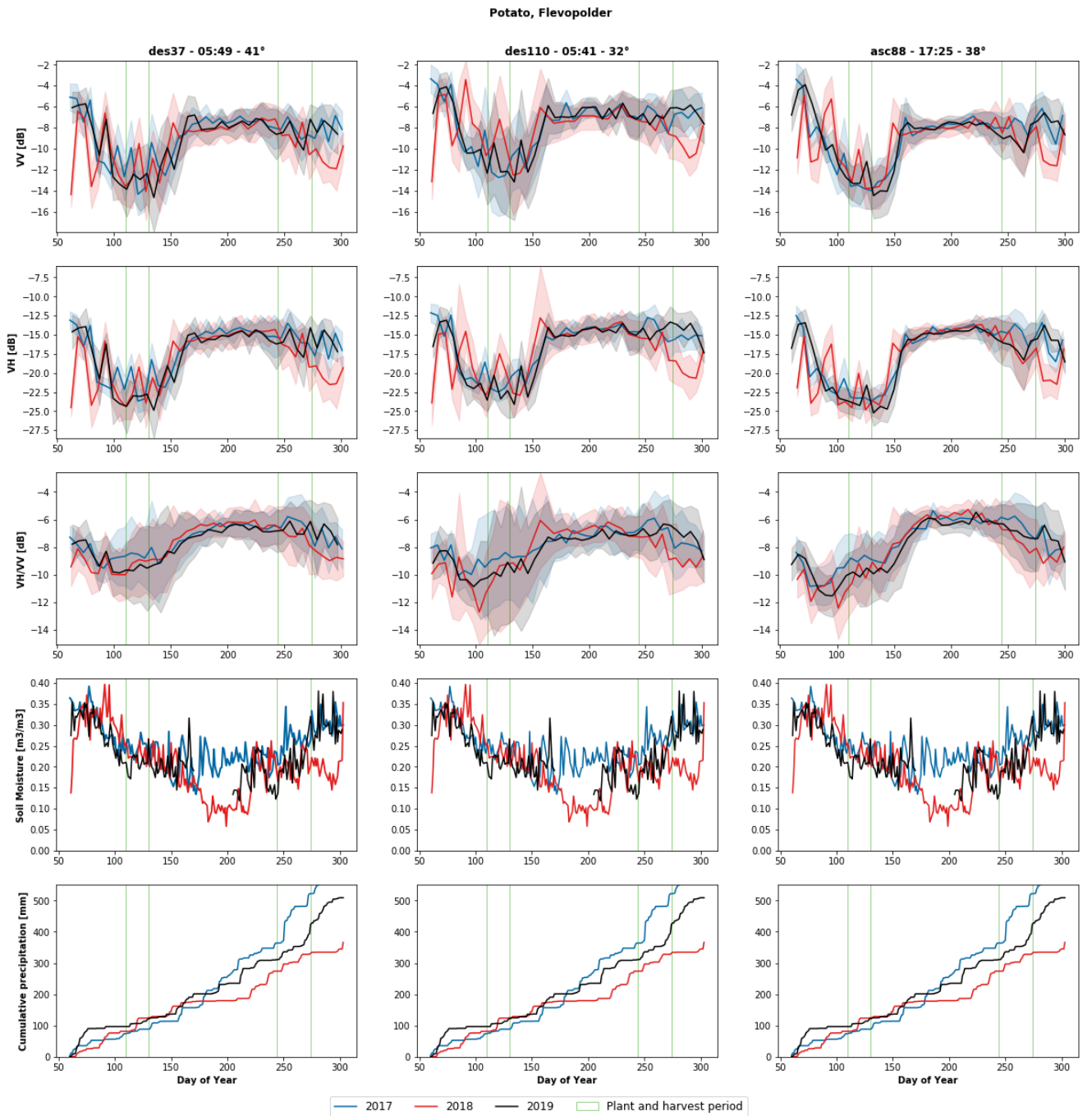


Figure D.8: 2017, 2018 and 2019 Sentinel-1 backscatter data for potato parcels, soil moisture and cumulative precipitation in the Flevopolder

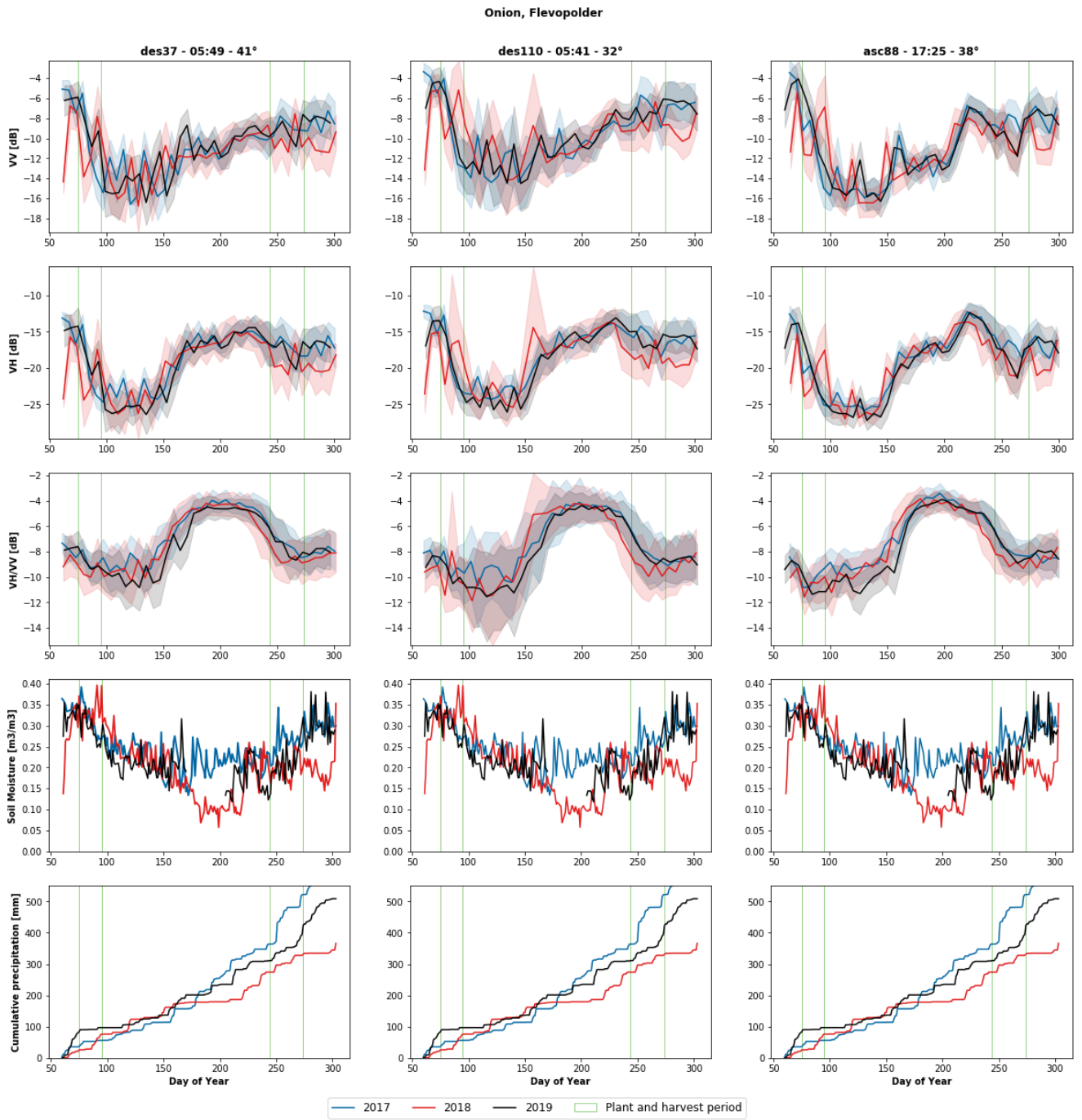


Figure D.9: 2017, 2018 and 2019 Sentinel-1 backscatter data for onion parcels, soil moisture and cumulative precipitation in Flevopolder.

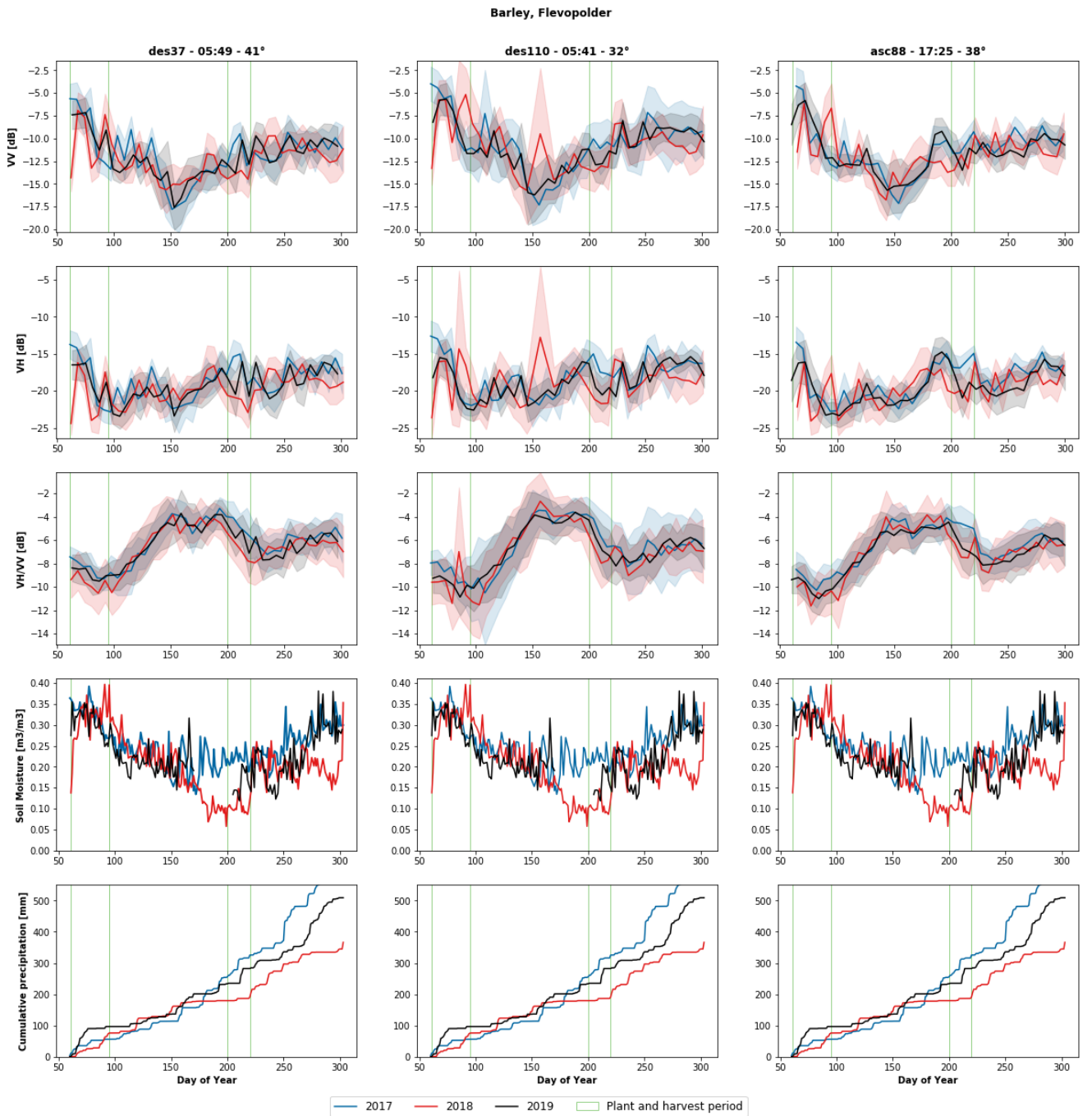


Figure D.10: 2017, 2018 and 2019 Sentinel-1 backscatter data for barley parcels, soil moisture and cumulative precipitation in the Flevopolder.